Investigating the antibiotic and metal binding properties of obafluorin

Melissa Joy Davie

John Innes Centre

Department of Molecular Microbiology

Norwich Research Park, Colney Lane, Norwich, NR4 7UH, UK

A thesis submitted to the University of East Anglia for the degree of Master of Philosophy

December 2021

Investigating the metal-binding and antibiotic properties of obafluorin

Melissa Joy Davie, John Innes Centre, December 2021

Abstract

Humans have utilised natural products (NPs) throughout history for a variety of different applications including in as pharmaceuticals; more than seventy percent of the antibiotics we use today are NPs or their derivatives. This project focusses on the NP, obafluorin, a broad-spectrum antibiotic produced by the bacterium *Pseudomonas fluorescens*. Its structure consists of a β-lactone core decorated with a catechol moiety and a 4-nitrophenyl group. β-lactones, although susceptible to hydrolysis and attack by β-lactamase enzymes, are components of various structurally diverse NPs with valuable biological activities.

The biosynthesis of obafluorin in *P. fluorescens* has been characterised previously and its molecular target has been identified as the threonyl-tRNA synthetase (ThrRS) enzyme. However, its mechanism of action remains elusive. Here, I report progress towards understanding the properties of obafluorin and their role in its mechanism of action. I used a biochemical approach to unpick the role of chemical constituents of the structure of obafluorin. The catechol was found to be essential for both the bioactivity and ferric iron binding properties of obafluorin. Through characterisation of the obafluorin-iron complex, I have found that iron binding is responsible for protecting the β-lactone of obafluorin from hydrolytic breakdown, and this to be vital for bioactivity. Unfortunately, studies on elucidation of the interaction between obafluorin and ThrRS were thwarted due to the reactivity of the compound *in vitro*. However, this report details significant progress made to understand the properties and bioactivity of this previously disregarded antibiotic.

These studies highlight the importance of further investigations into “old” antibiotics and demonstrate the potential of antibiotic-iron interactions. This could represent an underexplored area of antibiotic research which could hold great value in the fight against antimicrobial resistance.

Acknowledgements

I would like to express my gratitude to Prof. Barrie Wilkinson for his guidance throughout my studies at the John Innes Centre, and for his understanding with my decision to write up early. I am incredibly grateful to have had the opportunity to work in his research group and to have developed the knowledge and skills here that I have.

I owe special thanks to Dr. Sibyl Batey for sharing both her scientific and personal wisdom with me and for her invaluable guidance during my studies. So much thanks also to Dr. Claudio Greco for his unwavering kindness, understanding and support. I wish them both the best of luck with her future career as they well and truly deserve great success. I would like to thank Dr. Edward Hems for his help with the chemistry wizardry and his careful encouragement towards doing something different. Dr. Tung Le and Dr. Ngat Tran have a special place in my heart as some of the most amazingly dedicated scientists and deeply caring people I know. Thank you, Tung, for the Mars bars and dates, much needed science fuel!

The welcoming and friendly atmosphere in Molecular Microbiology is a credit to the attitude of Prof. Mark Buttner and all the members of his department. I feel privileged to have been part of such a community-minded department and to have made the friends here that I have. I would particularly like to thank Hannah McDonald for her cheer, her encouragement, and her reassurance for me and for everyone she meets. Also Dr. Martin Rejzeck, Dr. Matthew Bush and Dr. Joseph Sallmen for their advice, such interesting conversations, and friendship. It is with a heavy heart that I will say goodbye to everyone in Molly Micro and I wish them all the best!

Finally, I would like to thank my family and friends for their absolute love and support throughout the good and the more challenging times. Particularly to my brother, Dan, for being my best friend and inspiration in this life, and to Granny Liz for her worldly wisdom and her trust in me.

Author’s declaration

The research described in this thesis was conducted entirely at the John Innes Centre between October 2019 and December 2021. All the data described are original and were obtained by the author, except where specific acknowledgement has been made. No part of this thesis has previously been submitted as for a degree at this or any other academic institution.

Abbreviations

DHBA	2,3-dihydroxybenzoic acid
2-HBA	2-hydroxybenzoic acid
3-HBA	3-hydroxybenzoic acid
β-OH-α-AA	β-hydroxy-α-amino acid
A	Adenylation*
aaRS	Aminoacyl-tRNA synthetase
ACP	Acyl carrier protein
AMR	Antimicrobial resistance
AT	Acyl transferase
BA	Benzoic acid
BGC	Biosynthetic gene cluster
Bipy	2'2-bipyridyl
BSA	Bovine serum albumin
C	Condensation*
CAS	Chrome azurol S
coA	Coenzyme A
CV	Column volume
DH	Dehydratase
DMSO	Dimethyl sulfoxide
EcThrRS	*Escherichia coli* threonyl-tRNA synthetase
EDTA	Ethylenediaminetetraacetic acid
ELSD	Evaporative light scattering detector
ER	Enoyl reductase
Fur	Ferric uptake iron regulator
HDTMA	Hexadecatrimethylammonium
HPLC	High pressure liquid chromatography
HR-LCMS	High-resolution liquid chromatography mass spectrometry
HSL	*N*-acylhomoserine lactone
IleRS	Isoleucine tRNA synthetase
KR	Ketoreductase*
KS	Ketosynthase*
L-TTA	L-threonine transaldolase
LB	Luria Bertani
LC-MS/MS	Liquid chromatography tandem mass spectrometry
LCMS	Liquid chromatography mass spectrometry
MIC	Minimum inhibitory concentration
MRSA	Methicillin resistant *Staphylococcus aureus*
MSSA	Methicillin sensitive *Staphylococcus aureus*
MS	Mass spectrometry
NGS	Next-generation sequencing
NP	Natural product
NPD	Natural product discovery
NRPS	Non-ribosomal peptide synthetase
OPM	Obafluorin production medium

OPM-Fe	Obafluorin production media without iron added
PAR	4-(2-pyridylazo)-resorcinol
PCP	Peptidyl carrier protein*
PKS	Polyketide synthetase
QS	Quorum sensing
ROS	Reactive oxygen species
SDS-PAGE	Sodium dodecyl sulphate polyacrylamide gel electrophoresis
SILAC	Stable isotope labelling by amino acids in cell culture
SNA	Soft-nutrient agar
TB	Terrific broth
TBDT	TonB-dependent transporter
TBE	Tris-borate EDTA
TE	Tris-EDTA
TE	Thioesterase*
THA	Trojan-horse antibiotic
ThrRS	Threonyl tRNA synthetase
Thr-AMS	Threonyl adenosine monophosphate
WT	Wild-type
XRD	X-ray diffraction

* Those marked with an asterisk are domains from NRPS/PKSs

Compound Key

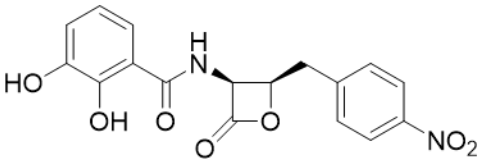

Obafluorin
1

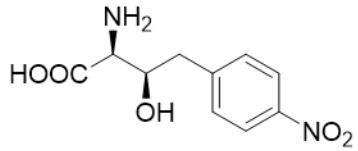

2S,3R)-2- amino-3-hydroxy
-4-(4-nitrophenyl)butanoate
2

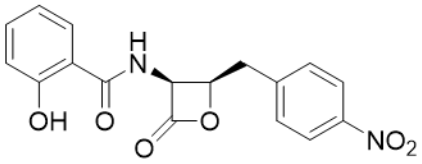

3

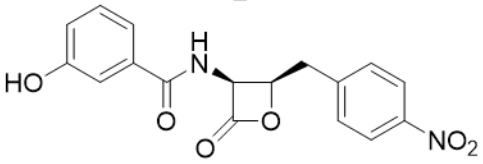

4

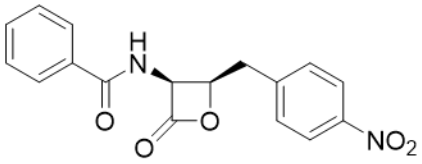

5

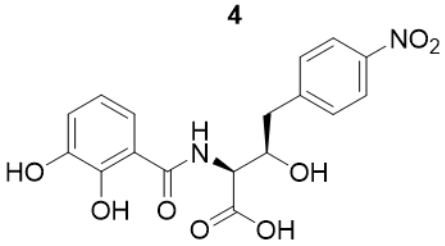

Hydrolysed obafluorin
6

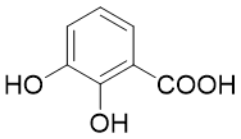

2,3-dihydroxybenzoic acid
DHBA

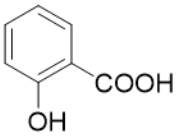

2-hydroxybenzoic acid
2-HBA

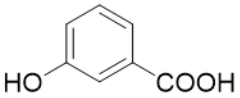

3-hydroxybenzoic acid
3-HBA

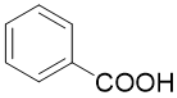

Benzoic acid
BA

Table of Contents

Index of Figures

Chapter 1:

Introduction

Chapter 1 : Introduction

1.1 Natural products

1.1.1 An introduction to natural products

Natural products (NPs), also known as specialised metabolites, are organic compounds produced by organisms in Nature. They are not active participants in the primary metabolism of the organism but often give some selective advantage in their environmental niche.[1] Humans can harness the potential of these naturally occurring compounds for various applications including in the agricultural and pharmaceutical industries.[2, 3] Sadly, the technological advancement of our species has involved too much encroachment onto natural habitats and withdrawal of the Earth's natural resources without replenishment. This has led to an age of global environmental instability and, as a result, humans are under increasing pressure to solve the consequent problems. Health issues are worsening due to antimicrobial resistance (AMR) and immense strain will face the agricultural industry to provide sufficient nutrition to the Earth's growing population using the current system. Therefore, we must return to Nature's archive of complex chemical diversity to look for inspiration for positive solutions for a more sustainable and harmonious future on this planet.

1.1.2 The rise and fall of natural product discovery

The use of natural products in traditional medicines has been documented throughout history and in many separate instances all over the world. The medicinal and physiological effects of plants and herbs were noted as early as 3500 B.C. when the properties of willow bark were utilised in Sumerian times and the Egyptians (2900 B.C.) documented over 700 different plant-based treatments in the Ebers Papyrus.[4, 5] The most famous modern natural product discovery was that of penicillin from the fungus *Penicillium notatum* by Sir Alexander Fleming in 1929.[4] This finding by Fleming, and the extraction and subsequent *in vivo* clinical studies of penicillin by Chain and Florey led to the three sharing the Nobel prize and the prevention of countless deaths from infection in the 1940s and the following years.[6] These events revolutionised the field of drug discovery research and led to screening efforts to find new microbial bioactive compounds, particularly from fungi and actinomycetes. Actinomycetes are a phylum of mainly Gram-positive, filamentous bacteria that have been one of the most prolific sources of antibiotics that we use today.[7] Successes include the discovery of various antibiotics produced by *Streptomyces* spp., many of which are still in clinical use today; these include streptomycin,[8] chloramphenicol,[9] chlortetracycline,[10] and vancomycin.[11] This led to investment from pharmaceutical

companies and the development of natural product discovery (NPD) programmes in the so-called “Golden-age of antibiotic discovery”.[2, 12, 13] This period, from 1940 to 1960, involved the systematic screening of fermentation extracts from bacteria and fungi for antagonistic activity against pathogens, leading to the discovery of over 1000 NPs with antibacterial and antifungal activity.[1] Some clinically important NPs and their biological activities are shown in Figure 1.1, highlighting the structural diversity of NP compounds.

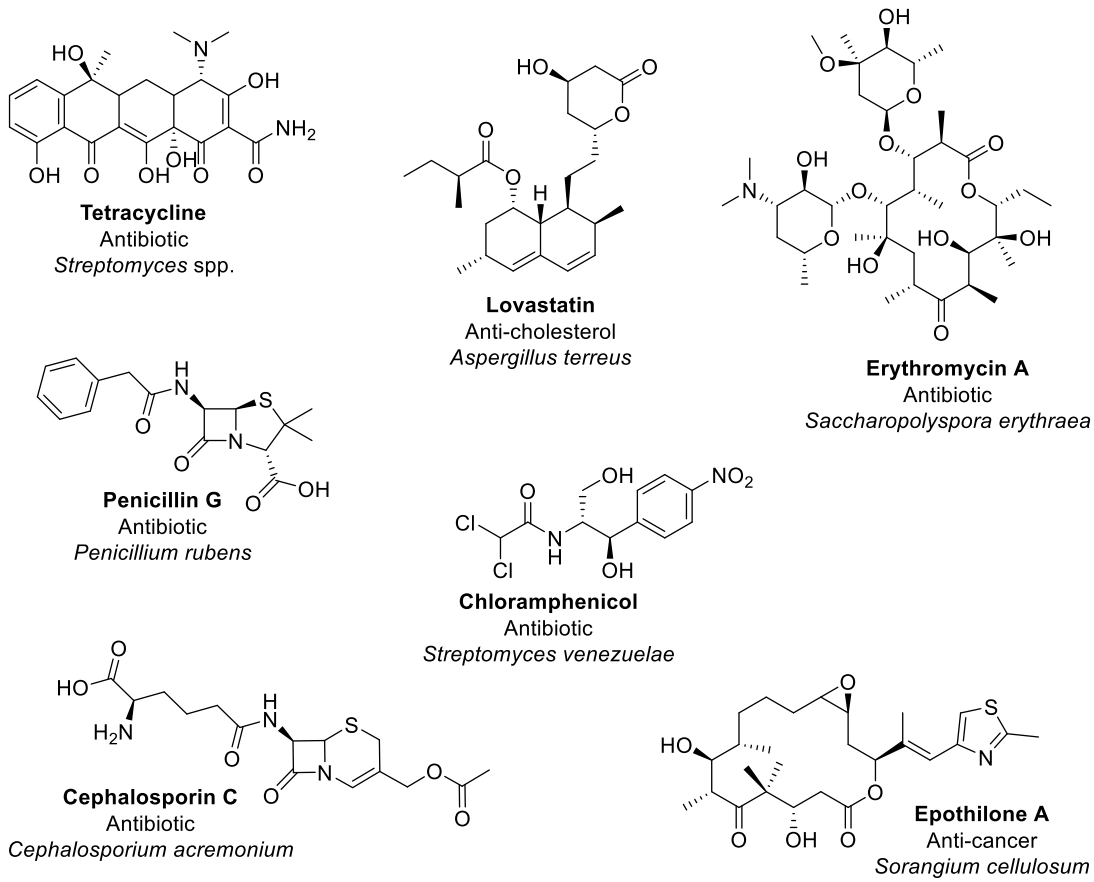

Figure 1.1: Structures of examples of clinically important natural products. Their biological activities and producing organisms are indicated.

Following this period, antibiotic development was mainly focused on creating synthetic versions of the natural scaffolds identified during the “Golden-age” of discovery. This was largely because many of the NPs discovered had pharmacological or toxicological drawbacks, and the development of resistance was already becoming a problem.[14] Combinatorial synthesises and high-throughput screening approaches were favoured by the pharmaceutical industry as they were deemed a more rapid route to generating huge compound libraries. These techniques involved the generation of thousands of unique compounds from chemical scaffolds

which could then be quickly screened via robotic target-based assays.[1] Unfortunately, these strategies did not reach their potential due to problems with reliable access and supply of targets, separation from complex mixtures and structural characterisation issues.[15] Additional problems included continual re-discovery of already known NPs and increased cost associated with screening and developing lead compounds.[15] Therefore, the de-emphasis on NPD programmes led to a decrease of new leads in the drug-development and approval pipeline,[3] which also coincided with the rise of AMR. The over- and misuse of antibiotics used to treat infection in human and animal diseases has created conditions that promote the selection of increasingly drug-resistant pathogens.[14] Therefore, our discoveries that led to the "miracles" of modern medicine also gave rise to significant further challenges, an example of how important it is to fully understand Nature's processes and to carefully consider the sustainability of our technological advancements.

1.1.3 The genomic era: a new "Golden Age" of natural products

After the decline of NPD, the number of new chemical entities reaching the drug market had fallen to a two-decade minimum in 2002.[16] The failures also involved the unrealistic expectations of combinatorial chemistry for discovering synthetic drugs.[1] NPs tend to be better adapted to access and interaction with biological targets as their chemistry has evolved for this specific process over millions of years.[17] Additionally, discussions on this decline of antibiotic productivity from the pharmaceutical industry are also complex and controversial. Short dosage times and the inherent low-profit nature of antibiotics mean that they are an economically unattractive area for big pharma; this has led to a lack of investment into their research and development. However, the need for new approaches for NP discovery is underlined by the alarming rise of bacterial infections that are resistant to almost all known antibiotics. Slowly, governments are realising that finding new antibiotics is a priority due to the significant threat of rising AMR and the risk of falling backwards into a situation akin to the pre-antibiotic era.

Thankfully, advancements in technologies including synthetic biology, genomics, metabolomics, and bioinformatics have led to a resurgence in NP discovery. After the publication of the first actinomycete genome sequence, *Streptomyces coelicolor* A3,[18] and the development of next generation sequencing (NGS) technologies there was a rapid expansion of available genomic data. This allowed assignment of previously orphan metabolites to biosynthetic gene clusters (BGCs) and highlighted the genetic potential of the strains to produce novel NPs. It was found that the genomes of

actinomycetes contained many putative BGCs encoding chemically diverse metabolites that were not expressed under laboratory conditions, so-called “cryptic BGCs”.[2] In fact, it is estimated that less than 10% of BGCs are expressed in sufficient quantities to be detected in routine fermentations; many require specialist conditions.[1] Specific triggers or environmental stimuli that are required to activate BGCs are lacking *in vitro*; biosynthetic genes are downregulated and so production yields of their resultant compounds are low. This represented a requirement for methods to sequence and genetically analyse strains to guide discovery and characterisation of NPs; a technique called “genome-mining”. The development of computational tools such as antiSMASH (antibiotics and secondary metabolite analysis shell)[19, 20] allows the semi-automated prediction of NPs from the sequences of BGCs. This means the wealth of genomic data can be analysed to connect BGCs to already known products, identify candidate BGCs encoding for potentially novel NPs and predict their structures. These methods bypass the tedious task of dereplication of already known NPs, which was a time consuming and restrictive aspect of “old-fashioned” NP isolation strategies.[1] An additional advancement was the development of strategies aiming to “switch-on” the expression of cryptic BGCs, which are generally not expressed constitutively due to the energetic cost of biosynthesis.[21] Moreover, the ability to sequence and clone biosynthetic genes opened up a whole host of new possibilities in the field of genetic engineering and combinatorial biosynthesis. These advancements have led to a reinvigoration of the field of NP discovery. It is now important that we fully understand the biosynthesis and bioactivity of these NPs before their application.

1.2 Natural product biosynthesis

The biosynthesis of NPs in bacteria and fungi is encoded for by pathways of multiple genes which are usually co-located in areas on the chromosome called BGCs. These genes can encode modular enzyme complexes that have evolved to assemble readily available building blocks, such as amino acids or acyl-coenzyme A (CoA) units, to longer product chains. The modular enzymes in question are called non-ribosomal peptide synthetases (NRPSs) and polyketide synthases (PKSs), respectively.[22-25] Both classes have modules that minimally comprise three functional components that are required to catalyse covalent attachment and extension of building block chains in an assembly-line fashion. Each module is generally responsible for addition of a single monomer unit to specific tethered intermediates in consecutive biosynthetic steps, meaning the number of modules correlates with the number of units in the chain.[25, 26] This is known as the principle of collinearity and is a

phenomenon that allows the prediction of the resulting NP structure based solely on NRPS or PKS sequence data in genome-mining strategies.[25, 27] The generation of chemical diversity from the action of these megasynthases arises from tailoring modifications as well as the ability to incorporate noncanonical substrates such as non-proteinogenic amino acids or carboxylic acids by NRPSs, and specialised acyl-CoA monomers by PKSs. The complexity and elegance of this biosynthetic machinery highlights the astounding achievements of evolution, and the development of technologies such as NGS and genome mining demonstrates the intellectual potential of humans to solve problems by harnessing the potential of Nature.

1.2.1 Non-ribosomal peptide synthetases (NRPSs)

NRPSs use amino acid building blocks to construct a broad range of bioactive peptides with magnificent structural diversity. These modular enzymes incorporate single amino acid monomers into a growing peptide chain by transferring it along modules in the assembly-line (Figure 1.2). The minimal three domains required in elongation modules are the adenylation (A), peptidyl carrier protein (PCP) and condensation (C) domains. The A domain is responsible for recognition and activation of a specific amino acid substrate which is then tethered to the adjacent PCP domain via a thioester bond. Finally, the C domain catalyses peptide bond formation between the new PCP-bound amino acid and the peptidyl intermediate bound to the PCP on the preceding module. The NRPS is completed by initial loading and final termination modules comprising of A and PCP domains only, or an additional thioesterase (TE) domain which catalyses release, and often cyclisation of the final peptide product, respectively.[24, 28]

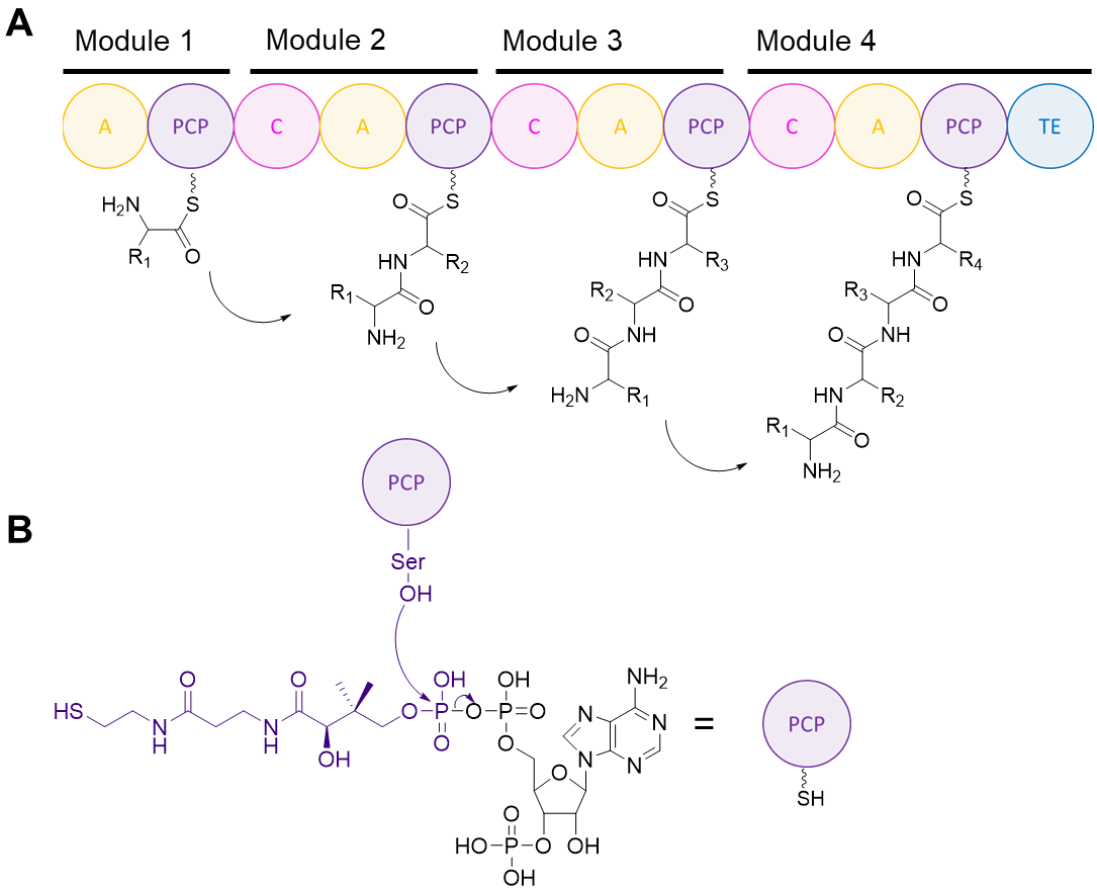

Figure 1.2: Illustration of non-ribosomal peptide synthetase (NRPS) biosynthetic logic. A) Chain elongation on a hypothetical, general NRPS showing the modular architecture. A specific substrate is activated onto the PCP domain where b) the C domain catalyses peptide bond formation and extension of the chain until the termination module where the TE domain catalyses release and cyclisation of the product. C = condensation, A = adenylation, PCP = peptidyl carrier protein and TE = thioesterase domains. B) The formation of the phosphopantetheinyl arm, represented by PCP~SH.

1.3 Iron and antibiotics

1.3.1 Iron is an essential nutrient for life

Iron is an essential nutrient for nearly all living organisms and plays a part in many enzymatic and metabolic processes. It is the fourth most plentiful element in the Earth's crust which meant it was an ideal choice for incorporation into proteins during the evolution of early life.[29] The biological utility of iron is due to its ability to cycle between two oxidation states; ferrous Fe(II), or ferric Fe(III). This means it can serve as a redox catalyst, thus playing a key role in many redox-sensing proteins. It is also a cofactor for a diverse range of biological processes including in Fe-S clusters and

haem groups and is essential for a plethora of vital systems including DNA replication, respiration, and oxygen transport.[30, 31] However, maintaining strict iron homeostasis is critical. Upon iron overload, the redox potential of iron generates cellular toxicity and oxidative stress. It can catalyse the formation of reactive oxygen species (ROSs) via the Fenton reaction (Eq. 1) which, in turn generates powerful hydroxyl radicals ($OH^{\cdot}$) that damage lipids, DNA and protein.

$$Fe^{2+} + H_2O_2 = Fe^{3+} + OH^{\cdot} + OH^{-} \ (Eq. 1)$$

After oxygenic photosynthesis started to pollute the atmosphere with molecular oxygen 2.2 to 2.7 million years ago, the predominant form of iron in the environment became the highly insoluble ferric form, Fe(III).[29] Thus, the availability of iron became a growth limiting factor within many ecological niches. Competition for iron became commonplace including in infectious processes; the pathogen utilises mechanisms for iron capture, whereas the invaded host tries to restrict pathogen access to iron, thereby limiting pathogen multiplication.[30]

1.3.2 Iron acquisition in bacteria: siderophore complexes

As iron exists in its insoluble form in the natural environment, microorganisms have developed strategies to overcome the restricted access to iron. These include the evolution of siderophores, low molecular weight compounds which form high affinity complexes with Fe(III) with great selectivity.[32, 33] These complexes are then taken up by the organism via their cognate membrane receptors, enabling the organism to scavenge iron from the environment by active transport (Figure 1.4).[33] Most siderophores are biosynthesised by NRPS enzymes[32, 34] and therefore often have a peptidic backbone structure which is modified by the attachment of iron-coordinating ligands.

Siderophore biosynthesis is typically regulated by the levels of iron in which the organism is located. It is induced by intracellular iron deficiency in a process mediated by the universal repressor Fur (*F*erric iron *u*ptake *r*egulator).[35] Under iron-rich conditions, promoters which contain a Fur box (Fur binding sequence) are bound by Fe(II)-Fur complexes which repress transcription.[35, 36] Conversely, in iron-depleted environments, repression is relieved and the target genes can be transcribed enabling siderophore biosynthesis and participation in iron homeostatic systems.[31] Siderophores are categorised into four main classes by their iron-binding moiety; hydroxamate, phenolate, carboxylate or catecholate groups.[32, 37] Examples of each of these classes are shown in Figure 1.3, with their iron-binding groups highlighted.

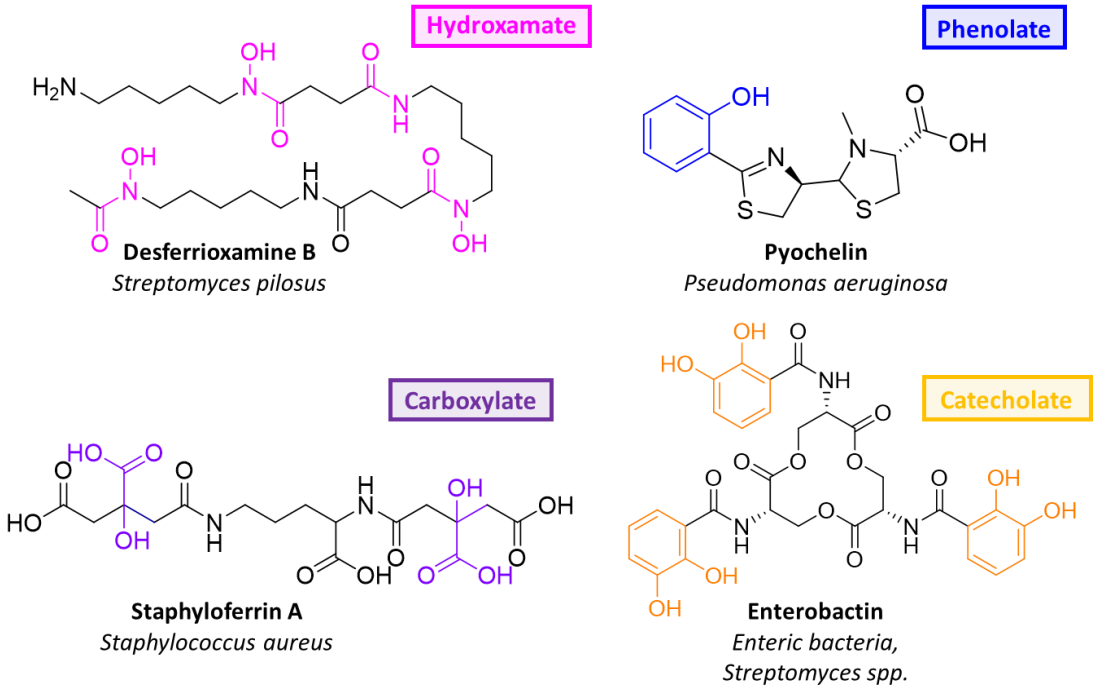

Figure 1.3: The four main types of siderophores. They are distinguished by their iron chelating moieties as highlighted; hydroxamate (pink), phenolate (blue), carboxylate (purple) and catecholate (orange). Representative examples of each class are shown with their producing bacterial species.

Siderophores selectively form high affinity complexes with Fe(III) over Fe(II) and other biologically relevant dipositive cations which are present at higher concentrations within the cell such as Zn(II), Cu(II) and Mn(II).[38] To give the greatest thermodynamic stability and therefore high affinity complexes, Fe(III) has various preferences due to the small, highly charged nature of the metal ion.[32] Hexadentate geometry to give an octahedral field is preferred, therefore higher denticity ligands and those constituted of negatively charged oxygen donor atoms form higher affinity complexes with Fe(III). To increase affinity, bidentate ligands can arrange themselves to bind to Fe(III) in a hexadentate fashion, for example in ferric enterobactin, the strongest known siderophore complex with an affinity of $K_a = 10^{52}$.[39] Enterobactin has three catecholate groups (Figure 1.3), that are deprotonated at neutral pH to give six oxyanion donors that are preorganised to bind to Fe(III) by the trilactone backbone making complex formation highly favourable.[40]

Once bound to Fe(III), the complex must be taken up into the bacterial cell. This process differs between Gram-positive and Gram-negative bacteria due to the latter's outer-membrane which provides a selective permeability barrier to higher MW molecules.[41] The iron-uptake system in Gram-positives is not as well studied as that

of Gram-negatives, but it is known that they have lipoprotein receptors and ABC transporters that are involved in iron acquisition.[32] In Gram-negatives, mechanisms to import these complexes have evolved which use a family of specific outer-membrane TonB-dependent transporters (TBDTs). These receptors selectively bind the Fe(III)-siderophore complex and translocate it into the periplasm of the cell using energy derived from the energy-transducing protein TonB.[33] For example, FepA, one of the six TBDTs of *E. coli*, has been structurally characterised and shown to be responsible for the uptake of the ferric-enterobactin complex.[42]

1.3.3 Trojan-horse antibiotics (THAs)

Bacteria have evolved an elegant mechanism to exploit these iron acquisition pathways by the evolution of "Trojan-horse" antibiotics (THAs) with structures that consist of a siderophore moiety conjugated to a toxic chemical warfare agent. These compounds bind to iron and are actively transported into the cells of competing bacteria; effectively hijacking the siderophore uptake machinery to deliver an antibiotic across the membrane (Figure 1.4).[31, 43]

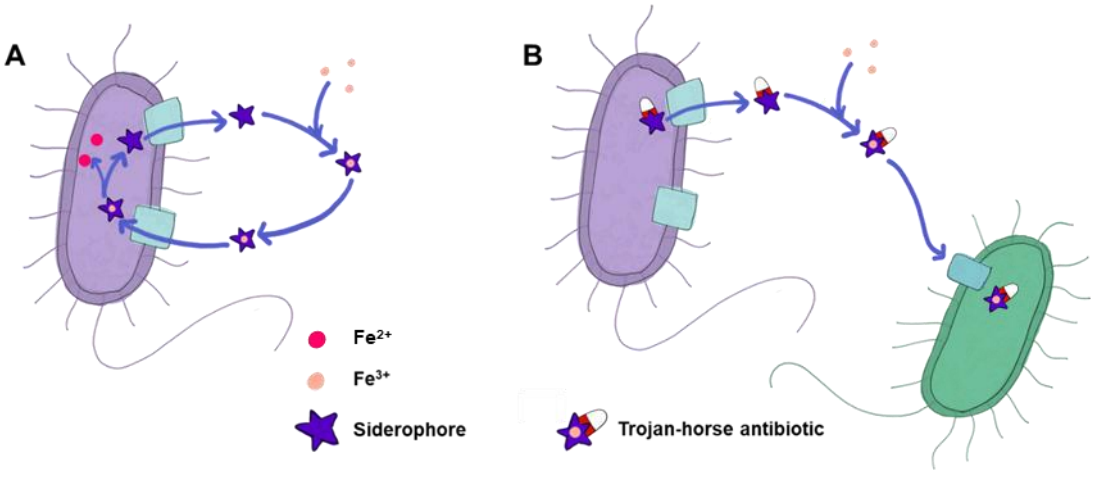

Figure 1.4: Schematic diagram to show mechanisms of bacterial iron acquisition. A) Bacterial iron uptake from the environment using siderophores; the apo-siderophore complex is excreted from the cell, binds to environmental Fe(III) and the siderophore-Fe(III) complex is recognised and actively transported inside the cell by TonB-dependent transporters (TBDTs) where upon entry, Fe(III) is enzymatically reduced to Fe(II) and released. B) Mechanism of trojan-horse antibiotics (THAs); bacteria biosynthesise and excrete the THA, which binds to Fe(III) and hijacks the iron uptake machinery of competing bacteria, where upon entry into the cell, the antibiotic has access to its target.

There are several examples of these compounds produced in nature including albomycin which is a potent seryl-tRNA synthetase inhibitor produced by *Streptomyces* spp.[44] This naturally occurring strategy has inspired the development of a class of semi-synthetic antibiotics where a siderophore is covalently linked to an antimicrobial compound. An example of these is cefiderocol, a clinically-used catechol siderophore-cephalosporin conjugate for the treatment of multi-drug resistant Gram-negative infections.[45] Several structural features, highlighted in Figure 1.5, give cefiderocol its potent antimicrobial activity: the covalent linker at position-3 is used to attach the catechol group for utilisation of the THA mechanism, the side-chain at carbon-7 confers stability against β-lactamase hydrolysis and the zwitterionic properties give enhanced water solubility.[46, 47]

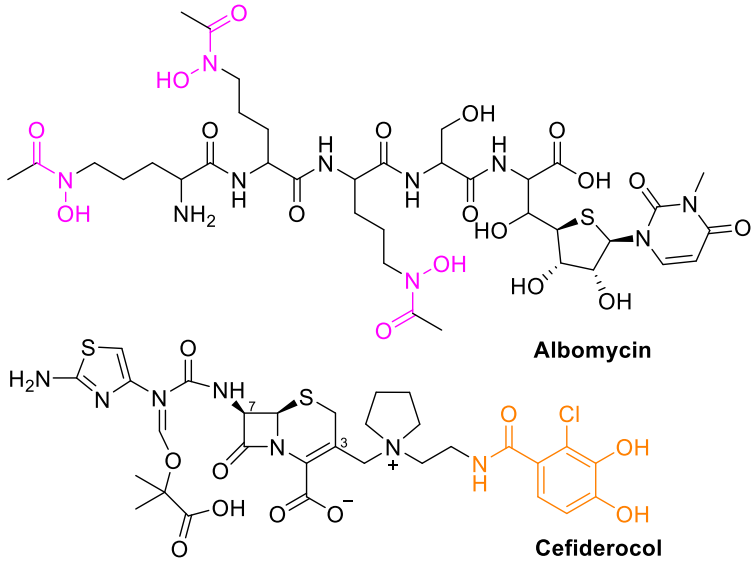

Figure 1.5: The chemical structure of the Trojan-horse antibiotic, cefiderocol. The iron-binding group is highlighted in orange.

Both naturally occurring and synthetic THAs mimic TBDT substrates meaning that they are actively transported into the bacterial cell via the TBDTs. This means this mechanism can be utilised for administering antimicrobials to Gram-negative pathogens such as *Pseudomonas aeruginosa* and *Acinetobacter baumannii*, as it can circumvent problems arising from the outer-membrane permeability barrier, an important resistance factor. Therefore, THAs have significant potential as new antibiotics in this era of increasing AMR.

1.4 β-lactone containing natural products

β-lactone rings can be found in a variety of NPs, biosynthesised by PKSs, NRPSs, hybrid PKS-NRPSs and other types of pathways, meaning their scaffolds possess

great chemical diversity. The highly reactive nature of β-lactones arises due to their strained 4-membered heterocycle, and means they readily undergo acid or base hydrolysis and are susceptible to thermal degradation.[48] Nevertheless, β-lactones are present in a variety of NPs with impressive biological activities.

The first β-lactone natural product, anisatin, a potent neurotoxin was discovered in the 50s and isolated from the fruit of a Japanese spice tree.[49] After this, it was not until after the "Golden-Age" of antibiotic discovery that the majority of β-lactone NPs were discovered. This is likely due to the instability of β-lactone rings in chemical workup procedures due to acid/base catalysed hydrolysis or reaction with nucleophiles following extraction from their producing organisms. The genome mining era has given access to 'orphan' β-lactones and enabled discovery of novel β-lactone containing NPs. There are now many members of the β-lactone class of NPs with highly diverse chemical structures (Figure 1.6). Clinically used examples include tetrahydrolipstatin, a β-lactone NP derivative commercially known as Orlistat, is used in the treatment of obesity[50]and salinosporamide A has potent anticancer activity.[51]

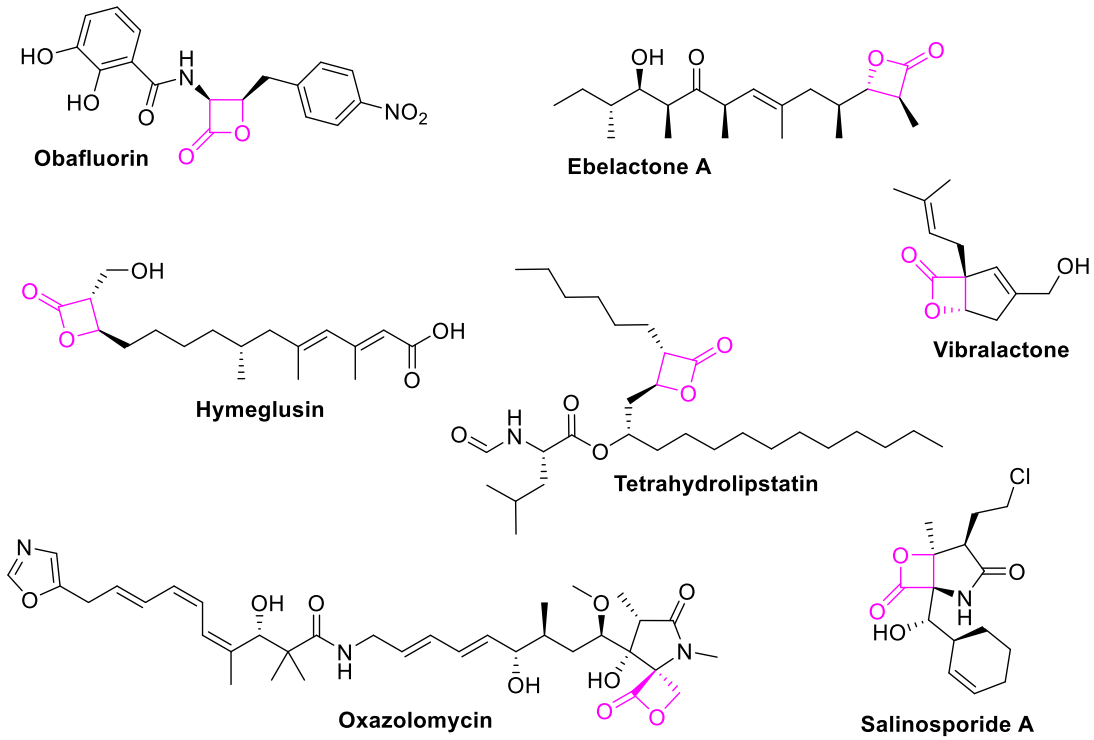

Figure 1.6: Examples of β-lactone containing NPs. The β-lactone motif is highlighted in pink.

The mechanism of action of β-lactone NPs, as with the structurally similar β-lactams, generally involves the acylation of a catalytic nucleophilic amino acid in their enzyme target resulting in covalent modification and inhibition.[52] The serine, cysteine or

threonine nucleophile will attack the electrophilic centre and open the strained 4-membered ring resulting in the formation of a covalent enzyme-lactone adduct as shown in Figure 1.7.[53]

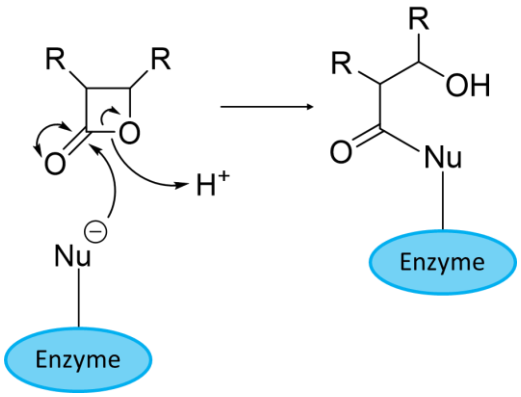

Figure 1.7: A schematic representation of the mechanism of covalent attachment of β-lactone NPs to their target enzyme. A nucleophilic residue attacks the carbonyl of the lactone opening the 4-membered ring.

1.5 Obafluorin, a β-lactone antibiotic from Pseudomonas fluorescens

Obafluorin, **1**, is a broad-spectrum antibiotic that was discovered by Sykes *et al.*[54] during the purification of the bioactive component of *Pseudomonas fluorescens* ATCC 39502 bacterial fermentations. They were using β-lactamase induction assays for the discovery of a variety of β-lactam containing NPs from bacterial fermentations. During these assays they also recorded several false positive results due to the presence of β-lactones which had little to no antibacterial activity, however, in this case the NP showed highly promising biological activity The structure of **1** was elucidated and proved to be an elaborate β-lactone decorated with a catechol and nitrophenyl group as shown in Figure 1.8.[55]

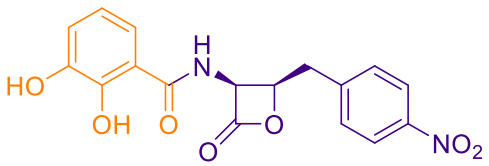

Figure 1.8: The structure of obafluorin, 1. A β-lactone natural product produced by *P. fluorescens* ATCC 39502. The regions of the molecule derived from DHBA and **2** (see section 1.4.1) are shown in orange and purple, respectively.

1.5.1 1 biosynthesis in *P. fluorescens*

After early work on the biosynthesis of **1** in the 1980s,[55-58] the study of the antibiotic slowed until improvements in sequencing technologies and genome mining allowed the identification of BGC for **1** production in *P. fluorescens* ATCC 39502. It was delineated by Dr. Thomas Scott *et al.* in our lab[59] and by others[60] using mutational analysis and *in vitro* reconstitution. **1** is assembled by ObaI, a bimodular NRPS which catalyses the linkage of 2,3-dihydroxybenzoic acid (DHBA) and the nonproteinogenic amino acid (2S,3R)-2- amino-3-hydroxy-4-(4-nitrophenyl)butanoate, **2**, via peptide bond formation. [59, 61] These two building blocks (Figure 1.8) are biosynthesised from chorismate by the proteins of two disparate pathways encoded for within the *oba* BGC as shown in Figure 1.9.

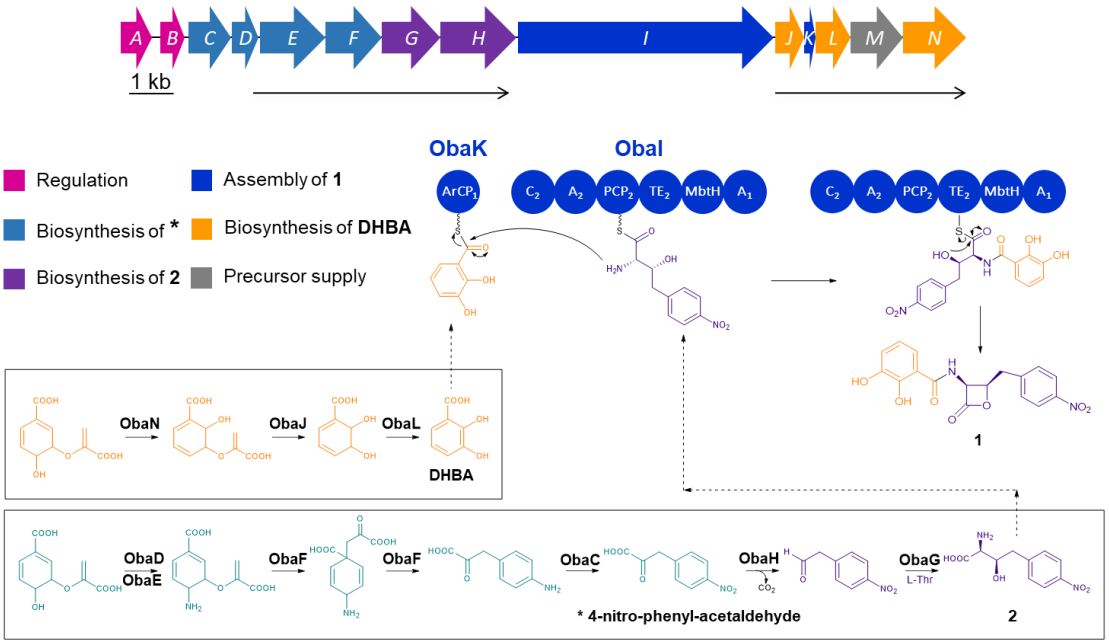

Figure 1.9: Biosynthesis of 1 in *P. fluorescens* ATCC 39502. The BGC of **1** production is shown at the top of the figure with gene function categorised by colour shown in the key. DHBA is biosynthesised from chorismate by the action of ObaN,J and L. **2** is biosynthesised from chorismate by ObaC-H; this includes ObaG, a rare L-threonine transaldolase (L-TTA) enzyme which converts 4-nitrophenylacetaldehyde to **2**. The arrow indicates the breakdown products of 4-nitrophenylacetaldehyde. The domain architectures of the NRPS, ObaI is shown and the anticipated mechanism of TE-catalysed peptide release and β-lactone ring closure.[59] Figure adapted from the thesis of Dr. Thomas Scott.

Table 1.1: Proteins comprising the 1 biosynthetic gene cluster (BGC). The cluster was subjected to mutational analysis by Dr Thomas Scott to confirm protein

function. Those proteins whose function remain proposed are marked with an asterisk.

Protein:	**Function:**
ObaA	Transcriptional regulator*
ObaB	*N*-acylhomoserine lactone synthase*
ObaC	*N*-oxygenase
ObaD	4-amino-4-deoxychorismate synthase component II
ObaE	4-amino-4-deoxychorismate synthase component I
ObaF	Bifunctional 4-aminochorismate mutase/4-aminoprephenate dehydrogenase
ObaG	L-threonine transaldolase
ObaH	4-nitrophenylpyruvate decarboxylase
ObaI	Dimodular nonribosomal peptide synthase
ObaJ	Isochorismatase
ObaK	Aryl carrier protein
ObaL	2,3-dihydro-2,3-dihydroxybenzoate dehydrogenase
ObaM	DAHP synthase*
ObaN	Isochorismate synthase

The ObaI NRPS contains a rare type I TE domain which catalyses the formation of the β-lactone from **2**. Importantly, the functional groups present in **2** are essential for β-lactone formation and its stereochemistry gives rise to the lactone's unusual *cis* stereochemistry.[62] **2** is a β-hydroxy-α-amino acid (β-OH-α-AA) and is biosynthesised from 4-nitrophenylacetaldehyde and L-threonine by ObaG, an L-TTA. L-TTAs are a rare family of fold-type I PLP-dependent enzymes that cleave L-threonine to yield glycine covalently attached to the cofactor, and subsequently catalyses C-C bond formation between this unit and an aldehyde substrate to give a β-OH-α-AA product. β-OH-α-AAs are important chiral building blocks in the biosynthesis of many pharmaceutically valuable NPs and their enzymatic production is sought after as it can set the two stereocentres in a single reaction under mild aqueous conditions.[59] The threonine aldolases, are a family of enzymes which can perform this reaction but low synthetic yields and poor diastereoselectivity hinders their use as industrial catalysts. L-TTAs, and therefore ObaG represents are an alternative enzyme with the potential to produce β-OH-α-AAs for asymmetric synthesis.

1.5.2 1 targets the threonyl-tRNA synthetase enzyme

After characterisation of the biosynthesis of **1**, attention turned to its bioactivity. Early studies showed that **1** is a broad-spectrum antibiotic and protects mice infected with clinical isolate of *Streptococcus pyogenes*, and it causes cell elongation in *Escherichia coli* grown at sub-lethal doses, all indications that **1** exhibits specific activity rather than acting as a general acylating agent.[55, 59] Indeed, the molecular target of **1** was identified as the essential enzyme, threonyl-tRNA synthetase (ThrRS), through an immunity guided approach by members of our lab.[61] A homologue of the house-keeping ThrRS, ObaO, is present in the native producer which gives the producer resistance to **1** and therefore enables its biosynthesis. *obaO* resides in the genomic neighbourhood of the **1** BGC and was identified by comparison of homologous BGCs; all had an *obaO* homologue which encoded for a putative ThrRS. Inactivation of o*baO* in *P. fluorescens* ATCC 39502 could only be performed in a Δ*obaL* background. *obaL* is an essential gene in the biosynthesis of DHBA, one of the building blocks of **1** biosynthesis and can be knocked out in *P. fluorescens* ATCC 39502 to give a strain termed Δ*obaL*. This strain is impaired in **1** biosynthesis meaning there is no selection pressure to lose a potential resistance determinant. The Δ*obaL*Δ*obaO* strain was generated and while this strain grows in the absence of exogenous DHBA, addition of DHBA to the growth medium abolished growth, as shown in Figure 1.10. This confirmed the function of o*baO* as an immunity gene.[61] Here, note that **1**-producing cultures exhibit a purple colouration.

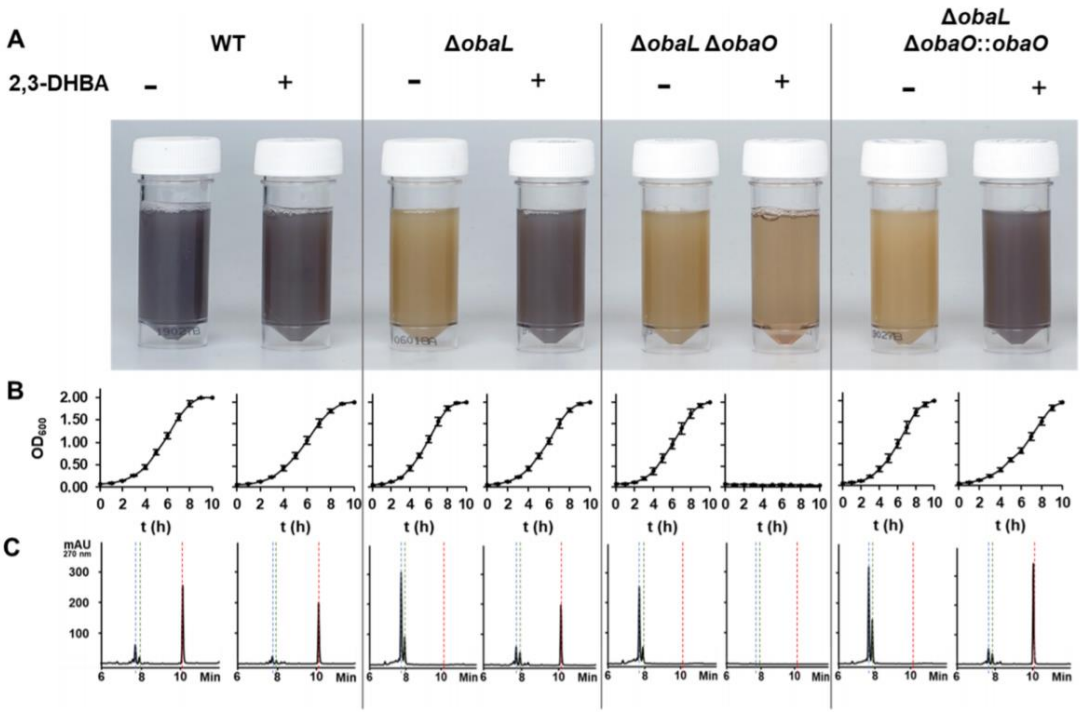

Figure 1.10: ObaO is the immunity determinant for 1 in the native producer, *P. fluorescens* ATCC 39502. Wild-type (WT), Δ*obaL*, Δ*obaL*Δ*obaO*, and Δ*obaL*Δ*obaO*::*obaO* strains were grown with and without DHBA. **1** production is restored by addition of DHBA to the Δ*obaL* strain, whereas for Δ*obaL*Δ*obaO*, growth is abolished. A) Samples of each strain after 14-hour growth; purple colour is an indication of **1** production. B) Growth curves showing no growth for Δ*obaL*Δ*obaO* strain fed with DHBA. C) HPLC chromatograms at 270 nm showing **1** production with a red dashed line, R_t = 10.1 min and the blue and green dashed lines representing shunt metabolites of the pathway.[61]

An *in vitro* assay measuring the formation of Thr-tRNA^{Thr} was performed to monitor the inhibition of a sensitive ThrRS from *Escherichia coli* (EcThrRS) compared to ObaO by 0-5 μM **1**, as shown in Figure 1.11. It was found **1** is a potent inhibitor of EcThrRS, with an IC_{50} of 92 ± 21 nM, whereas, unexpectedly for a resistance determinant, ObaO was partially inhibited by **1**. As **1** concentration increased the aminoacylation activity of ObaO decreased but, even at the highest concentrations of **1**, a fractional residual activity of 35% was retained.[61] This shows that ObaO is exhibiting an unusual partial inhibition mechanism of immunity which is interesting to note when considering the mode of action of **1**.

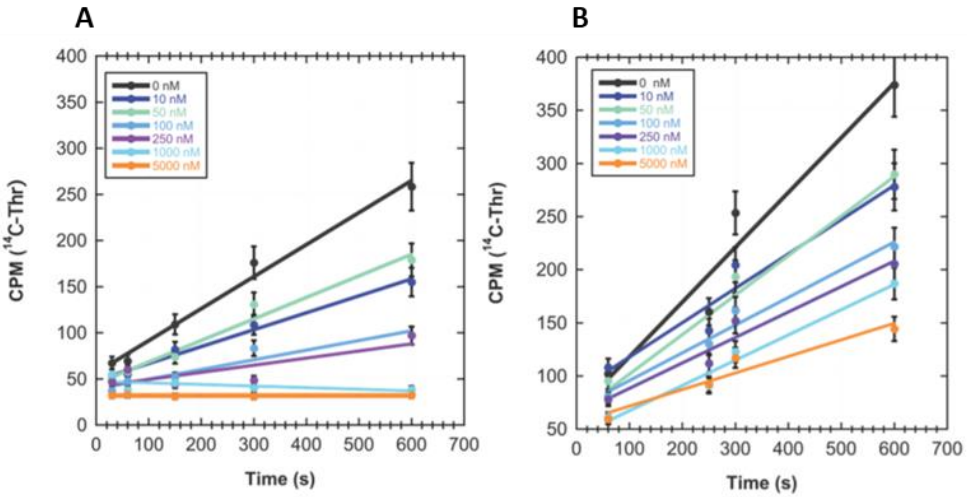

Figure 1.11: Complete and partial inhibition of EcThrRS and ObaO by 1, respectively. Progress curves of aminoacylation assays for A) EcThrRS and B) ObaO with increasing concentrations of **1** (0-5 μM).[61]

As described, this immunity-guided approach was successful in the identification of the molecular target of **1** as the ThrRS enzyme; an aminoacyl-tRNA synthetase (aaRS).[61] aaRSs are essential enzymes responsible for the ligation of an amino acid to its cognate tRNA to form an aminoacyl-tRNA during protein synthesis. This two-step aminoacylation reaction involves the condensation of an amino acid with ATP to give an aminoacyl-AMP intermediate, then the transfer of the amino acyl group to the 3' end of the tRNA. The resulting aminoacyl-tRNA then enters the ribosome for mRNA translation, therefore this process is essential in protein synthesis.[63, 64] aaRSs have three distinct binding pockets for each substrate, the amino acid, ATP and tRNA and are therefore structurally complex enzymes.

The divergence of aaRSs has led to the evolution of NP antibiotics which can be used as selective anti-infective agents, for example, mupirocin is an isoleucyl-tRNA synthetase (IleRS) inhibitor which is used topically to treat skin infections.[65] Several features of these enzymes mean they are well suited as drug targets: 1) the divergence between prokaryotic and eukaryotic aaRSs gives selectivity; 2) the high conservation of aaRS structure within kingdoms means an inhibitor is likely to be active across bacterial species; and, 3) there are twenty distinct aaRSs, one for each proteinogenic amino acid substrate, and each represents an independent drug target.[66] Therefore, research to improve mechanistic understanding of the inhibition of these enzymes is valuable.

1.5.3 Project outlook

After the characterisation of the biosynthesis of **1**, the focus of investigations by the Wilkinson Group shifted to the bioactivity of the antibiotic. With knowledge of the mechanism of action of characterised β-lactone NPs,[52, 67] we formed a hypothesis about the mechanism of action of **1**. We propose that **1** binds to its target enzyme, ThrRS, via the attack of a specific nucleophilic residue onto the carbonyl of the β-lactone ring, generating a covalently modified ThrRS (Figure 1.12). We therefore aimed to characterise the mechanism of **1** on a ThrRS from the **1**-sensitive *E. coli*, EcThrRS, and investigate differences between that and the immunity copy, ObaO. The partial inhibition mechanism of ObaO by **1** suggests that it may bind at a site close to, but not overlapping with, the active site meaning that the ability of the enzyme to execute conformational changes is hindered.[61] We aimed to apply conventional methods to study antibiotic mode of action including those previously used to characterise that of other β-lactone NPs. This would allow us to investigate the validity of our hypothesis for how **1** works, with a goal to identify the specific nucleophilic amino acid of ThrRS that we propose as a covalent attachment point for **1**.

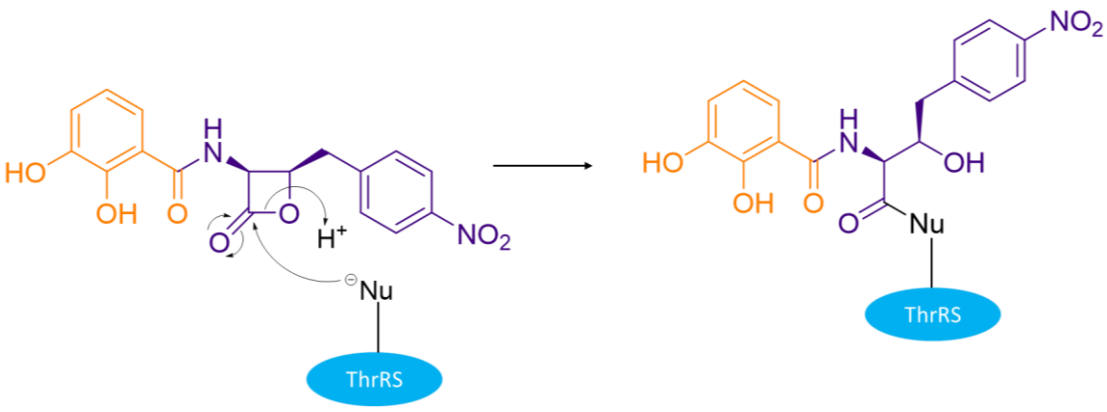

Figure 1.12: The proposed mechanism of covalent attachment of 1 to ThrRS. Based on the mechanism of action of other β-lactone containing NPs, we propose a specific nucleophilic residue of the target enzyme, ThrRS attacks the electrophilic carbon of the β-lactone and the 4-membered ring opens to leave the **1** covalently attached.

It is also important to consider the role of other chemical components in the structure of **1** when investigating its mechanism of action. After the β-lactone, another important structural feature of **1** is the catechol ring. The precedence of these moieties in siderophore compounds and THAs suggested to us that **1** could utilise mechanisms involved in iron acquisition as part of the antibiotic mechanism of action. Therefore,

my project aims to understand the role of the catechol and its effect on the biological properties of **1** by application of chemical and biochemical methods. Specific objectives are to purify analogues of **1** which have a disrupted catechol and use these to investigate the role of this chemical motif in the bioactivity and metal binding properties of **1**.

To summarise, my project aims to unpick the mechanism of action of **1** by investigating: 1) the role of the catechol in the bioactivity of **1**; 2) the metal binding ability of the catechol and its influence on the bioactivity of **1**; 3) the interaction between **1** and ThrRS. These studies are important to gain a deeper understanding of the antibiotic activity of **1** and how it inhibits ThrRS. They will give insight into the mechanism of action of β-lactone antibiotics and routes to the inhibition, and in turn potential resistance, of aaRS enzymes.

Chapter 2:

Materials and Methods

Chapter 2 : Materials and Methods

2. 1 General materials

Chemicals and reagents were purchased from Alfa-Aesar and Merck Life Sciences (previously Sigma Aldrich) and were used without further purification. All solvents used for HPLC were obtained from Fisher Scientific.

2.2 Bacterial strains, plasmids and oligonucleotides

2.2.1 Bacterial strains

Bacterial strains used in this study are listed in Table 2.1

All strains were maintained on solid LB medium (with appropriate selection) at 37°C (*E. coli*) or 28 °C (*P. fluorescens*).

Table 2.1: Strains used in this work.

Strain	Description	Reference
B. subtilis EC 1524	Bioassay strain; *trpC2*, Subtilin BGC deleted	O'Rourke *et al*., 2017[68]
E. coli ATCC 25922	Bioassay strain; WT	ATCC, USA
E. coli BW25113	Bioassay strain; WT	Grinter *et al*., 2019[41]
E. coli BW25113 Δ3	Bioassay strain; TonB dependent transporters, FhuA, FecA, CirA, deleted	"
E. coli BW25113 Δ6	Bioassay strain; TonB dependent transporters, FhuA, FecA, CirA, FepA, FhuE and Fiu are deleted	"
E. coli DH5α	Host for general cloning; F- endA1 glnV44 thi-1 recA1 relA1 gyrA96 deoR nupG ϕ80dlacΔ(lacZ)M15 Δ(lacIZYA-argF)U169 hsdR17(rK- mK+) λ–	Hanahan, 1983[69]
E. coli NiCo21(DE3):pLysS	Expression strain; *can::CBD*, *fhuA2*, *[lon] ompT*, *gal* (λ DE3) *[dcm] arnA::CBD*, *slyD::CBD*, *glmS6Ala*, Δ*hsdS* λ DE3 = λ *sBamHIo* Δ*EcoRI-B int::(lacI::PlacUV5::T7 gene1) i21*, Δ*nin5*. PLysS subsequently introduced	New England Biolabs

E. coli NiCo21(DE3):pLysS:pET28a(+)-*EcThrRS*	NiCo21(DE3):pLysS carrying a WT copy of the *E. coli thrRS* gene as an *Nde*I-*Xho*I fragment for production of the ThrRS protein with an N-terminal hexahistidine tag in pET28a(+)	Thesis of Dr. Thomas A. Scott
E. coli NiCo21(DE3):pLysS: pET29a(+)-*ΔN-EcThrRS*	NiCo21(DE3):pLysS carrying a WT copy of the *E. coli thrRS* gene as an *Nde*I-*Xho*I fragment for production of the ThrRS protein with a C-terminal hexahistidine tag in pET29a(+)	Thesis of Dr. Thomas A. Scott
E. coli NR698	Bioassay strain; MC4100 (F^- *araD139* Δ(*argF-lac*)*U169*, *rpsL150*, *relA1*, *flbB5301*, *deoC1*, *ptsF25*, *rbsR*), *imp4213*	Ruiz *et al*., 2005[70]
E. coli S17-1 λ(pir)	Conjugation strain; *recA*, *thi*, *pro*, *hsd*(R^- M^+)RP4: 2- Tc::Mu-Km::Tn7 λpir SM^R Tp^R	Simon *et al*., 1983[71]
P. fluorescens ATCC 39502	Obafluorin-producing strain, WT	ATCC, USA
P. fluorescens Δ*obaL*	ATCC 39502 with an in-frame truncation in the *obaL* and *obaO* genes	Scott *et al*., 2017[59]
P. fluorescens Δ*obaL*Δ*obaO*	ATCC 39502 with an in-frame truncation in the *obaL* gene	Scott and Batey *et al*., 2019[61]
P. fluorescens Δ*obaLobaO*:pJH10TS-EcThrRS *K200A*	Δ*obaLobaO* strain carrying a copy of the EcThrRS gene with a K200A mutation cloned into pJH10TS for complementation by expression *in trans*	This work
P. fluorescens Δ*obaLobaO*:pJH10TS-EcThrRS *K314A*	Δ*obaLobaO* strain carrying a copy of the EcThrRS gene with a K314A mutation cloned into pJH10TS for complementation by expression *in trans*	This work
P. fluorescens Δ*obaLobaO*:pJH10TS-EcThrRS *K419A*	Δ*obaLobaO* strain carrying a copy of the EcThrRS gene with a K419A mutation cloned into pJH10TS for complementation by expression *in trans*	This work
S. cerevisiae Meyen ex E.C. Hansen, MTA-3666	VL6-48; aerobic; 25-30 °C; biosafety level 1; ATCC medium #1069, #1245, #200; Genotype: MATa, his3-	ATCC, USA

	delta200, trpl-delta1, ura3-52, ade2-101, lys2, psi+cirÂ°	
S. aureus subsp. aureus Rosenbach 6538P	Bioassay strain; WT	ATCC, USA
Staphylococcus aureus subsp. aureus Rosenbach BAA-1717 (Methicillin-resistant)	Bioassay strain; methicillin-resistant, *pvl* positive	ATCC, USA

2.2.2 Plasmids

Plasmids used in this work are listed in Table 2.2

Table 2.2: Plasmids used in this work.

Plasmid	Genotype/description	Reference
pET28a(+)	Expression vector; $Kan^{R,}$ the transcription of the cloned gene is driven by the T7 RNA polymerase and controlled by the LacI repressor, *ColE1* replicon	Novagen
pET29a(+)	Expression vector; $Kan^{R,}$ the transcription of the cloned gene is driven by the T7 RNA polymerase and controlled by the LacI repressor, *ColE1* replicon	Novagen
pJH10TS	Vector for complementation studies by *in trans* expression in *P. fluorescens* ATCC 39502 Δ strains; pOLE1 with *IncC1* deleted, *Eco*RI-*Sac*I polycloning site, Tc^R from pDM1.2, modified with an expanded cloning site	Scott *et al*., 2017[59]
pLysS	Vector for basal expression from the T7 promoter by producing T7 lysozyme; p15A replicon, Cm^R	Novagen

2.2.3 Primers

Primers used in this study are listed in Table 2.3

Table 2.3: Primers used in this study.

Primer	Sequence 5'-3'	Function
K200A Fw	GTAAGCCCCTGCCGTTGCCATTAGTTTGAAATG ATGGCAGAAAC	Primers for QuikChange™ mutagenesis of EcThrRS in pJH10TS
K200A Rv	GTTTCTGCCATCATTTCAAACTAATGGCAACGG CAGGGGCTTAC	
K314A Fw	TGTGGTGAACATTGCATCTGCGTAGTTGTCCCA GTGACCG	
K314A Rv	CGGTCACTGGGACAACTACGCAGATGCAATGTT CACCACA	

K419A Fw	CAGGACGAGTGGAGAGTGCGACGACGATCTTC TCGA	
K419A Rv	TCGAGAAGATCGTCGTCGCACTCTCCACTCGTC CTG	

2.3 Media, buffers and solutions

2.3.1 Culture media

Luria Bertani (LB)

Difco™ Bacto tryptone	10 g/L
Difco™ yeast extract	10 g/L
NaCl	5 g/L
Glucose	1 g/L

Terrific broth (TB)

Difco™ Bacto tryptone	12 g/L
Difco™ yeast extract	24 g/L
Glycerol	4 mL/L

Obafluorin production medium (OPM)

Difco™ yeast extract	5 g/L
D-Glucose	5 g/L
$FeSO_4$	0.1 g/L
$MgSO_4$	0.1 g/L

Obafluorin production medium without added iron (OPM-Fe)

Difco™ yeast extract	5 g/L
D-Glucose	5 g/L
$MgSO_4$	0.1 g/L

SOC medium

Tryptone	20 g/L
Yeast extract	5 g/L
NaCl	0.58 g/L
KCl	0.19 g/L
$MgCl_2$	2 g/L
$MgSO_4$	2.5 g/L

Soft Nutrient Agar (SNA)

Difco™ Nutrient Broth	8 g/L
Agar	7 g/L

2.3.2 Buffers and solutions

4-(2-pyridylazo)-resorcinol (PAR) solution

PAR	7.1 mg/L	30 µM
PBS (pH 7.0)		

Chrome azurol S (CAS) assay solution

Prepared as described by Alexander and Zuberer.[72] 21.9 mg hexadecatrimethylammonium (HDTMA) (601 µM final conc.) was dissolved in 25 mL ddH_2O while stirring constantly over low heat. 1.5 mL of 1 mM $FeCl_3 \cdot 6H_2O$ (15µM final conc., dissolved in 10 mM HCl) was mixed with 7.5 mL of 2 mM CAS (150 µM final conc.). The resulting solution was gradually added to the HDTMA with stirring. 9.76 g MES (500 mM final conc.) was dissolved in 50 mL ddH_2O pH 5.6 (adjusted with 50% KOH) and applied to the dye solution. ddH_2O was added to a final volume of 100 mL.

***E. coli* threonyl-tRNA synthetase (EcThrRS) purification buffer**

HEPES/HCl (pH 7.8)	6 g/L	25 mM
NaCl	17.5 g/L	300 mM
$MgCl_2$	952 mg/L	10 mM
Imidazole*	17 g/L	250 mM

Running buffer for SDS-PAGE

Tris/HCl (pH 8.0)	3 g/L	25 mM
Glycine	14.4 g/L	192 mM
SDS (25%)	1 g/L	0.1% (w/v)

Tris-Borate-EDTA (TBE) buffer, pH 8.3

Trizma base	10.8 g/L	89 mM
Boric acid	5.5 g/L	89 mM
EDTA	930 mg/L	3 mM

Tris-EDTA (TE) buffer, pH 8

Tris/HCl (pH 8.0)	1.2 g/L	10 mM

EDTA	292 mg/L	1 mM

*Imidazole only included in elution buffer for Ni affinity chromatography.

2.4 High-pressure liquid chromatography (HPLC) instruments and methods

Flash chromatography was performed on a Biotage Isolera system using a 30 g C18 cartridge and monitoring at wavelengths of 254 and 270 nm with a flow rate of 25 mL/min. Mobile phase A = water, B = acetonitrile. The following elution gradient was used: 4.5 CV 0% B; 1 CV 0-30% B; 7.5 CV 30-80% B; 0.5 CV 80-100% B; 2 CV 100% B. (CV = column volume).

Preparative-HPLC was performed on a Dionex UltiMate 3000 HPLC system using a Phenomenex Gemini 5 µm C18 110Å 150 x 21.2 mm column and a monitoring wavelength of 276 nm with a flow rate of 20 mL/min. Mobile phase A = water, B = acetonitrile. The following elution gradient was used: 0-2 min 5% B; 2-4 min 5-45% B; 4-12 min 45-80% B; 12-14 min 80% B; 14-15 min 80-5%.

Analytical HPLC was performed on multiple instruments during this work. These included an Agilent 1100 system, Agilent 1290 system (JIC Metabolomics facility), and an Agilent 1290 system (JIC Chatt Chemistry Lab). Method details are described below. DAD signals were acquired at 210, 254, 270, 365 and 418 nm, with a bandwidth of 4 nm. For the evaporative light scattering detector (ELSD), evaporator and nebuliser temperatures were 40 °C, with a gas flow rate of 1.6 SLM and data rate of 10 Hz. The injection volume was 10 µL for all samples. Data were analysed with Agilent ChemStation software.

Agilent 1290 (JIC Chatt Chemistry Lab) system details: Agilent 1290 Infinity II LC system with a 1290-Infinity II Diode Array Detector FS and a 380-Evaporative Light Scattering Detector. Samples were analysed using a Kinetex 2.6 µm XB-C18 100 Å LC column, 100 x 4.6 mm (Phenomenex) with a flow rate of 1 mL/min. Mobile phase A = water + 0.1% (v/v) trifluoroacetic acid (TFA), B = acetonitrile. The following elution gradient was used: 0 - 1 min 10% B; 1 - 11 min 10% to 98% B; 11-13 min 98% B; 13 – 13.1 min 98 to 10% B; 13.1 – 15 min 10% B.

Agilent 1100 and Agilent 1290 (JIC Metabolomics facility) details: a Gemini 3 µm NX-C18 110 Å, 150 x 4.6 mm column (Phenomenex) with a flow rate of 1 mL/min. Mobile phase A = 0.1% (v/v) TFA (water), B = acetonitrile. The following gradient gradient

was used: 0-15 min 10-100% B; 15–16 min 100% B; 16–16.50 min 100-10% B; 16.50–23 min 10% B.

2.5 1 and analogue (3-5) extraction and purification

Obafluorin production media (OPM; 100 mL) was inoculated with a single colony of *P. fluorescens* ATCC 39502 (WT for **1** production or *ΔobaL* for analogue production) and incubated at 25 ˚C with shaking at 300 rpm. After 24 h, 8 L of OPM (12 x 500 mL in 2L flasks) were each inoculated with 5 mL from the starter culture and further incubated at 25 ˚C and 250 rpm. For analogue production cultures were fed with the appropriate volume of a 100 mM stock solution of the corresponding DHBA derivative in DMSO (to give final concentration 0.4 mM for 2-HBA, 3-HBA and BA and 0.2 mM for DHBA). After a further 14 h incubation, ethyl acetate (500 mL) was added to each flask and the cultures were shaken vigorously and then left to stand for ~ 2 h. The organic phase was then separated and the solvent removed under pressure. The resulting crude extract was dissolved in acetonitrile:water (1:1; total volume 4 mL), loaded to a Biotage C18 30 g cartridge and purified by Biotage Isolera flash chromatography. For the peak corresponding to the desired analogue, the solvent was removed under reduced pressure and the resulting material was further purified (if necessary) using the preparative HPLC system and methods described above. After removal of the solvent from combined fractions containing the target compound, residual solvent was removed under high vacuum to yield the pure product.

This process was repeated on multiple occasions, but the optimal results were achieved after a collaborative scale-up process was organised between myself, Dr. Sibyl Batey and Dr. Edward Hems. The purification process was optimised by Dr. Edward Hems and the final yields of each analogue are shown in Table 3.1

The analogues were characterised by ^{1}H, ^{13}C NMR, optical rotation and HRMS as described below.

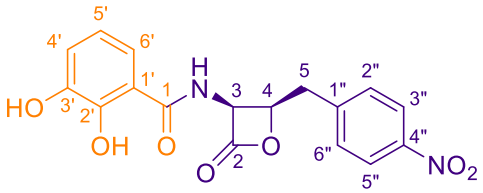

1: 1467.8 mg, 20.4 mg/L, δ_H (400 MHz, d_6-acetone) 11.95 (s, 0.6 H, O*H*), 9.06 (d, $J_{NH,H3}$ = 7.8 Hz, 0.6 H, N*H*), 8.18 (d, $J_{H2'',H3''}$ = 8.8 Hz, 2H, H3''), 7.96 (s, 0.6 H, O*H*), 7.59 (d, $J_{H2'',H3''}$ = 8.8 Hz, 2H, H2''), 7.39 (d, $J_{4',5'}$ = 8.2 Hz, 1H, H4'), 7.07 (dd, $J_{5',6'}$ = 7.9 Hz, $J_{4',6'}$ = 1.2 Hz, 1H, H6'), 6.82 (dd, $J_{4',5'}$ = 8.0, Hz, $J_{5',6'}$ = 8.0 Hz, 1H, H5'), 6.06-

6.03 (m, 1H, H3), 5.26-5.21 (m, 1H, H4), 3.55 (dd, $J_{4,5a}$ = 9.3 Hz, $J_{5a,5b}$ = 14.9 Hz, 1H, H5a), 3.42 (dd, $J_{4,5b}$ = 4.7 Hz, $J_{5a,5b}$ = 14.9 Hz, 1H, H5b); δ_C (101 MHz, d_6-acetone) 170.5 (C1), 168.5 (C2), 149.9 (C2'), 147.1 (C3'), 146.7 (C4''), 144.7 (C1''), 130.4 (C2''/6''), 123.6 (C3''/5''), 119.6 (C6'), 119.6 (C5'), 117.4 (C4'), 113.8 (C1'), 77.2 (C4), 58.9 (C3), 35.3 (C5); HRMS calc. for $C_{17}H_{15}N_2O_7$ ($[M+H]^+$) 359.0874, found 359.0872 ($[M+H]^+$), Δ = -0.56 ppm.

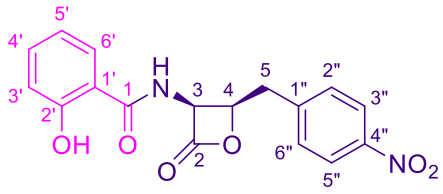

3: 326.7 mg, 13.6 mg/L, $[\alpha]_D$ +115 (*c* 1.0, EtOAc); δ_H (400 MHz, d_6-acetone) 11.80 (s, 0.8 H, O*H*), 9.11 (d, $J_{NH,H3}$ = 7.7 Hz, 0.8H, N*H*), 8.16 (d, $J_{H2'',H3''}$ = 8.8 Hz, 2H, H3''), 7.90 (dd, $J_{H5',H6'}$ = 8.0 Hz, $J_{H4',6'}$ = 1.5 Hz, 1H, H6'), 7.61 (d, $J_{H2'',H3''}$ = 8.8 Hz, 2H, H2''), 7.52-7.48 (m, 1H, H4'), 6.98-6.93 (m, 2H, H3',5'), 6.07-6.04 (m, 1H, H3), 5.26-5.21 (m, 1H, H4), 3.55 (dd, $J_{4,5a}$ = 9.4 Hz, $J_{5a,5b}$ = 15.0 Hz, 1H, H5a), 3.41 (dd, $J_{4,5b}$ = 4.7 Hz, $J_{5a,5b}$ = 15.0 Hz, 1H, H5b); δ_C (101 MHz, d_6-acetone) 170.1 (C2), 167.9 (C1), 161.3 (C2'), 147.0 (C4''), 144.9 (C1''), 134.9 (C4'), 130.3 (C2''), 127.3 (C6'), 123.5 (C3''), 119.0 (C5'), 117.9 (C3'), 113.8 (C1'), 77.4 (C4), 58.9 (C3), 35.4 (C5); HRMS calc. for $C_{17}H_{15}N_2O_6^+$ ($[M+H]^+$) 343.0925 found 343.0930 ($[M+H]^+$), Δ = 1.46 ppm.

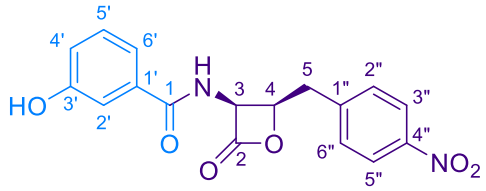

4: 181.9 mg, 7.6 mg/L, $[\alpha]_D$ +66 (*c* 0.5, EtOAc); δ_H (400 MHz, d_6-acetone) 8.69 (d, $J_{NH,H3}$ = 8.6 Hz, 1H, N*H*), 8.19 (d, $J_{H2'',H3''}$ = 8.8 Hz, 2H, H3''), 7.62 (d, $J_{H2'',H3''}$ = 8.8 Hz, 2H, H2''), 7.43-7.42 (m, 2H, H2',6'), 7.34 (dd, $J_{H5',H4'}$ = 8.0 Hz, $J_{H5',H6'}$ = 8.0 Hz, 1H, H5'), 7.09-7.06 (m, 1H, H4'), 6.02-5.98 (m, 1H, H3), 5.20-5.15 (m, 1H, H4), 3.53 (dd, $J_{4,5a}$ = 9.4 Hz, $J_{5a,5b}$ = 15.0 Hz, 1H, H5a), 3.39 (dd, $J_{4,5b}$ = 4.7 Hz, $J_{5a,5b}$ = 15.0 Hz, 1H, H5b); δ_C (101 MHz, d_6-acetone) 168.5 (C2), 166.6 (C1), 157.5 (C3'), 147.0 (C4''), 144.9 (C1''), 134.7 (C1'), 130.3 (C2''), 129.7 (C5'), 123.5 (C3''), 118.9 (C4'), 118.3 (C6'), 114.4 (C2'), 77.5 (C4), 59.4 (C3), 35.2 (C5); HRMS calc. for $C_{17}H_{15}N_2O_6^+$ ($[M+H]^+$) 343.0925 found 343.0933 ($[M+H]^+$), Δ = 2.33 ppm.

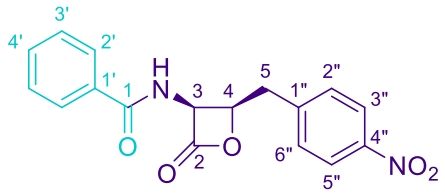

5: 396.9 mg, 12.4 mg/L, $[\alpha]_D$ +45° (*c* 0.16, EtOAc); δ_H (400 MHz, d_6-acetone) 8.78 (d, $J_{NH,H3}$ = 8.1 Hz, 0.4H, N*H*), 8.19 (d, $J_{H2'',H3''}$ = 8.9 Hz, 2H, H3''), 7.97 (dd, $J_{2',3'}$ = 8.9 Hz, $J_{2',4'}$ = 1.6 Hz, 2H, H2'), 7.64-7.60 (m, 3H, H2'',4'), 7.56-7.51 (m, 2H, H3'), 6.04-6.00 (m, 1H, H3), 5.22-5.17 (m, 1H, H4), 3.54 (dd, $J_{4,5a}$ = 9.4 Hz, $J_{5a,5b}$ = 15.0 Hz, 1H, H5a), 3.40 (dd, $J_{4,5b}$ = 4.5 Hz, $J_{5a,5b}$ = 15.0 Hz, 1H, H5b); δ_C (101 MHz, d_6-acetone) 168.5 (C2), 166.5 (C1), 147.0 (C4''), 144.9 (C1''), 133.2 (C1'), 132.0 C4'), 130.3 (C2''), 128.6 (C3'), 127.4 (C2'), 123.5 (C3''), 77.5 (C4), 59.4 (C3), 35.2 (C5); HRMS calc. for $C_{17}H_{15}N_2O_5$ ($[M+H]^+$) 327.09755 found 327.0990 ($[M+H]^+$), Δ = 4.43 ppm.

2.6 Hydrolysis of 1

Hydrolysis of **1**; **1** (4mg) was dissolved in aqueous NaOH (0.05 mM; 500 µL) and stirred for 3 h at room temperature. One drop of HCl (1 M) was then added and the compound was extracted with ethyl acetate (3 x 500 µL). The organic phase was dried *in vacuo* to give **6** (2.8 mg) as a brown solid.

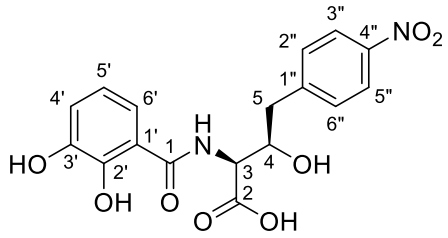

6: 2.8 mg - δ_H (400 MHz, d_6-acetone), 12.26 (d, $^4J_{3,OH}$ = 3.3 Hz, 1H, COO*H*), 8.19 (d, $J_{H3''/H5'',H2''/H6''}$ = 8.9 Hz, 2H, H3"/5"), 7.90 (d, $J_{NH,H3}$ = 7.2 Hz, 1H, N*H*), 7.64 (d, $J_{H2''/H6'',H3''/H5''}$ = 8.9 Hz, 2H, H2"/6"), 7.44 (ddd, $J_{4',5'}$ = 8.1 Hz, $^4J_{4',6'}$ = $^4J_{4',3'\text{-OH}}$ = 1.4 Hz, 1H, H4'), 7.06 (dd, $J_{H6',H5'}$ = 8.0 Hz, $^4J_{H6',H4'}$ = 1.4 Hz, 1H, H6'), 6.83 (ddd, $J_{4',5'}$ = 8.1 Hz, $J_{5',6'}$ = 7.8 Hz $^5J_{5',3'\text{-OH}}$ = 1.5 Hz, 1H, H5'), 4.89-4.86 (m, 1H, H3), 4.79 (d, $J_{4\text{-OH,}}$ = 6.6 Hz, 0.4H, O*H*), 4.69-4.63 (m, 1H, H4), 3.18 (dd, $J_{5a,4}$ = 4.7 Hz, $J_{5a,5b}$ = 13.7 Hz, 1H, H5a), 3.07 (dd, $J_{5b,4}$ = 8.3 Hz, $J_{5a,5b}$ = 13.7 Hz, 1H, H5b), δ_C (101 MHz, d_6-acetone), 198.4 (C1), 170.7 (C2) 170.3 (3'-O*H*), 149.3 (2'-O*H*), 146.9 (C1"), 146.8 (C4"), 146.2, 130.7 (C2"/C6"), 123.2 (C3"/5"), 118.9 (C6'), 118.6 (C5'), 117.6 (C4'),

114.7 (C1'), 71.9 (C4), 56.2 (C3), 40.5 (C5), HRMS calc. for $C_{17}H_{15}N_2O_7$ ([M-H]$^-$) 375.0834, found 375.0831 ([M-H]$^-$), Δ = 0.8 ppm.

2.7 ΔN-EcThrRS and EcThrRS protein purification

E. coli NiCo21(DE3):pLysS strains carrying pET28a(+)-EcThrRS or pET29a(+)-*ΔN-EcThrRS*, for expression of the full length or N-terminally truncated version of the E. coli ThrRS, respectively, were cultivated in Terrific Broth (TB) medium at 28°C and 250 rpm on a rotary shaker until they reached as of OD_{600} = 0.5-0.7. Protein expression was induced by addition of a 1 mM stock solution of IPTG (to give a final concentration of 0.1 mM) and the cultures were incubated at 18°C and 200 rpm for 18 h. Cells were harvested at 4 °C by centrifugation at 6,000 rpm, and cell pellets were re-suspended in purification buffer. After disruption with an EmulsiFlex-B15 high pressure homogeniser (Avestin, Inc.), insoluble cell debris was removed by centrifugation at 15,000 rpm at 4 °C for 30 min. The lysed supernatant was purified by chitin resin (NEB) chromatography to remove any endogenous *E. coli* metal-binding proteins. The sample was loaded onto a HisTrap excel (GE Healthcare) Ni-NTA column using an ÄKTA pure (GE Healthcare) system and eluted with 250 mM imidazole-containing purification buffer. Further purification was performed by size exclusion chromatography over a HiLoad 16/600 Superdex 200 pg column (GE Healthcare). Protein-containing fractions were identified by sodium dodecyl sulphate polyacrylamide gel electrophoresis (SDS-PAGE) and were combined and applied to an Amicon column (10 kDa MWCO). The imidazole was removed by exchange into non-imidazole-containing EcThrRS buffer by centrifugation at 6000 rpm at 4 °C, then the protein was concentrated before analysis with SDS-PAGE.

2.8 Sodium dodecyl sulphate polyacrylamide gel electrophoresis (SDS-PAGE)

Protein samples were prepared by addition of loading dye in a 1:3 ratio and denaturing them by heating at 90 °C for 2 min. 10 µL samples were loaded onto a 12% RunBlue (Expedeon Ltd.) polyacrylamide gel using 5 µL of Color Prestained Protein Standard (NEB) for reference. Electrophoresis was performed at 150 V in SDS-PAGE running buffer using an XCell SureLock™ Mini-Cell electrophoresis system (Thermo Fisher Scientific). Gels were subsequently stained using InstantBlue (Expedeon Ltd.) and de-stained in water.

2.9 ΔN-EcThRS and EcThrRS mass spectrometry with 1

2.9.1 Sample preparation

Purified ΔN-EcThrRS protein (18 µL of 20 mg/mL) in 20 mM Tris/HCl (pH 8.0) buffer containing 500 mM NaCl, 10 mM $MgCl_2$, 5 mM L-threonine was incubated with **1** (2 µL of a 10 mg/mL stock solution prepared in DMSO) for 15 min at room temperature.

An aliquot of each sample was taken for measurement of intact mass and the rest of each sample was prepared for tryptic digest experiments as follows. Proteins were separated by SDS–PAGE and the appropriately sized protein band was cut into slices and prepared for LC–MS/MS as described by Petre *et al*.[73] The subsequent HRMS analyses were carried out by Dr. Carlo de-Oliveira Martins from the JIC proteomics facility.

2.9.2 LCMS analysis for measurement of protein intact mass

Intact protein mass was analysed by LCMS on a Synapt G2-Si mass spectrometer coupled to an Acquity UPLC system (Waters, Manchester, UK). Aliquots of the samples were injected onto an Aeris WIDEPORE 3.6 µm C4 column, 2.1 mm x 50 mm, (Phenomenex, Macclesfield, UK) with a flow rate of 0.4 mL/min. Mobile phase A = water + 0.1 % FA, B = acetonitrile. The following elution gradient was used: 0-5 min 5% to 90% B. The mass spectrometer was controlled by the Masslynx 4.1 software (Waters) and operated in positive MS-TOF and resolution mode with a capillary voltage of 2.5 kV and a cone voltage of 40 V. Calibration was performed in the m/z range of 50-2000 using sodium formate according to the manufacturer. Leu-enkephalin peptide (0.5 µM in 50% methanol/0.1% formic acid, Waters) was infused at 10 µL/min as a lock mass and measured and applied every 30 s. The data were processed in Masslynx 4.1 after combining relevant spectra using the background subtract and smooth options. The protein mass was determined by deconvolution using the MaxEnt 1 option, and the peaks were centred.

2.9.3 Protein digestion via tryptic digest and analysis of peptides using LC-MS/MS

Proteins were prepared for LC-MS/MS as follows. Trypsin (Promega) was used as the proteolytic enzyme for digestion, at a ratio of 1:20 (trypsin:target protein). The reaction was run for 8 h at room temperature, and pH 7.5. LC–MS/MS analysis was performed with an Orbitrap Eclipse tribrid mass spectrometer (Thermo Fisher Scientific) and a nanoflow HPLC system (Dionex Ultimate3000, Thermo Fisher Scientific) as described by Bender *et al*,[74] with the following differences: 1) MS/MS

peak lists were exported in the Mascot generic file format using MaxQuant v.1.6[75]; 2) the database searched with Mascot v.2.7 (Matrix Science) was the *E. coli K12* protein database with the inclusion of sequences of common contaminants such as keratins and chymotrypsin; 3) carbamidomethylation of cysteine residues and modification by **1** at C, K, S, T, Y were specified as variable modifications. The other Mascot parameters used were as follows: 1) mass values were monoisotopic and the protein mass was unrestricted; 2) the peptide mass tolerance was 6 ppm and the fragment mass tolerance was 0.6 Da; 3) one missed cleavage was allowed with trypsin. All Mascot searches were collated and verified with Scaffold (Proteome Software), and the subset database was searched with the Mascot server v.2.7. Accepted proteins passed the following threshold in Scaffold: 95% confidence for protein match and minimum of two unique peptide matches with 95% confidence.

2.10 ΔN-EcThrRS crystallography with 1

Crystal trials were set up using the sitting drop vapour diffusion method with Morpheus HT-96 MD1-47, PEG (Qiagen), Structure and MIDAS screens (Molecular dimensions). Co-crystallisations were set up with 20 mg/mL ΔN-EcThrRS in 20 mM Tris/HCl (pH 8.0) buffer containing 500 mM NaCl, 10 mM $MgCl_2$ and 5 mM threonine. Either **1** or its analogue **3**-**6** were added to a final concentration of 1 mg/mL (using a stock solution of 10 mg/mL in DMSO). Soaks were performed with successfully obtained crystals protein-only crystals where **1** or its analogue **3**-**6** were added to a final concentration of 1 mg/mL (using a stock solution of 10 mg/mL in DMSO) and a cryoprotectant specific to the conditions of the drop in which the crystals had formed.

Table 2.4: Summary of conditions tested in crystal trials of 1 with ΔN-EcThrRS. Summary of the conditions tested in co-crystallisations and soaks with **1** or analogues.

Screen	**Co-crystallisation with:**	**Soaked with:**
PEG	**6**, **1**-Fe(III)	**6**, **3**, **4**, **5**, **1**-Fe(III)
Morpheus	**1**, **3**, **4**	
MIDAS	**1**	
Structure	**3**, **4**	

2.11 QuikChange mutagenesis

Single-site mutations were performed using the QuikChange™ kit purchased from Agilent. All PCR reactions were performed in a T100™ Thermal Cycler (Bio-Rad). PCR reactions of 50 µL containing the reagents described in Table 2.6 as per the manufacturers' instructions. Control reactions were performed using the pWhitescript control plasmid and the primers provided in the kit. The PCR cycles were performed as described in Table 2.7.

Table 2.5: QuikChange™ PCR reaction mix

Component	Volume (µL)	Final concentration
10× reaction buffer	10	1×
Forward primer	1.25	1 µM
Reverse primer	1.25	1 µM
dNTPs	1	200 µM
DNA template	1	~50 ng
PfuTurbo polymerase	1	2.5 U

Table 2.6: QuikChange™ PCR programme

Cycle	Temperature (°C)	Time	Repeat (×)
Initial denaturation	95	2 min	1
Denaturation	95	20 s	18
Annealing	55-65	10 s	
Elongation	68	1 min/kb	
Final elongation	68	5 min	1
Cooling	12	1 min	1

The PCR reactions were treated with 2 µL of *Dpn*I at 37°C for 5 min and then a 1 µL aliquot of each reaction was transformed respectively into *E. coli* DH5α competent cells by heat shock. The transformed cells were grown on a LB-tetracycline[12.5] plate (or LB–ampicillin[50] agar plates containing 80 µg/mL X-gal and 20 mM IPTG for the control reaction) and incubated at 37 °C overnight. The number of blue colonies on the control plate was analysed and used as an indirect indication of PCR amplification efficiency. To verify the mutations, colony PCR using Q5 polymerase in 50 µL reaction volumes, as shown in Table 2.8 and Table 2.9, was performed on four colonies from

each reaction plate. Cells from a single colony were applied to 50 µL dH_2O with a toothpick which was used as template. PCR products were purified using a QIAquick® PCR Purification Kit (Qiagen), were analysed by agarose gel electrophoresis and sent for sequencing.

Table 2.7: High-fidelity Q5 PCR reaction mix

Component	Volume (µL)	Final concentration
5× reaction buffer	10	1×
Forward primer	2.5	0.5 µM
Reverse primer	2.5	0.5 µM
dNTPs	1	200 µM
DNA template	2	~50 ng
Q5 polymerase	0.5	0.5 U

Table 2.8: High-fidelity Q5 PCR programme

Cycle	Temperature (°C)	Time	Repeat (×)
Initial denaturation	98	3 min	1
Denaturation	98	30 s	30
Annealing	55-65	30 s	
Elongation	72	30 s/kb	
Final elongation	72	10 min	1
Cooling	12	1 min	1

2.11.1 Agarose gel electrophoresis

Agarose gels were prepared by adding agarose to TAE buffer to a final concentration of 1%. 10 µg/mL ethidium bromide was added for visualisation under ultraviolet (UV) light. 1 kb ladder (NEB) was used as a comparison to the DNA samples to be analysed which were prepared by addition of loading dye before gel application. Gel electrophoresis was performed in TBE buffer using a PowerPac™ Universal Power Supply (Bio-Rad) at 80-120 V, until sufficient separation between DNA fragments was achieved. Gel visualisation was performed using a UV Transilluminator and Gel Documentation System (UVP).

2.12 Isothermal Titration Calorimetry (ITC) of EcThrRS or BSA with 1

ITC measurements were obtained by using a Malvern Microcal PEAQ-ITC. The cell contained 20 μM protein (EcThrRS or BSA) that had been dialysed overnight into EcThrRS buffer containing 5% DMSO. The syringe contained 200 μM **1** prepared in the same buffer system. ITC experiments were performed at 25 °C. The titrant was delivered in 2 μL aliquots with 250 s between injections, while it was stirred at 750 rpm with a reference power of 10 μcal/s. Control experiments included 200 μM **1** into buffer only and buffer into 20 μM protein.

2.12.1 Monitoring hydrolysis of 1 under ITC conditions

Samples of **1** in EcThrRS buffer with the same concentration used in ITC experiments were prepared in HPLC vials and monitored by HPLC with repeated injections over the time frame of the experiment. UV chromatograms were analysed at 270 nm to monitor **1** and **6** proportions.

2.13 Monitoring pH-dependence of 1 hydrolysis

Samples were prepared in HPLC vials with a glass insert: 10 μL **1** (1 mg/mL in DMSO stock) was added to 90 μL buffer solution (Tris-HCl at pH 6.0, 6.5, 7.0, 7.5, or 8.0). Samples were incubated for 30 min before HPLC analysis using the Agilent 1100 system and method. UV chromatograms were analysed at 270 nm.

2.14 *P. fluorescens ΔobaLΔobaO* growth and compound production time course

These experiments were performed with Dr. Sibyl Batey.

OPM (100 mL in a 250 mL flask) was inoculated with a single colony of *P. fluorescens* ATCC 39502/*ΔobaLΔobaO* and incubated at 25 ˚C with shaking at 300 rpm. After 24 h, 5 × 100 mL (in 500 mL flask) production cultures were inoculated with 1 mL of the *ΔobaLΔobaO* seed culture and an aliquot of a 100 mM stock solution of the corresponding DHBA derivative in DMSO was added (to give final concentration of 0.4 mM for 2'-HBA, 3'-HBA and BA and 0.2 mM for DHBA). Cultures were incubated at 25 ˚C with shaking at 300 rpm for 12 h. Every hour the OD_{600} was recorded, and a 1 mL aliquot was removed and stored at -20 ˚C for subsequent HPLC analysis. The 1 mL HPLC aliquots were extracted by shaking with ethyl acetate (1 mL) for 15 min and centrifuging at 13,300 rpm for 1 min. The resulting organic phase was separated,

and the solvent removed under *vacuo* and the resulting residue dissolved in 250 µL acetonitrile then analysed by HPLC using the Agilent 1100 system and method.

2.15 Antibacterial activity (MIC) assays

Indicator strains were grown for 16−18 h in 5 mL LB cultures. 500 µL of each culture was used to inoculate 50 mL LB cultures (in 250 mL flasks), which were incubated at 37 °C with shaking at 250 rpm until they reached an OD_{600} = 0.3−0.4. Cultures were diluted 1:10 with molten soft nutrient agar (SNA), before pouring into appropriately sized Petri dishes to set. Serial dilutions of the test compounds (from 1000 µg/mL to 1 µg/mL) were prepared in acetonitrile, and 4 µL of each dilution was applied directly onto the SNA surface. Kanamycin (500 µg/mL in water) was used as a positive control, and acetonitrile or water (4 µL) was used as a negative control. Plates were then incubated at 37 °C for 16−18 h. The MIC was defined as the lowest concentration of compound that resulted in a zone of inhibition. Experiments were carried out in at least triplicate for each strain.

2.15.1 Antibacterial activity assays under iron depleted/excess iron conditions

The method was the same as the antibacterial MIC assays described above, however, the conditions are altered for excess iron ($FeNO_3.9H_2O$ stock was added to give a final concentration of 2 mM) or iron depletion (2,2'-bipyridyl stock was added to give a final concentration of 150 µM). Compounds were further diluted to lower concentrations due to a decrease in MIC under excess iron conditions. The effect of excess iron on the MIC of alternative antibiotics was determined by performing a serial dilution of carbenicillin, kanamycin, streptomycin, nitrofurantoin and chloramphenicol.

2.15.2 Trojan-horse antibacterial assays

This method is the same as the antibacterial MIC assays described above. Indicator strains used were *E. coli* BW25113 and siderophore TBDT transporter knock-out mutants Δ1 to Δ6 described by Grinter *et al.*[41] Conditions were altered for iron depleted or excess iron concentrations as described above.

2.16 Metal binding assays

2.16.1 Chrome azurol S (CAS); Fe(III) binding

CAS assay for iron binding; a serial dilution of **1** (dissolved in DMSO) was performed and 90 µL CAS solution was added to 10 µL of each dilution to give final concentrations of **1** between 5000 to 5 µM in a 96-well-plate. The negative control was 10% DMSO in CAS solution. A full UV spectrum (200-800 nm) was recorded on a microplate reader (Clariostar).

2.16.2 4-(2-pyridylazo)-resorcinol (PAR); Zn (II) binding

To make $Zn(PAR)_2$ solution, 100 µL of a 10 mM aqueous $ZnSO_4$ solution was added to 8.9 mL PAR assay solution. A serial dilution of **1** (dissolved in DMSO) was performed and 90 µL $Zn(PAR)_2$ solution was added to 10 µL of each dilution to give final concentrations of **1** between 5000 to 5 µM in a 96-well-plate. The negative control was 10% DMSO in $Zn(PAR)_2$ solution, the positive control was 10% DMSO in PAR-only solution. A full UV spectrum (200-800 nm) was recorded on a microplate reader.

2.16.3 Mass spectrometry of 1 with metal ions

To determine whether **1** can form a complex with different metal ions detectable by high-resolution mass spectrometry (HRMS) a sample of each metal ion stock solution (1 µL of $FeSO_4$, $FeCl_3$, $ZnSO_4$, $MgSO_4$ or $MnCl_2$; 200 mM in water) was added to 20 µL of **1** (1 mg/mL stock solution prepared in DMSO) in a HPLC vial insert and diluted with acetonitrile (180 µL). Samples were subjected to HRMS by HRMS by Dr. Carlo de-Oliviera Martins of the JIC Proteomics Platform.

For HRMS, the samples prepared above were diluted into 50% methanol/0.1% formic acid and infused into a Synapt G2-Si mass spectrometer (Waters, Manchester, UK) at 10 µl/min using a Harvard Apparatus syringe pump. The mass spectrometer was controlled by Masslynx 4.1 software (Waters). It was operated in positive ion mode and calibrated using sodium iodide. The sample was analysed for 1 min with a 1 s MS scan time over the range of 50-1200 m/z with 3.0 kV capillary voltage, 40 V cone voltage, 115 °C cone temperature. Leu-enkephalin peptide (1 ng/µL, Waters) was infused at 10 µL/min as a lock mass (m/z = 556.2766) and measured every 10 s. Spectra were generated in Masslynx 4.1 and peaks were centred using automatic peak detection with lock mass correction.

2.17 Single crystal X-ray diffraction (XRD) of 1

A saturated solution of **1** was prepared by addition of 90 µL acetonitrile to 3 mg of compound in a 2 mL HPLC vial. 10 µL of 200 mM $FeCl_3$ in water was added and the vial was capped with a slit lid. The solution was left in the fridge for 3 months, after which, long oblong-shaped transparent crystals had formed. The following steps were performed at the University of East Anglia (UEA) by Dr. Joseph Wright, associate Professor in the School of Chemistry, and Dr. David Hughes a retired chemical crystallographer. Dr. Joseph Wright harvested the crystals and collected diffraction data and the structure was solved by Dr. David Hughes.

2.18 Determination of 1-Fe(III) complex stoichiometry via UV-visible spectroscopy

To determine the stoichiometry of the **1**-Fe(III) complex, the change in absorbance at λ_{max} of the complex with mole fraction of **1**:Fe(III) was measured by UV-visible spectroscopy. A mole fraction range of **1**:Fe(III) from 0.1 to 0.9 was prepared across a series of wells in a 96-well-plate as follows. An aliquot of **1** (from 10 to 90 µL of a 1 mM stock solution in DMSO) and an aliquot of $Fe(NO_3)_3.9H_2O$ (from 90 to 10 µL of a 1 mM stock solution in water) were added across a row in a 96-well-plate. An example is given here; well A3 contains 30 µL **1** (1 mM stock solution in DMSO) and 70 µL $Fe(NO_3)_3.9H_2O$ (1 mM stock solution in water). The solutions were left at room temperature for 15 min to allow equilibration, then the UV-visible spectrum was measured using a microplate reader (Clariostar). Salicylic acid (1 mM in DMSO) was used in replacement of **1** as a positive control, as it forms a 1:1 complex with Fe(III) with λ_{max} absorbance at 535 nm.[76] The absorbance at λ_{max} of the **1**-Fe(III) complex was determined as 690 nm, this was plotted against mole fraction to give a Job's plot with a maximum at 0.5 molar ratio; a 1:1 complex.

2.19 Spectophotometric titration experiments for complex stability determination

The change in absorbance with increasing concentration of the **1**-Fe(III) complex was measured by UV-visible spectroscopy to determine its λ_{max} and extinction coefficient under these conditions. A concentration range of the **1**-Fe(III) complex (with final concentrations from 0.1 to 1 mM) was prepared in a series of wells across a row in a 96-well-plate as follows. An aliquot of **1** (10 µL of a stock solution varying in

concentration from 1 to 10 mM in DMSO) was added to each well then an aliquot of $Fe(NO_3)_3.9H_2O$ (10 µL of a stock solution varying in concentration from 1 to 10 mM in water) was added. Then the solutions were buffered with 80 µL MES solution, pH 6.0 and ionic strength 0.1 M (KNO3). An example is given here; well A3 contains 10 µL **1** (3 mM stock solution in DMSO), 10 µL $Fe(NO_3)_3.9H_2O$ (3 mM stock in water) and 80 µL MES solution, pH 6.0 and ionic strength 0.1 M (KNO3). The absorbance was measured and λ_{max} of the **1**-Fe(III) complex was found to be 560 nm in these conditions.

To determine the stability constant, K, of the **1**-Fe(III) complex, the ability of EDTA to outcompete **1** for Fe(III) binding was monitored by UV-visible spectroscopy. A solution of **1**-Fe(III) was prepared in each well across a row in a 96-well-plate (with a constant final concentration of 1 mM) then an aliquot of EDTA was added (varying in final concentration across the row from 0.1 to 0.9 mM) as follows. A solution of **1** (10 µL of a 10 mM stock solution in DMSO) and $Fe(NO_3)_3.9H_2O$ (10 µL of a 10 mM stock solution in water) was added to each well across the row, then EDTA (10 µL of a stock solution varying in concentration from 1 to 12 mM) was added and the solutions were buffered with 70 µL MES solution, pH 6.0 and ionic strength 0.1 M (KNO_3). An example is given here; well A3 contains 10 µL **1** (10 mM stock solution in DMSO), 10 µL $Fe(NO_3)_3.9H_2O$ (10 mM stock solution in water), 10 µL EDTA (3 mM stock solution in water) and 70 µL MES solution, pH 6.0 and ionic strength 0.1 M (KNO_3). The full UV absorbance spectrum was measured in a plate reader.

2.20 Monitoring the ability of 1 to act as a siderophore for *P. fluorescens*

To monitor the ability of **1** to act as a siderophore for *P. fluorescens* ATCC 39502 the effect on growth and compound production of the organism with changes in iron bioavailability was measured by OD_{600} and HPLC, respectively. A series of *P. fluorescens* ATCC 39502 cultures were grown in media conditions prepared with increasing 2'2-bipyridyl (bipy) or $Fe(NO_3)_3.9H_2O$ concentrations (to give a final concentration range of 0 to 350 µM) to decrease or increase the available concentration of Fe(III), respectively, as follows. OPM (50 mL in a 250 mL flask) was inoculated with a single colony of *P. fluorescens* ATCC 39502 and incubated at 25 ˚C with shaking at 300 rpm for 24 h. Aliquots of OPM-Fe (10 mL in 50 mL falcon tubes sealed with bungs) were prepared to give a concentration range of bipy or $Fe(NO_3)_3.9H_2O$; 100 µL of a stock solution in DMSO varying in concentration from 5

to 35 mM was added. Then, the cultures were inoculated with 1 mL *P. fluorescens* ATCC 39502 starter culture and were incubated at 25 ˚C with shaking at 300 rpm for a further 14 h. Following this, 1 mL aliquots were removed and prepared for subsequent HPLC analysis by shaking with ethyl acetate (1 mL) for 15 min and centrifuging at 13,300 rpm for 1 min. The resulting organic phase was separated, and the solvent removed under *vacuo* and the resulting residue dissolved in 250 µL acetonitrile then analysed by HPLC using the Agilent 1290 (Chem Lab) system and method described. The UV chromatograms were analysed at 270 nm and the proportion of **1** vs. **6** was quantified by peak areas.

For OD_{600} measurements, the conditions described above were replicated in a 96-well-plate. A series of *P. fluorescens* ATCC 39502 cultures were grown in media conditions prepared with increasing 2'2-bipyridyl (bipy) or $Fe(NO_3)_3.9H_2O$ concentrations (to give a final concentration range of 0 to 350 µM) across a row in a 96-well-plate as follows. Aliquots of OPM-Fe media (147.5 µL) were prepared to give a concentration range of bipy or $Fe(NO_3)_3.9H_2O$; 1.5 µL of a stock solution in DMSO varying in concentration from 5 to 35 mM was added. Then the cultures were inoculated with 1.5 µL *P. fluorescens* ATCC 39502 starter culture and were incubated for 24 h at 25 ˚C with double orbital shaking at 600 rpm in a Clariostar plate reader (BMG Labtech). The UV absorbance at 600 nm was recorded every 30 min.

2.21 Monitoring the hydrolysis protection effect of Fe(III) binding for 1 and the analogues by HPLC

Samples of **1** or the analogues **3**-**5** (10 µL of a 10 mM stock solution in DMSO) were incubated with $Fe(NO_3)_3.9H_2O$ (10 µL of a 10 mM stock solution in water) and 80 uL Na_2HPO_4 buffer (100 mM, pH 8) for 30 min. The respective control samples (without Fe(III)) were prepared with 10 µL water instead of $Fe(NO_3)_3.9H_2O$ stock solution. After 30 min incubation the samples were analysed by HPLC using the Agilent 1290 (Chem Lab) system and method. UV chromatograms were analysed at 270 nm and the proportion of compound with ring-closed vs. ring-open β-lactone (eg. **1** vs. **6**) was quantified using peak area. Additional peaks detected by HPLC were identified by MS as products of the nucleophilic attack of buffer components to ring open the lactone ring of compounds.

2.22 Measuring the hydrolysis of 1 in *P. fluorescens* cultures of OPM vs. OPM-Fe

OPM or OPM-Fe (100 mL in 250 mL flasks) was inoculated with a single colony of *P. fluorescens* ATCC 39502 and incubated at 25 ˚C with shaking at 300 rpm. After 24 h, 1 mL of each starter culture was used to inoculate OPM or OPM-Fe (100 mL in 250 mL flasks) production cultures. These were incubated at 25 ˚C at 300 rpm for a further 14 h after which 1 mL aliquots were removed for subsequent HPLC analysis and the colour of the cultures was recorded. Following this, an aliquot of $FeCl_2$ or $FeCl_3$ (10 mg dissolved in 500 µL H_2O) was added to the cultures to give final concentrations of 0.1 g/L Fe(II) or Fe(III), respectively. Further 1 mL aliquots were taken for subsequent HPLC analysis, and the colour change of the cultures was recorded. The 1 mL aliquots were prepared by shaking with ethyl acetate (1 mL) for 15 min and centrifuging at 13,300 rpm for 1 min. The resulting organic phase was separated, and the solvent removed under *vacuo* and the resulting residue dissolved in 250 µL acetonitrile then analysed by HPLC using the Agilent 1100 system and method described.

Chapter 3:

Investigating the role of the catechol moiety of **1** via a mutasynthetic approach

Chapter 3 : Investigating the role of the catechol moiety of 1 via a mutasynthetic approach

3.1 Introduction

The structure of **1** contains a catechol ring, which is a common binding motif in siderophore compounds[32, 42] and THAs.[33] We therefore hypothesised that the catechol moiety could participate in a metal binding interaction which, in turn, could be involved in the mechanism of action of **1**. To test this hypothesis, we investigated the role of the catechol on the biochemical properties of **1** and the interplay between metal binding and bioactivity of **1**.

To systematically assess the role of the catechol, the first aim was to produce a suite of analogues which were deficient in either one or both of its hydroxyl groups. To do this a mutasynthetic approach was applied to the producing organism, *P. fluorescens* ATCC 35902. **1** is assembled by ObaI, a bimodular NRPS which catalyses the linkage of 2,3-dihydroxybenzoic acid (DHBA) and the nonproteinogenic amino acid (2*S*,3*R*)-2- amino-3-hydroxy-4-(4-nitrophenyl)butanoate, (**2**), via peptide bond formation with subsequent release from the enzyme involving β-lactone formation (Figure 1.9).[59, 61] During previous biosynthetic studies by Dr Thomas Scott in our lab[59] it was shown that ObaJ, ObaL and ObaN are involved in the production of DHBA, an essential precursor of **1** biosynthesis via gene deletions, and that addition of exogenous DHBA to cultures of the deletion strains results in restoration of the phenotype.[59] We chose the Δ*obaL* strain for further mutasynthesis work.

It was further shown that, in addition to the native substrate, DHBA, ObaI has sufficient promiscuity to accept alternative substrates, 2'-hydroxybenzoic acid (2-HBA), 3'-hydroxybenzoic acid (3-HBA) and benzoic acid (BA). These alternative building blocks are incorporated in place of DHBA by the Δ*obaL* strain during biosynthesis to give analogues **3**, **4**, and **5**, respectively (Figure 3.1). This gave a suite of catecholate analogues that could be tested in a series of biochemical assays, allowing investigations into the role of the catechol to be undertaken.

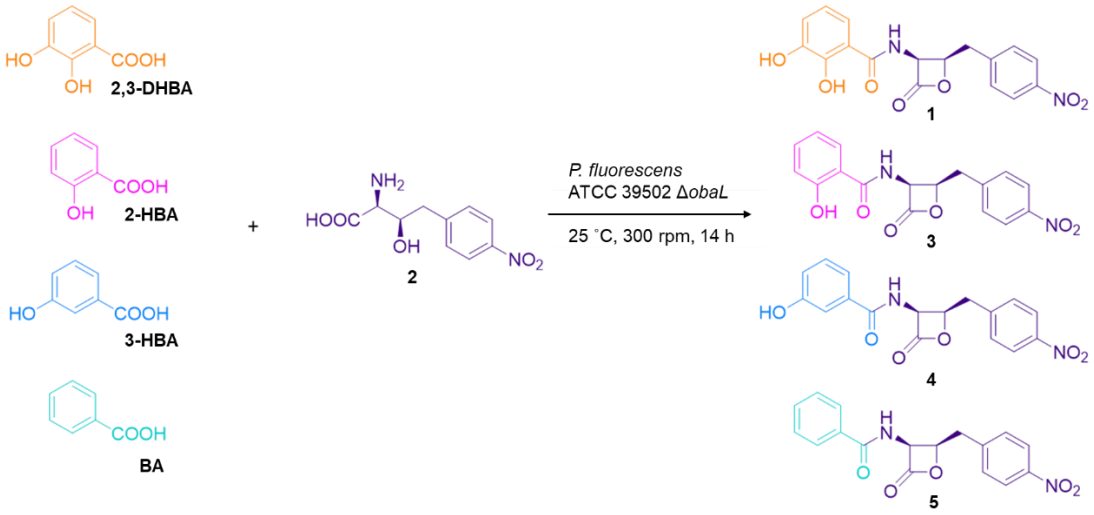

Figure 3.1: Schematic representation of the formation of 1 analogues. *P. fluorescens* ATCC 39502 Δ*obaL* cultures are fed with DHBA or building block derivatives which react with **2** in a reaction catalysed by the NRPS, ObaI, to form the respective analogue; **1**, **3**, **4** or **5**.

3.2 Extraction and purification of 1 and catecholate analogues (3-5)

The first objective of my project was to work with Dr. Sibyl Batey and Dr. Edward Hems to extend previous small-scale production of **3**, **4** and **5** using *P. fluorescens* Δ*obaL* which had enabled their purification by HPLC and structural characterisation by LCMS and NMR. The aim of my work was to repeat and refine this procedure and then scale up production. The following experiments were conducted by me and Dr. Sibyl Batey. Firstly, we grew small-scale cultures of the Δ*obaL* strain (100 mL) and added exogenous DHBA or the relevant alternative building block, 2-HBA, 3-HBA or BA, along with the unfed culture and WT *P. fluorescens* as controls. After 14 h I analysed the metabolites present in the cultures by HPLC; aliquots (1 mL) of the cultures were extracted with an equal volume of ethyl acetate, the solvent removed *in vacuo*, re-dissolved in acetonitrile (250 µL) and analysed using an Agilent HPLC. This confirmed previous results showing that Δ*obaL* cultures fed with DHBA analogues produce the corresponding **1** analogue; **3** elutes at 11.15 min, **4** at 9.47 min and **5** at 10.73 min (Figure 3.2). Interestingly, the purple colouration of cultures normally associated with **1** production was not seen for analogue-producing cultures. This indicated that the purple colouration is associated with the presence of the DHBA catechol moiety and suggested that it may be due to the formation of a **1**-metal ion complex which will be discussed later.

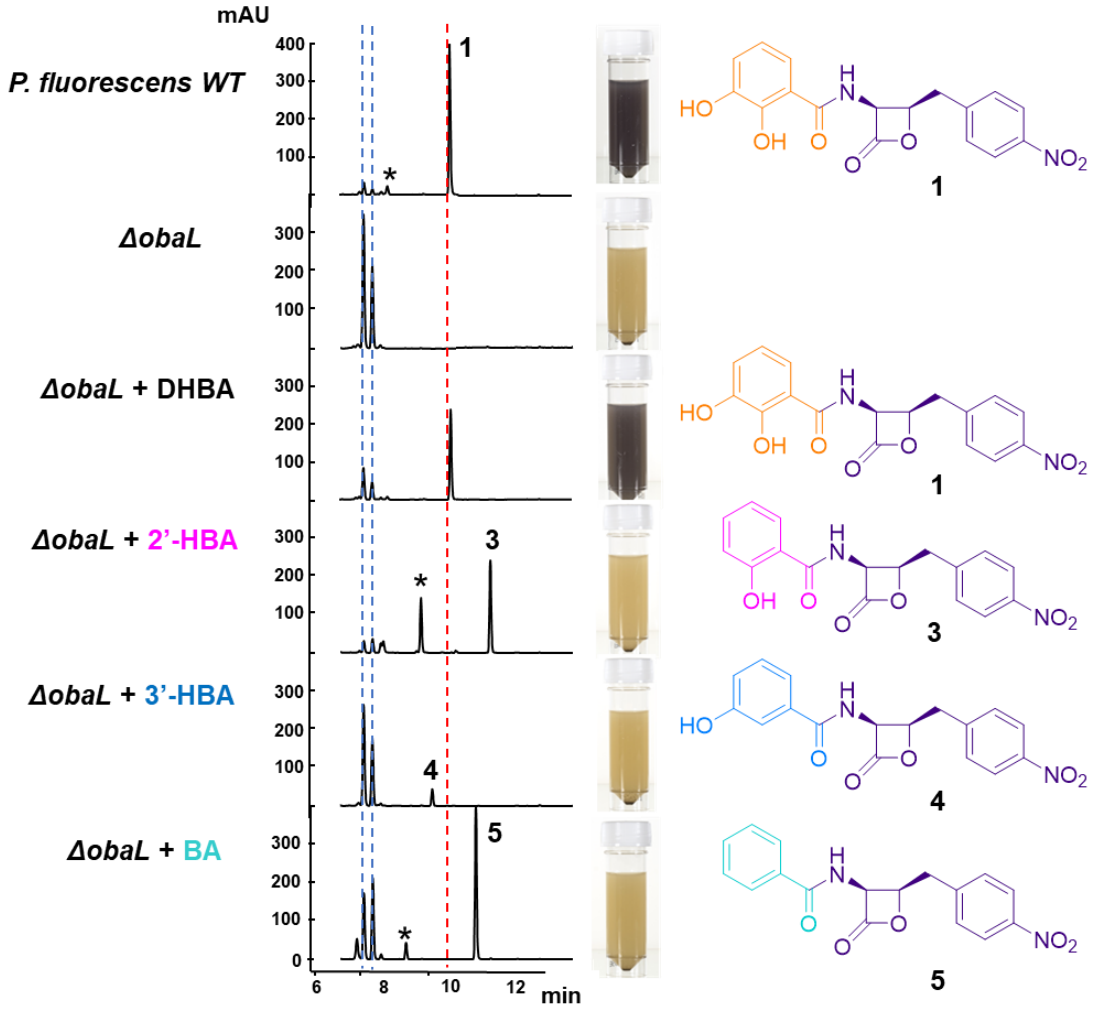

Figure 3.2: Small-scale detection of 1 and catecholate analogues. HPLC chromatograms at 270 nm showing the production of **1** in *P. fluorescens* wild-type (WT), shunt metabolites in unfed Δ*obaL* and the corresponding product, **1** or analogues **3**, **4** and **5** from Δ*ObaL* cultures fed with the respective exogenous building blocks, DHBA, 2-HBA, 3-HBA and BA. The red dashed line marks the retention time of **1**. Analogue retention times are **3**, 11.15 min, **4**, 9.47 min, **5**, 10.73 min. The blue dashed lines mark shunt metabolites of the pathway. Peaks highlighted with an asterisk mark the corresponding hydrolysis product of each analogue (as confirmed by LCMS analysis). Pictures of culture aliquots after 14 h growth show the lack of purple colouration in analogue-producing cultures.

Following this, we scaled up production and purification of **1**, **3**, **4** and **5** for further study using bioassays and metal binding assays. Cultures (8 x 1 L) of *P. fluorescens* ATCC 39502 WT or the *ΔobaL* strain fed with the appropriate DHBA derivative were conducted in conjunction with Dr. Sibyl Batey. After 14 hours of growth these were extracted using and equal volume of ethyl acetate and purified using a combination

of Biotage Isolera flash chromatography and preparative HPLC if further purification was required; this part of the work was conducted by Dr. Edward Hems. This process was repeated in additional batches of 8 L, leading to the production of each compound in good yield (Table 3.1).

Table 3.1: Breakdown of scale-up procedure for extraction/purification of catecholate analogues. Total culture volumes processed for each analogue and their average titre and yield isolated in the purification process.

Analogue	Total culture volume / L	Average titre / mg/L	Total yield / mg
1	72	20.4	1467.8
2	24	13.6	326.7
3	24	7.6	181.9
4	32	12.4	396.9

3.3 Investigating the bioactivity of 1 analogues *in vivo*

Following their isolation, we assessed the antibacterial activity of these compounds. Bioassays of **1** and **3**-**5** against various indicator strains were performed. We used a clinical isolate of methicillin-resistant *Staphylococcus aureus* (MRSA), *Bacillus subtilis*, *E. coli* 25922 and *E. coli* NR698 (a membrane permeabilised strain of *E. coli*) repeating analysis previously performed by Dr. Sibyl Batey. A representative example of this work is given below for MRSA as the indicator strain (Figure 3.3).

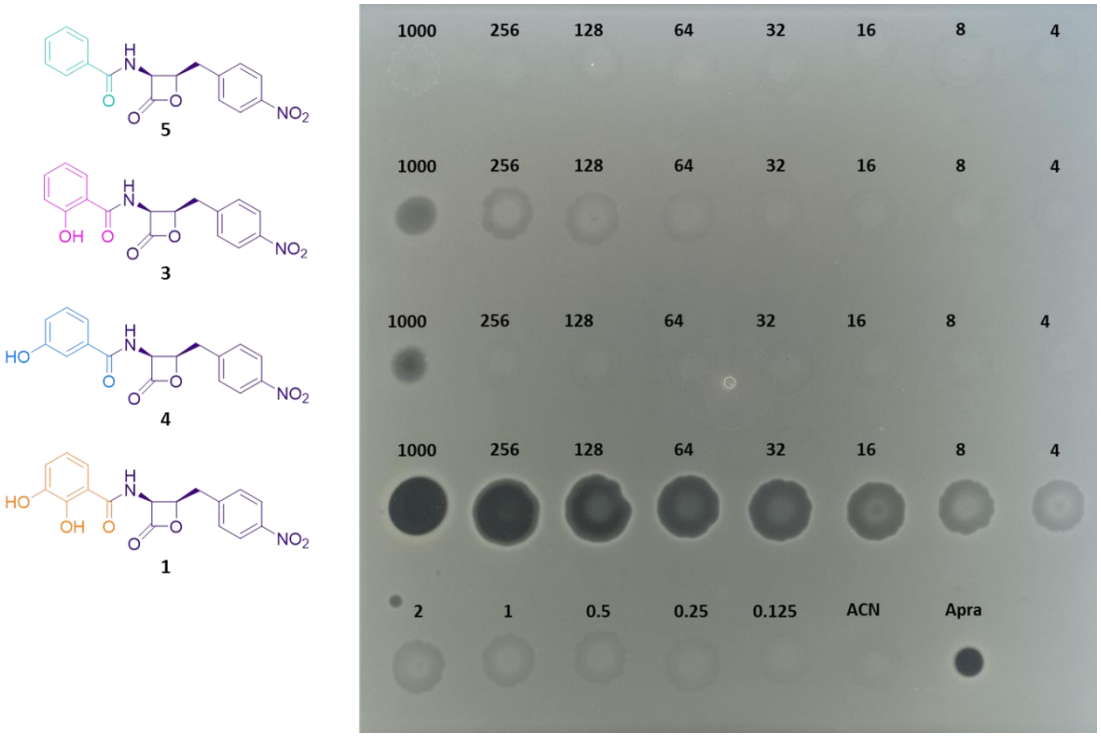

Figure 3.3: The catechol is essential for the bioactivity of 1. Spot on lawn bioassay of **1**, **3**, **4** and **5** with MRSA. Minimum inhibitory concentrations are **1**: 4 µg/mL; **3** and **4**: 1 mg/mL; **5**: > 1 mg/mL. Acetonitrile and apramycin were used as negative and positive controls respectively.

To extend this analysis, I performed bioassays with *Saccharomyces cerevisiae* as a representative eukaryote. The minimum inhibitory concentrations (MICs) for each compound are shown in Table 3.2.

Table 3.2: MIC of 1 increases with variation of the catechol moiety. The minimum inhibitory concentrations (MICs in µg/mL) of **1**, **3**, **4** and **5** against a set of indicator strains; methicillin-resistant *Staphylococcus aureus* (MRSA), *Bacillus subtilis* EC 1524, *E. coli* 25922, membrane permeabilised *E. coli* NR698 and *Saccharomyces cerevisiae* MTA-3666.

Analogue	**MIC / µg/mL**				
	MRSA	***B. Subtilis***	***E. coli* 25922**	***E. coli* NR698**	***S. cerevisiae***
1	4	8	128	4	1000
3	>1000	>1000	>1000	>1000	>1000
4	800	1000	>1000	>1000	>1000
5	1000	1000	>1000	>1000	>1000

MRSA, *B. subtilis* and *E. coli* are all sensitive to **1**, with membrane disruption increasing the sensitivity of *E. coli* (as shown by the decrease in MIC between strains 25922 and NR698). This and the encouraging finding that *S. cerevisiae* is not sensitive to **1** indicate its potential as an antibiotic for treating Gram-positive infections. However, the analogues **3**-**5** do not exhibit inhibitory activity on any of the indicator strains tested. This confirms the catechol moiety of **1** is essential for its bioactivity *in vivo*.

After these findings, our next aim was to investigate the ability of the analogues to inhibit the molecular target of **1**, the housekeeping enzyme, ThrRS. To do this, the experiment described in Figure 1.10 was repeated but modified to test the ability of the analogues **3**-**5** to inhibit the housekeeping ThrRS of *P. fluorescens*. ATCC 39502 Dr. Sibyl Batey and I grew *ΔobaLΔobaO* cultures in the presence of the building block compounds (or DHBA as a control) and monitored cell growth (by OD_{600} measurements) and the production of **1** or **3**-**5** at hourly timepoints by HPLC. As described in section 1.4.2, when strain *ΔobaLΔobaO* is cultured in the presence of DHBA to restore **1** production, growth is abolished due to inhibition of the house-keeping ThrRS enzyme.[61] The same was observed in this experiment, however Figure 3.4 shows that cultures fed with 2HBA, 3HBA or BA produced the corresponding analogue, **3**-**5**, and can grow normally but with a somewhat delayed growth for the culture producing **5**. HPLC analysis showed that **3**-**5** were still produced despite the cultures lacking the immunity determinant, ObaO. This further validates out hypothesis that the catechol moiety of **1** is essential for its antibacterial activity.

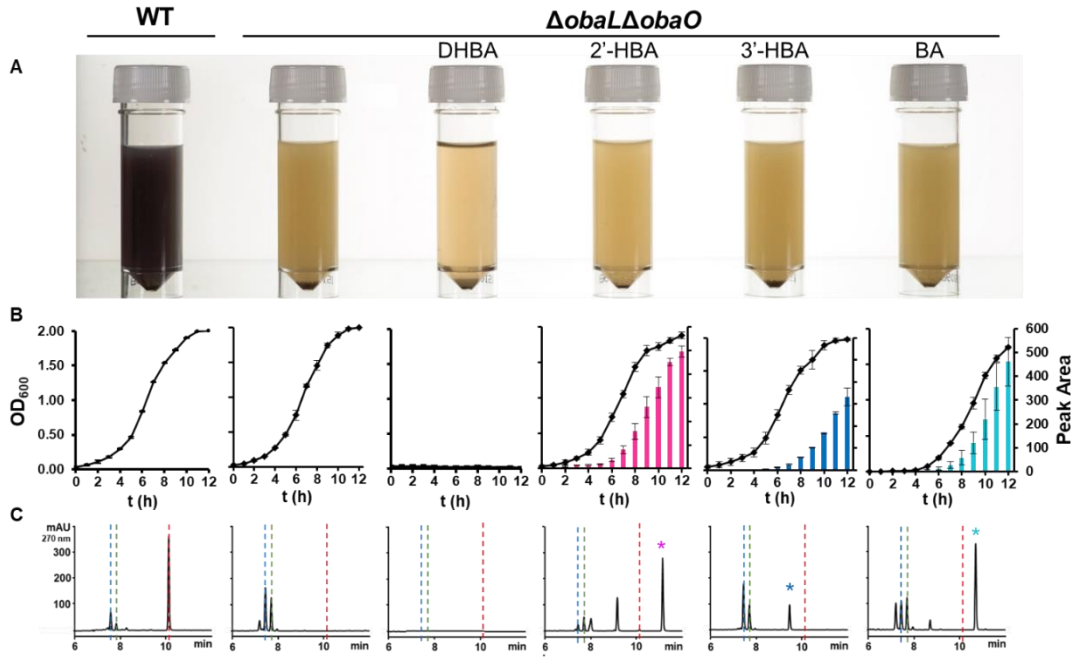

Figure 3.4: Catecholate analogues of 1 cannot inhibit the housekeeping ThrRS *in vivo*. *P. fluorescens* ATCC 39502 WT and the Δ*obaL*Δ*obaO* strain unfed and fed with DHBA, 2-HBA, 3-HBA and BA and producing **1**, **3**, **4** and **5** respectively. A) Samples of each strain after 14 h growth; purple colour is an indication of **1** production. B) Growth curves showing no growth for Δ*obaL*Δ*obaO* fed with DHBA and almost normal growth for the strain when fed with 2-HBA, 3-HBA and BA (area under corresponding analogue peak in HPLC is shown). C) HPLC chromatograms at 270 nm showing **1** production with red dashed line, R_t = 10.1 min, analogue peaks are highlighted with an asterisk; blue and green dashed lines indicate shunt metabolites of the pathway.

We wanted to address the question; what is the role of the catechol in the mechanism of action of **1**? Could it form a direct interaction with the target ThrRS enzyme, potentially via the essential zinc ion of the ThrRS[77]? Alternatively, could it be indirectly involved, for example it could be responsible for iron binding allowing increased uptake of **1** via a Trojan-horse strategy? The results reported above suggest that **1** is more likely to be involved in a direct interaction as it seems that when analogues of **1** lacking hydroxyl groups on the catechol moiety are present inside the cell, but they are unable to inhibit the housekeeping enzyme, ThrRS.

3.4 Investigating the metal binding properties of the catechol moiety

Considering the well-established iron binding function of catechols,[32] we first wanted to test the ability of **1** to bind to iron using established Chrome Azurol S (CAS) assays.

These are colourimetric competition-based assays that test the ability of a ligand to bind to ferric iron. CAS solution is prepared which is bright blue in colouration due to a complex of CAS and hexadecyltrimethylammonium (HDTMA) ligands with Fe(III).[78] Upon addition of a competing ligand, a colour change from blue through pink to orange is observed as the compound disrupts the Fe(III)-CAS complex by binding Fe(III) and displacing CAS.[78]

I performed these assays with **1** and the catecholate analogues, **3**-**5**, as well as with DHBA and the building block compounds, 2-HBA, 3-HBA and BA. A significant colour change was observed for **1** showing that it exhibits strong ability to bind to Fe(III). A slight colour change occurred at the highest concentration of **3** but there is no colour change for the analogues **4** and **5** (Figure 3.5). This suggests that although the 2'-hydroxyl group seems to be more important, both hydroxyl groups are required for effective Fe(III) binding, i.e. the full catechol moiety is essential for this property. Therefore, Fe(III) binding ability correlates with bioactivity. Interesting, DHBA is a known siderophore,[79] yet appears to exhibit much weaker binding to Fe(III) than **1** suggesting that another functional group present in **1** contributes to its Fe(III) binding ability.

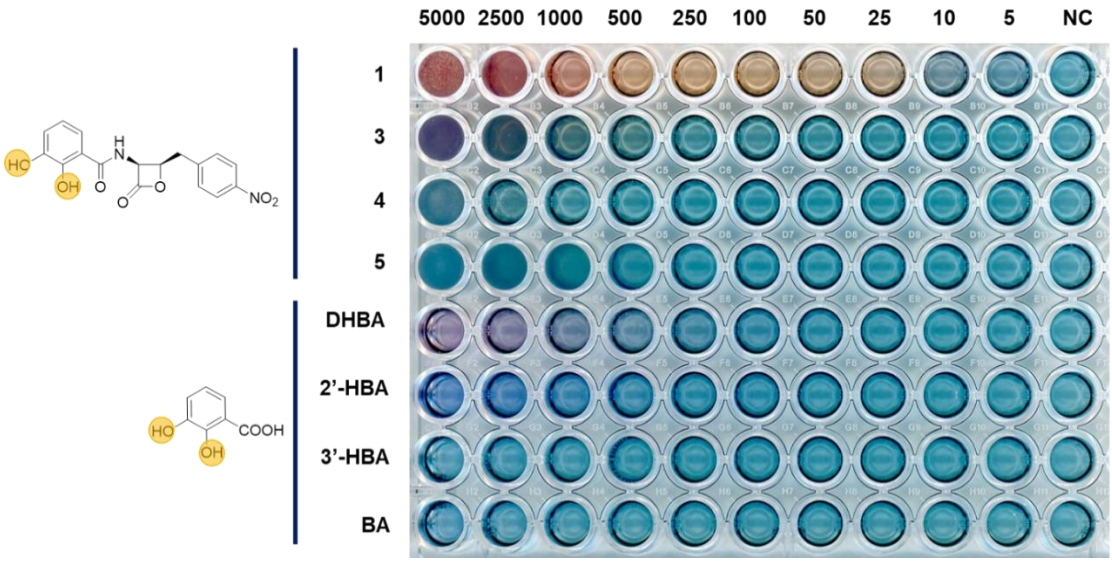

Figure 3.5: The catechol is essential for Fe(III) binding ability of 1. Chrome azurol S (CAS) assay monitoring the Fe(III) binding ability of **1**, the analogues **3**, **4** and **5**, and the building block compounds, DHBA, 2-HBA, 3-HBA and BA. Concentrations are in mM. NC (negative control) = 10% DMSO in CAS.

In addition to iron, we were also interested to test the zinc binding ability of **1**. This was due to knowledge of the presence of an essential zinc ion in the active site of the

ThrRS target enzyme,[77, 80] and the results of the Δ*obaL*Δ*obaO* time course experiments indicating the possibility of a direct interaction between **1** and ThrRS. We hypothesised that **1** could bind to the Zn(II) ion at the active site and block the threonyl adenosine monophosphate (Thr-AMS) native substrate from binding, therefore inhibiting the enzyme's activity.

To test this, I performed 4-(2-pyridylazo)-resorcinol (PAR) assays. These are similar dye displacement assays, like CAS, in which a colour change from orange to yellow is observed when PAR is displaced from the orange $Zn(PAR)_2$ complex as a compound is added that binds Zn(II).[81] For **1** and the analogues **3**-**5,** no colour change is observed confirming they exhibit no zinc binding activity (Figure 3.6). The building blocks show a colour change above a concentration of 1000 mM which is independent of the presence of both hydroxyl groups on the catechol suggesting that zinc binding by these compounds is mediated by the carboxylic acid group.

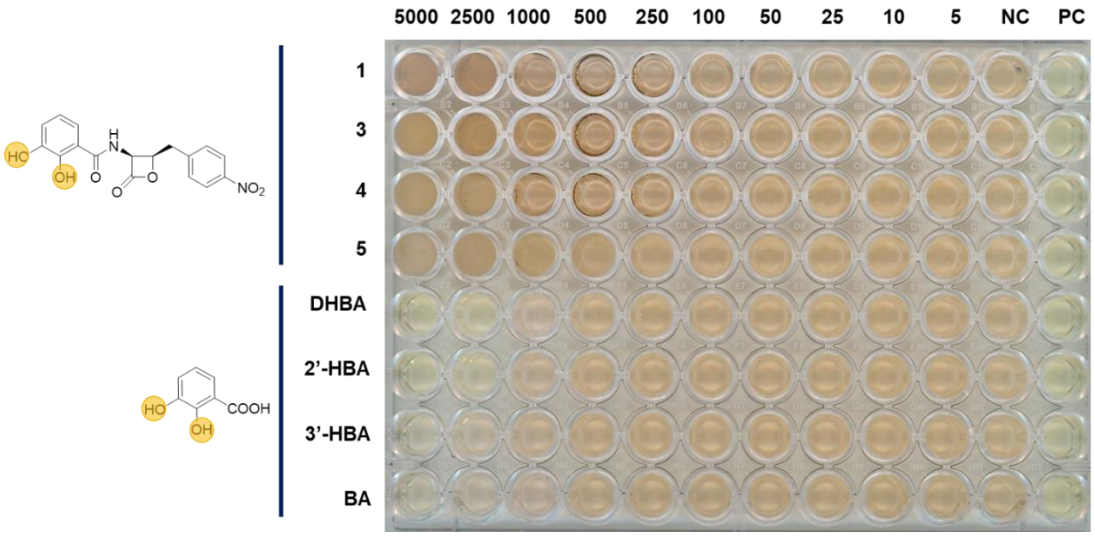

Figure 3.6: The catechol of 1 is not responsible for Zn(II) binding. PAR assay monitoring the Zn(II) binding ability of **1** and the analogues **3**, **4** and **5**, and the DHBA building blocks. Concentrations are in mM. NC (negative control) = 10% DMSO in $Zn(PAR)_2$ solution. PC (positive control) = 10% DMSO in PAR only solution.

3.5 Discussion

Access to the genomic data of *P. fluorescens* ATCC 39502 was vital for the identification of the **1** BGC and enabled the identification of function of the pathway's constituent enzymes. This knowledge was essential for rational design of the mutasynthetic approach described here to produce **1** catecholate analogues. Harnessing the strain's ability to produce this suite of compounds gave us the

opportunity to systematically assess the role of the catechol moiety in the mechanism of action of **1**.

We demonstrated the efficacy of a large-scale extraction and purification procedure to give access to **1** and its analogues **3**-**5** in ample quantities for further experiments. Spot-on-lawn bioassays showed an increase in MIC to 1000 µg/mL or above for catecholate analogues **3**-**5** and highlighted the importance of retention of both hydroxyl groups for the bioactivity of **1**. Feeding experiments with the *P. fluorescens* double mutant strain, Δ*obaL*Δ*obaO*, enabled us to indirectly assess the ability of these analogues to interact with the house-keeping copy (PfThrRS) of the target enzyme, ThrRS, in sensitive bacteria. Using HPLC to monitor compound production and OD_{600} to measure culture growth we showed that although the catecholate analogues could be produced inside the cell, the cultures were still able to grow essentially normally. Therefore, in contrast to **1**, it seems they are unable to inhibit the activity of ThrRS, suggesting that both hydroxyl groups on the catechol moiety are required for a direct interaction with the target enzyme. Biochemical metal binding assays showed that the catechol is responsible for a binding interaction between **1** and Fe(III), but not Zn(II), so it is unlikely that the direct interaction with the target enzyme is through binding the essential zinc ion at the active site.[77] The iron binding ability of **1** could implicate the role of the catechol to be involved in the mechanism of action of **1** via active uptake or as a Trojan-horse antibiotic.

In summary, the results of *in vivo* bioassays and biochemical metal binding assays have shown that the catechol moiety of **1** is essential for both its antibacterial and iron binding properties. Interestingly, they also highlight the correlation between these properties and lead us to further questions regarding why this may be. The requirement of the catechol moiety for metal binding ability and bioactivity and the indications that it is responsible for a direct interaction with ThrRS could suggest a dual role in its function. Perhaps iron binding results in enhanced uptake of **1** into the cell where, following an iron release mechanism, the catechol can form a specific interaction with the target enzyme leading to its inhibition.

This research underlines the importance of understanding the role of biosynthetic enzymes in NP pathways for the development of engineering strategies to structurally diversify their products. It also highlights the practicalities of using systematically designed analogues of NPs to further understand the role of structural components in their mechanism of action.

Chapter 4:

Characterising the obafluorin-iron interaction

Chapter 4 : Characterising the obafluorin-iron interaction

4.1 Introduction

The findings described in Chapter 3, namely the correlation between the bioactivity and iron binding properties of **1**, raised a series of questions that required investigation to further understand the role of the catechol moiety, and in turn, the iron binding role of **1** in its mechanism of action.

Studies concerning possible effects of iron bioavailability on antibiotic activity are relatively scarce and results are highly variable. This is largely due to the lack of standardised methods in the establishment of specific iron concentrations. Three distinct methods tend to be used; 1) addition of iron to the medium, 2) addition of the iron chelator, 2'2-biypydyl (bipy), to the medium,[41, 82, 83] 3) using specific genetic backgrounds which alter intracellular iron homeostasis.[84] However, there are multiple caveats concerning the accuracy of iron concentration control. Additional iron sources such as water and glassware may result in the actual concentration being different to that assumed, and alteration of iron concentrations may lead to pleotropic effects including inhibition of iron-containing proteins. Additionally, free iron can be toxic under aerobic conditions due to its ability to catalyse the formation of ROSs via the Fenton reaction, leading to oxidative stress.[30] The involvement of iron in essential cellular processes adds to the complexity of studies and can lead to ambiguous results.

This chapter details work conducted to unpick the role played by the iron binding properties of **1** in its antibacterial activity. As discussed, the **1**-Fe(III) complex could participate in 1) a direct interaction with the target enzyme, ThrRS, 2) a Trojan-horse mechanism where the **1**-Fe(III) complex is involved in active transport, or 3) a stability effect for the molecule. Additionally, it could be involved in a more complex mechanism involving more than one of these roles. Using both chemical and biological methods I aimed to understand the properties of the **1**-Fe(III) complex and evaluate differences in activity, uptake and production of **1** in varying iron conditions. By undertaking experiments using methods based on each of the three approaches that can be used to vary iron concentrations, a more holistic understanding of the system can be obtained.

4.2 Chemical characterisation of the 1-Fe(III) complex

My first aim was to chemically characterise the **1**-Fe(III) complex and investigate the binding mode and properties of the interaction. This will provide additional useful

information for experimental design of studies to investigate the biological role of **1**'s iron binding properties.

4.2.1 Single crystal X-ray diffraction (XRD)

CAS assays described in Chapter 3 show that the catechol is essential for iron binding but also suggested another group in **1**'s structure aids this moiety in formation of the complex. The 3D structure of the molecule demonstrates that the aromatic rings pi-stack to give a butterfly-like conformation,[55] so we hypothesised that the nitro group could be participating in this interaction as it is effectively pre-organised for binding. However, there is no literature precedent to suggest an aromatic nitro group could participate in binding to Fe(III), although there are several examples of NPs with this structural moiety.[85]

To characterise the binding mode, I aimed to obtain a crystal structure of the **1**-iron complex by single crystal X-ray diffraction. I set up crystal trials of solutions of the **1**-Fe(III) complex in a water, acetonitrile solvent system as was used by Tymiak *et al*.[55] Upon addition of a solution of Fe(III) ions to a solution of pure **1** dissolved in acetonitrile, a colour change to a deep blue solution is observed. After performing the experiment with other controls, the colouration was attributed to the formation of the **1**-Fe(III) complex. UV-visible spectroscopy showed a shift in absorbance from λ_{max} 270 nm for **1**, typical for π-π* transitions in catecholate compounds, to λ_{max} 590 nm. After slow evaporation from a pierced HPLC vial, crystals formed and were sent to the University of East Anglia for diffraction and structure solution, performed by Dr. Joseph Wright and Dr. David Hughes, respectively. Unfortunately, it was found that although the crystals formed from the bright blue **1**-Fe(III) solution, they were clear in colouration and there was no iron present in the 3D structure. Moreover, the structure obtained was identical to that reported previously by Tymiak *et al*.[55] (Figure 4.2). We also see coordination of an acetonitrile ligand to **1**, which along with previous observations such as the fading of the blue **1**-Fe(III) complex colour in acetonitrile solutions over time and detection of adduct peaks via mass spectrometry (Figure 4.3), suggests that acetonitrile can complex with **1** and outcompete iron.

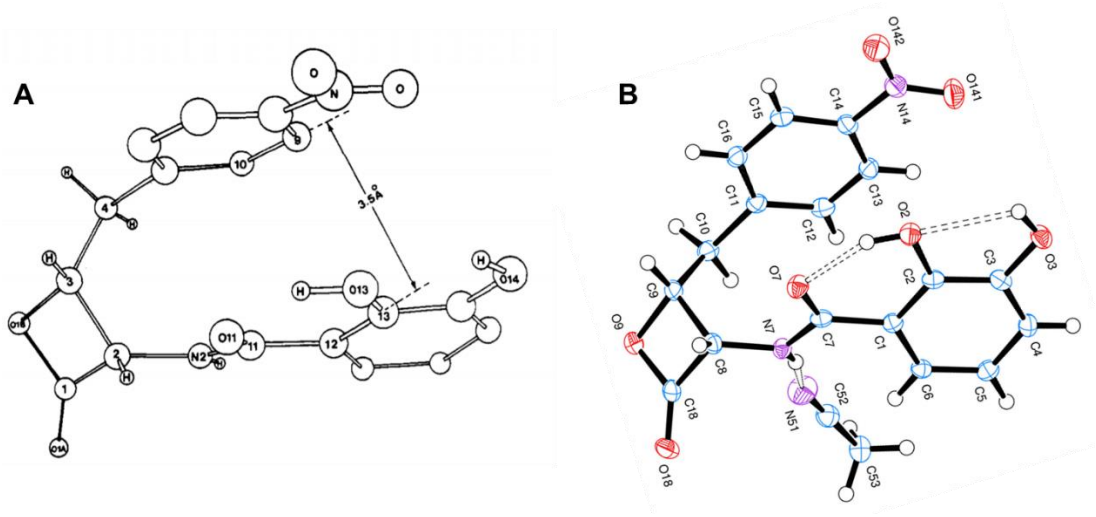

Figure 4.1: Single crystal X-ray diffraction structures of 1. A) Structure published by Tymiak et al.[55] with **1** in butterfly-like conformation. B) Structure recorded by Joseph Wright and David Hughes from the University of East Anglia showing **1** in the same conformation (here the acetonitrile ligand coordinating through hydrogen bonding with the amide proton N7**H** is shown).

This experiment shows that crystallisation of the **1**-Fe(III) complex will be unlikely in the presence of acetonitrile. However, further crystallographic trials were hindered by the solubility and stability of **1**; acetonitrile, ethyl acetate and DMSO are generally used as solvents. Unfortunately, methanol cannot be used as a solvent for **1** due to the nucleophilic nature of methanol which can react with the β-lactone forming the methylester. DMSO is not compatible with crystallisation trials using slow evaporation due to its high boiling point. I tried a variety of other solvent systems including ethyl acetate:hexane and acetone:water, but no further crystals were obtained. Additionally, to investigate the role of the nitroaromatic group, a hydrogenation reaction was attempted using H_2/palladium on carbon. However, instead of reduction of the nitroaromatic group of **1** leading to the corresponding aniline derivative, we observed a complex mixture of products, possibly due to intermolecular reaction of the aniline with the beta-lactone ring. Therefore, we have been unable to confirm whether the aromatic nitro group can aid the catechol moiety in Fe(III)-binding by this approach.

4.2.2 Mass spectrometry

To complement the CAS and PAR assays described in Chapter 3, I performed mass spectrometric analysis of **1** metal binding using electrospray ionisation mass spectrometry (ESI-MS), a soft ionisation technique which can be used to detect metal

ion complexes.[86, 87] Different metal ion salts were added in excess to a solution of **1** and the formation of a metal ion complex was monitored by direct injection HRMS. If **1** exhibits binding activity I expect to see depletion of the **1** $[M+H]^+$ peak and formation of a new peak corresponding to the **1**-metal ion complex. This experiment was performed with a selection of biologically relevant metal ion solutions: Fe(II), Fe(III), Zn(II), Mg(II) and Mn(II) and Ga(III). The results are shown in Table 4.1 and example spectra in Figure 4.3.

Table 4.1: 1 selectively forms a complex with Fe(III) detectable by MS. Results of ESI-HRMS experiments of samples of **1** incubated with biologically relevant metal ions recorded on a Synapt G2-Si MS. The base peak in the mass spectrum is shown and the mass shift from the $[M+H]^+$ peak in the **1** only sample. Species was determined from mass shift and isotopic pattern. Note the intensity and proportion of **1**:complex peak varies between repeats so only the base peak is shown for simplicity.

Sample	**Base Peak in MS / m/z**	**Mass shift from 1 $[M+H]^+$ / m/z**	**Species**	**Error, Δ / ppm**
1 only	359.0872	n.a	**1** $[M+H]^+$	**nd**
1 + Fe(II)	359.0879	/	**1** $[M+H]^+$	***/***
1 + Fe(III)	411.9980	52.9108	[**1**-2H+Fe(III)]$^+$	-3.40
1 + Zn(II)	359.0867	/	**1** $[M+H]^+$	***/***
1 + Mg(II)	359.0869	/	**1** $[M+H]^+$	***/***
1 + Mn(II)	412.0089	52.9217	[**1**-1H+Mn(II)]$^+$	-3.45
1 + Ga(III)	359.0879	/	**1** $[M+H]^+$	***/***
1 + mix	411.9992	52.9118	[**1**-2H+Fe(III)]$^+$	-0.47

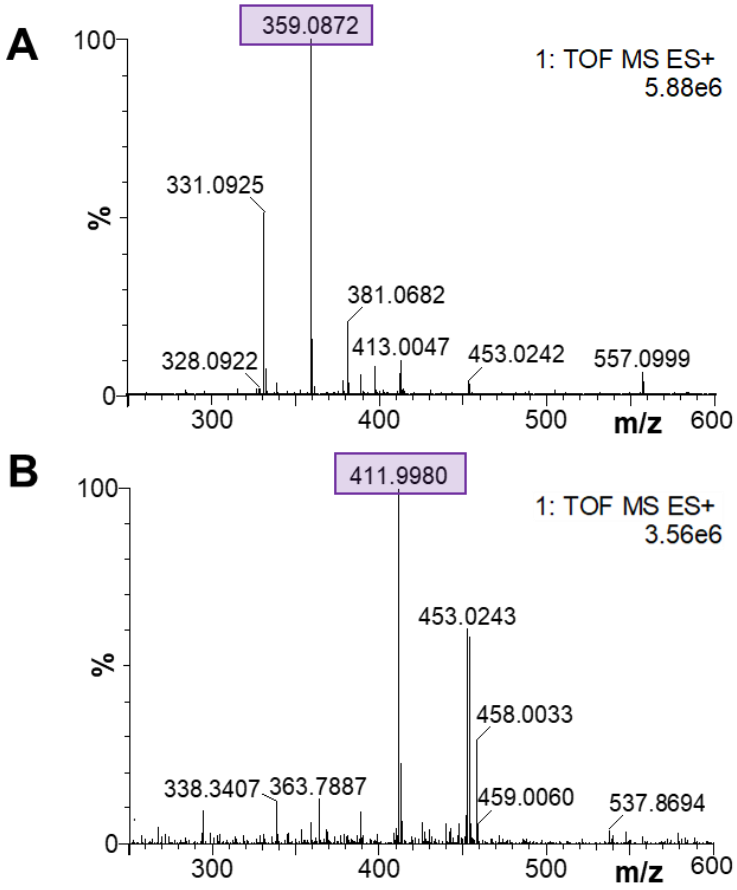

Figure 4.2: Example mass spectra showing formation of 1-Fe(III) complex detectable by MS. HRMS spectra shown between m/z 250 and 600 for samples of A) **1** only and B) **1** + Fe(III). Base peaks are highlighted in purple and correspond to $[M+H]^+$ and $[M-2H+Fe(III)]^+$, respectively. Note the peak at m/z 453.0243 matches the mass expected for the **1**-Fe(III) complex with an acetonitrile ligand bound. Note these experiments were performed using 1:1 **1**:metal ion concentrations and with an excess concentration of metal ion (the spectra shown above are the latter).

This shows that Fe(III) forms a complex with **1** under these experimental conditions; a mass shift was observed, from 359.0872 Da, **1** $[M+H]^+$, to 411.9980 Da which corresponds to [**1**-2H+Fe(III)]$^+$. This indicates that ferric iron binds to **1** via the deprotonated catechol, a motif seen often in catecholate siderophores.[42, 88, 89] A mass shift was also seen for solutions of Mn(II), which corresponds to the [**1**-1H+Mn(II)]$^+$ complex. In contrast to the Fe(III) solution, the peak corresponding to **1**-only was not fully depleted to give the **1**-Mn(II) complex peak, suggesting this could be a weaker complex. To test the selectivity of binding, I performed the same experiments with a mixture of the metal ions present in a single sample. Here, the base peak was 411.9992, corresponding to the [**1**-2H+Fe(III)]$^+$ complex with an error of -0.47 ppm,

suggesting that **1** selectively binds to Fe(III). These experiments confirm that **1** forms a strong interaction with Fe(III) that can be detected by using mass spectrometry.

4.2.3 Job's method for measuring complex stoichiometry by UV-visible spectroscopy

To further consolidate the MS experimental data that suggested the **1**:Fe(III) interaction is via a 1:1 stoichiometry the following experiments were carried out. Firstly, the λ_{max} of the **1**:iron complex was determined to be 690 nm in a 1:1 DMSO:water solvent system. This system was chosen due to the solubilities of **1** and $Fe(NO_3)_3.9H_2O$ in DMSO and water, respectively. Then, I performed spectrophotometric titration experiments where the concentration of compound relative to that of iron is varied and the formation of the complex is monitored by UV-visible spectroscopy. This is known as the Job's method of continuous variation.[90] Across a row in a 96-well-plate the proportion of **1**:Fe(III) was varied so wells 1 to 9 are increasing in mole fraction of **1**, with well 5 representing a mole fraction of 0.5 i.e a 1:1 mixture. The absorbance from each well at 690 nm was plotted against the mole fraction to generate a Job's plot as shown in Figure 4.4. An absorbance maximum is observed at a mole fraction of 0.5 which indicates that **1** forms a 1:1 complex with Fe(III), similarly to salicylic acid which was used as a positive control.

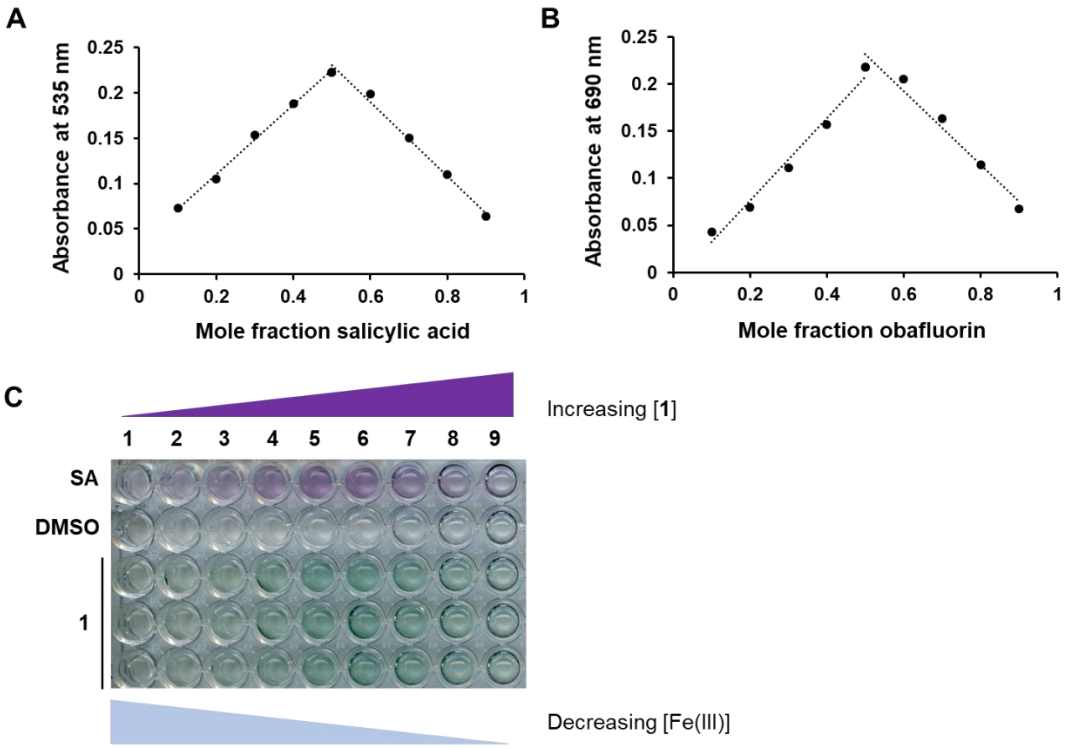

Figure 4.3: Job's plots for measuring iron complex stoichiometry via UV-visible spectroscopy. A) Salicylic acid (positive control) and B) **1** Job's plots show maximum

absorbance at λ_{max} of the respective complex at mole fraction 0.5, indicating a 1:1 ratio of compound:Fe(III). C) 96-well plate with increasing **1**:Fe(III) ratio from column 1-9 showing complex colouration. Rows are different compounds; SA, salicylic acid (positive control), DMSO only (negative control) and **1** in triplicate. The experiment was performed in triplicate and error bars are shown but are too small to be visible.

These results indicate that the **1**-Fe(III) complex has 1:1 stoichiometry. Binding of **1** to Fe(III) in this manner would not, however, give an octahedral ligand field around the central ion, as is preferentially adopted in complexes of Fe(III). I hypothesise that the other free binding sites are occupied by other ligands, likely water, or chloride ions in a biological system.

It is important to note here that assays of this type are usually performed in a buffered system.[91, 92] However attempts made to perform these experiments in HEPES or phosphate buffer at pH 7.0 and 6.4 resulted in the hydrolysis of **1**. The breakdown of the β-lactone of **1** is shown in Figure 4.5 and gives the ring-open, hydrolysed product which will be referred to as **6**. This reaction can be performed to isolate **6** from a solution of **1** as will be described in section 4.6.

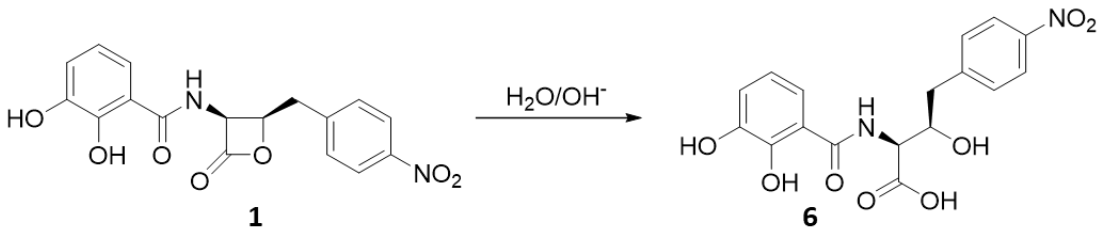

Figure 4.4: Reaction scheme of the hydrolysis of 1. The hydrolysis and ring opening of the β-lactone moiety of **1** to give its hydrolysed product, **6**.

The experiments trialled in a buffered system were set up identically to those described above with an increasing mole fraction of **1** from wells 1 to 9 across a row in a 96-well-plate. A variation in the colour of the complex was observed in wells 7, 8 and 9 so aliquots were taken immediately for HPLC analysis. This showed that **1** was stable to hydrolysis in wells with a higher proportion of Fe(III), but in wells 7, 8 and 9, where the proportion of Fe(III) is lower, **1** had hydrolysed to **6**, or had reacted with components of the buffer (Figure 4.6).

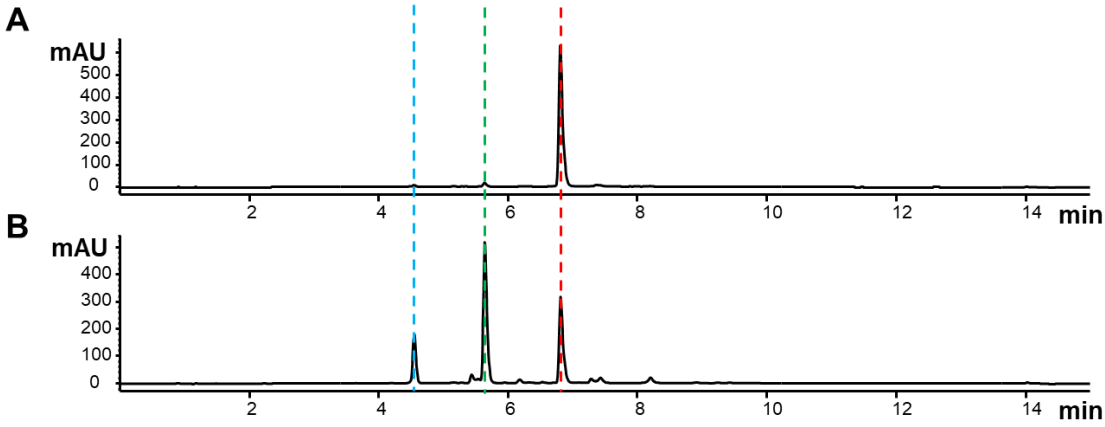

Figure 4.5: 1 is more susceptible to β-lactone ring-opening in lower Fe(III) concentrations. HPLC UV chromatograms at 270 nm from extracts of wells in the Job's plot stoichiometry experiments. A) Extract from well C5 = 1:1 ratio of **1**:Fe(III), showing **1** (highlighted with red line) as its stable ring-closed form. B) Extract from well C9 = 9:1 ratio of **1**:Fe(III), showing **1** has been hydrolysed to **6** (highlighted with green line) and reacted with buffer (highlighted with blue line and confirmed by LCMS; m/z of base peak corresponds to theoretical m/z of **1** covalently attached to buffer).

When the ratio of **1**:Fe(III) is 1:1, essentially no hydrolysis is observed. This suggests that, upon complexation to Fe(III), **1** is protected from hydrolysis. This was an interesting finding that I wanted to pursue, especially considering the susceptibility of **1** to hydrolysis noted by members of our lab,[59, 61] and others.[55, 93]

4.2.3 UV-Visible spectrophotometric titrations to determine 1-Fe(III) complex stability constant

After finding a concentration range of the **1**-Fe(III) complex suitable for these experiments by monitoring the colouration and so change in absorbance of the complex over a concentration range, I attempted to determine the stability constant of the **1**-Fe(III) complex. To do this, I used spectrophotometric titrations which are commonly reported for this purpose in the literature,[32, 94, 95] using ethylenediaminetetraacetic acid (EDTA) in a competition experiment. The principle is that as the EDTA-Fe(III) complex is colourless,[96] if EDTA is titrated into a solution of the **1**-Fe(III) complex, a colour change will be observed from deep blue to colourless, as EDTA outcompetes **1** for Fe(III) binding. The change in absorbance was monitored via UV-visible spectroscopy and, indeed, a trend of decreasing absorbance with increasing EDTA concentration was observed (Figure 4.7).

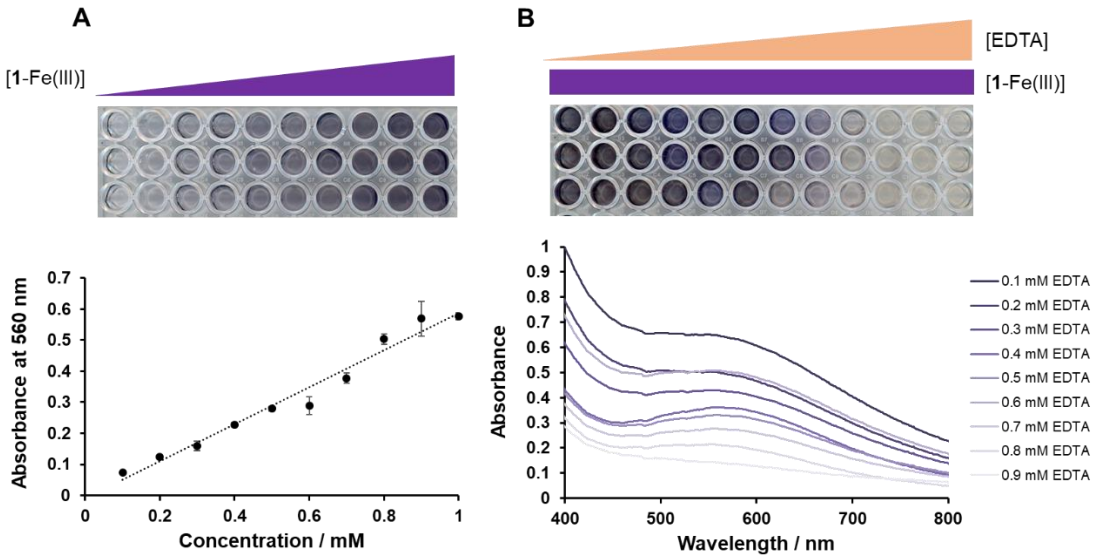

Figure 4.6: Spectrophotometric measurements of 1-Fe(III) and competition by EDTA. A) The change in absorbance at λ_{max} of the **1**-Fe(III) complex (560 nm in these conditions) with increasing concentration of the complex. B) A decrease in absorbance of the **1**-Fe(III) complex is seen with increasing concentrations of EDTA due to competition for Fe(III) binding.

Following these experiments, the results should be interpreted using the Beer-Lambert law, and should incorporate calculations of extinction coefficient, ε, and pKa values.[97] Generally, pKa values are determined via potentiometric titrations which involve addition of an acid/base,.[32, 96] and therefore are unsuitable for experiments with **1** due to complications with hydrolysis. This can be addressed in future work, for which the software, HypSpec, should ideally be used.[98]

4.3 Investigating the effect of Fe(III) on antibacterial activity of 1

With information gathered during characterisation of the **1**-Fe(III) interaction, I next aimed to understand the biological implications of the iron binding properties of **1**. To investigate the importance of this mechanism *in vivo*, I endeavoured to test the effect of iron in bioassays of **1** against representative Gram-positive (*S. aureus*) and Gram-negative (*E. coli* 25922 and *P. aeruginosa*) organisms. To do this, I performed spot-on-lawn antibacterial bioassays with additional Fe(III) added to the media.

Firstly, I performed a range of bioassays with increasing concentrations of Fe(III) added to the media (from 500 μM – 2 mM) against *E.coli* 25922 and *P. aeruginosa*. Unexpectedly, a drastic decrease in the MIC of **1** is observed with increasing

concentrations of Fe(III) above 500 µM (Table 4.2). At concentrations below 500 µM, no effect on the MIC of **1** was observed.

Table 4.2: Minimum inhibitory concentrations (MICs) of 1 against *E. coli* 25922 and *P. aeruginosa*. Determined from spot-on-lawn bioassays performed with increasing concentrations of Fe(III) added to the media.

	1 MIC / µg/mL	
Fe(III) added / mM	***E. coli* 25922**	***P. aeruginosa***
0.0	256	256
0.5	128	64
1.0	32	4
1.5	2	2
2.0	0.5	1

To clearly show this change in the MIC of **1** in the presence of additional Fe(III), I performed bioassays without Fe(III) supplementation and compared these to bioassays performed with the addition of the highest concentration of Fe(III) before growth defects of the indicator strain were observed (2 mM for E. coli 25922 and 1.5 mM for *P. aeruginosa*). The results are shown in Figure 4.8.

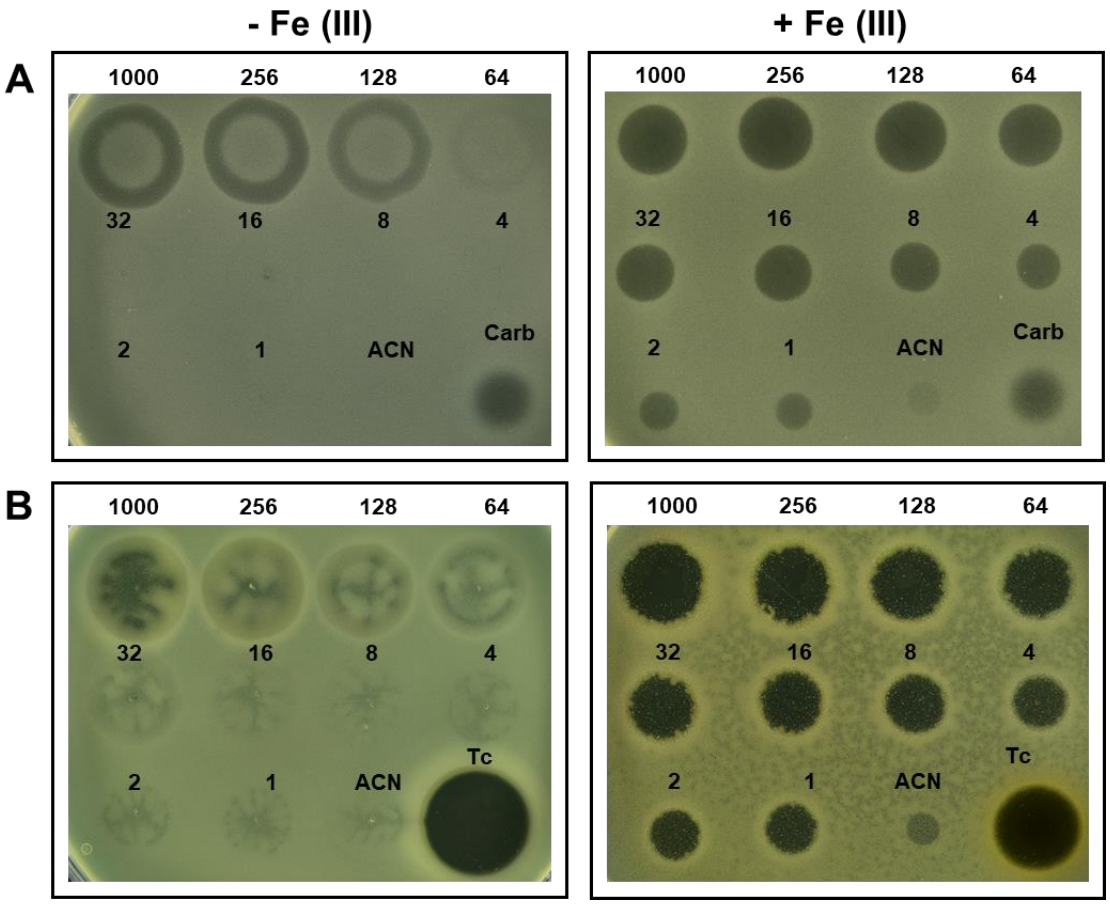

Figure 4.7: The presence of additional Fe(III) increases the bioactivity of 1 against Gram-negative strains. Spot-on-lawn bioassays of **1** against A) reference strain *E. coli* 25922 in the absence of Fe(III) supplementation vs. with additional Fe(III) added to growth media (2 mM), B) a clinical isolate of *P. aeruginosa* in the absence of Fe(III) supplementation vs. with additional Fe(III) added to growth media (1.5 mM). Zones of clearing indicate inhibition of growth. Numbers indicate concentrations of **1** (in µg/mL). Acetonitrile (ACN) was used as a negative control and carbenicillin(Carb)/ tetracycline (Tc), (1000 µg/mL), was used as a positive control for *E. coli* 25922/ *P. aeruginosa* respectively.

The addition of Fe(III) resulted in a drastic decrease in the MIC of **1** against *E. coli* 25922, from 256 to 2 µg/mL and from 256 µg/mL to 1 µg/mL for *P. aeruginosa* (Figure 4.8). I used carbenicillin and tetracycline as controls as they gave an inhibition zone against *E. coli* 25922 and *P. aeruginosa*, respectively, in bioassays performed in conditions both with and without addition of Fe(III). These results clearly show that the addition of Fe(III) has a significant effect on the antibacterial activity of **1** against Gram-negative organisms.

Next, I wanted to test the effect of addition of 2 mM Fe(III) on the MIC of **1** against the Gram-positive organism, *S. aureus*. Firstly, however, I wanted to test whether the decrease in MIC seen with additional Fe(III) is also seen with other antibiotics, as well as **1**. Therefore, to investigate whether the effects observed are **1**-dependant, I tested a concentration range (from 50 to 5000 µg/mL) of commonly used antibiotics against *E. coli* 25922 and *S. aureus* in normal conditions versus excess iron (2 mM). As I was looking for differences in activity profiles between normal and excess iron conditions, I did not test concentrations all the way down to MIC. I also used high concentrations after previously observing decreased antibacterial activity of other antibiotics in the presence of additional Fe(III). The results are summarised in Table 4.3, from which I can conclude that this effect observed for **1** upon addition of iron is not observed to as great an extent for other antibiotics.

Table 4.3: Changes to antibacterial activity of antibiotics with additional Fe(III). The lowest concentrations tested of a range of antibiotics which gave an inhibition zone against *S. aureus* and *E. coli* 25922 in bioassay conditions with and without additional Fe(III) (2 mM).

	Lowest concentration of antibiotic tested which gave an inhibition zone against the indicator strain / µg/mL			
	S.aureus		***E. coli* 25922**	
Antibiotic	**- Fe(III)**	**+ Fe(III)**	**- Fe(III)**	**+ Fe(III)**
Carbenicillin	50	50	1000	1000
Kanamycin	50	500	50	250
Streptomycin	50	500	50	100
Nitrofurantoin	500	250	500	100
Chloramphenicol	1000	250	1000	500
Apramycin	50	1000	50	1000

For the antibacterial assays with *S. aureus*, I chose to use carbenicillin as a control as its bioactivity did not seem to be affected by the Fe(III) in the media, concluded from the results above. The effect of 2 mM Fe(III) on the MIC of **1** against *S. aureus* is not as great as was observed for the Gram-negatives, but a decrease in the MIC of **1** is also observed; from 16 to 2 µg/mL (Figure 4.9).

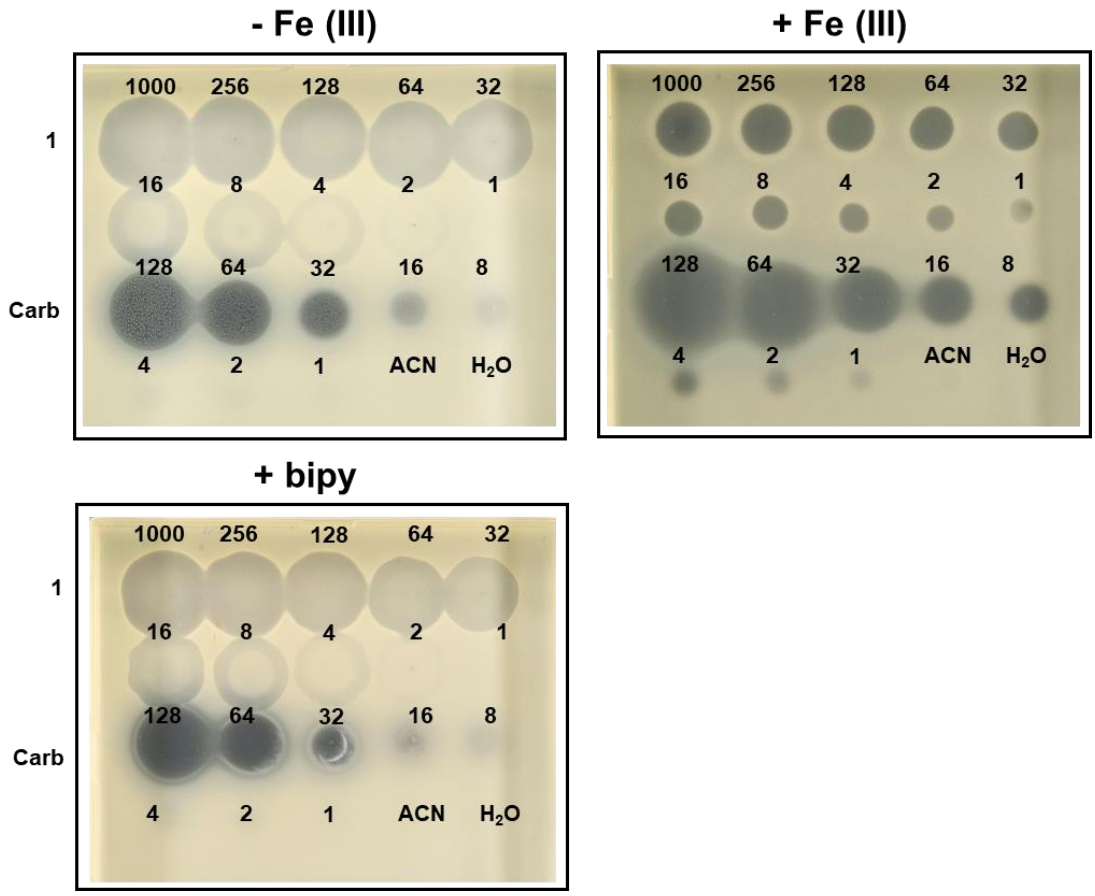

Figure 4.8: The effect of increasing and decreasing Fe(III) concentration on the MIC of 1 against MSSA. Spot-on-lawn bioassays of **1** against reference strain methicillin sensitive *S. aureus* (MSSA) in normal conditions vs. with additional Fe(III) (2 mM) or bipy (150 μM) added to growth media. Zones of clearing indicate inhibition of growth. Numbers indicate concentrations of **1** (in μg/mL). Carbenicillin is used as a control antibiotic which should exhibit the same MIC in each condition (but note here we see a decrease in MIC with additional Fe(III)). Acetonitrile (ACN) and water were used as negative controls.

However, here it is important to note that a decrease in MIC of carbenicillin was observed with additional Fe(III), as well as for **1**. Also, I noted that for the spots with the highest concentrations of **1** on the bioassay plates containing additional Fe(III), it is possible to see a purple colouration with the naked-eye. These results suggest that the formation of the **1**-Fe(III) complex occurs *in situ* and increases the bioactivity of the antibiotic. There are several hypotheses for why this may be: the **1**-Fe(III) complex could 1) directly partake in an interaction with ThrRS (assuming this complex is stable once inside the bacterium for long enough to have an effect and seems unlikely); 2) be involved in an iron acquisition mechanism as a siderophore or THA; 3) provide increased stability for the molecule leading to an enhanced effective concentration;

or 4) some combination of 1-3. Several strands of the data supported so far suggest that it could be involved in a stability effect by protection of the molecule against hydrolysis. However, I first investigated the second hypothesis.

4.4 Testing the ability of 1 to act as a siderophore or Trojan-horse antibiotic

To test the ability of **1** to act as a THA, I performed bioassays of **1** against *E. coli* 25922 in iron depleted conditions by addition of 2,2'-bipyridyl (bipy), a chelator added to diminish the concentration of free iron. For THAs a decrease in MIC is observed upon iron depletion as the indicator strain actively transports the THA-Fe(III) complex into the cell.[33, 99-101] However, upon the addition of 150 μM bipy to the growth media, no change in the MIC of **1** was observed compared to normal assay conditions, suggesting **1** is not acting as a THA.

To confirm this, I acquired the archetypal *E. coli* strain BW25113, and a set of its mutants, Δ1-6, in which each of the six siderophore TonB-dependent transporters (TBDTs), FhuA, FecA, CirA, FepA, FhuE and Fiu are progressively deleted as reported by Grinter *et al.*[41] It has been shown that Cir and Fiu are responsible for the uptake of catecholate containing compounds,[84] including THAs,[33] so I hypothesised that **1** could be utilising these membrane transporters if a THA uptake mechanism was involved in its activity. Upon iron depletion using the addition of bipy, no change in MIC was observed for Δ3, the strain deficient in FhuA, FecA and CirA, showing that none of these transporters are used for uptake. Unfortunately, Δ6, the strain deficient in all the TBDTs including Fiu, is unable to grow in iron deplete conditions. However, these results support our hypothesis that **1** does not act as a THA and show that it does not use FhuA, FecA or CirA transporters for uptake. Given the observations above, I also performed bioassays against these strains in the presence of excess Fe(III), and again I observed a drastic decrease in MIC of **1** with excess iron. (Table 4.4). These results are inconsistent the hypothesis that **1** can act as a THA.

Table 4.4: 1 does not act as a THA. Minimum inhibitory concentrations (MICs) of *E. coli* 25922, BW25113 and siderophore TonB dependent transporter (TBDT) knock-out mutants, Δ3 and Δ6. Δ3 = ΔFhuA,FecA,CirA and Δ6 = ΔFhuA,FecA,CirA,FepA,FhuE,Fiu). Determined from spot-on-lawn bioassays in normal conditions vs. iron depleted (+ 150 μM 2,2'-bipyridyl) and iron excess (+ 2 mM Fe(III)) conditions. Note the strain Δ6 is unable to grow in iron depleted conditions.

	1 MIC / μg/mL		
Organism	**Normal conditions**	**Iron depleted**	**Iron excess**
***E. coli* ATCC 25922**	256	256	2
***E. coli* BW25113**	256	256	2
***E. coli* BW25113 Δ3**	256	256	2
***E. coli* BW25113 Δ6**	256	/	2

Following this, I was interested to investigate whether **1** acts as a siderophore for iron acquisition in the producing organism, *P. fluorescens*. I performed bacterial growth experiments in which OD_{600} and the production of **1** was monitored in iron deplete and replenished conditions. If a compound functions as a siderophore, a concomitant increase in its production would be observed upon iron limitation, functioning to aid iron uptake and growth of the producing organism.[32] However, an increased concentration of bipy resulted in both reduced production of **1** and reduced *P. fluorescens* growth. Inversely, increasing the concentration of Fe(III) added to the media led to an increase in the production of **1** and related metabolites which was not simply due to enhanced growth of the organism as additional Fe(III) had no significant effect on OD_{600} (Figure 4.10). Interestingly, I also noticed an increase in the proportion of **1** compared to its hydrolysis product, **6**, as the concentration of Fe(III) increased. These results suggest that **1** does not act as a siderophore but is consistent with the hypothesis that Fe(III) binding protects **1** from hydrolysis.

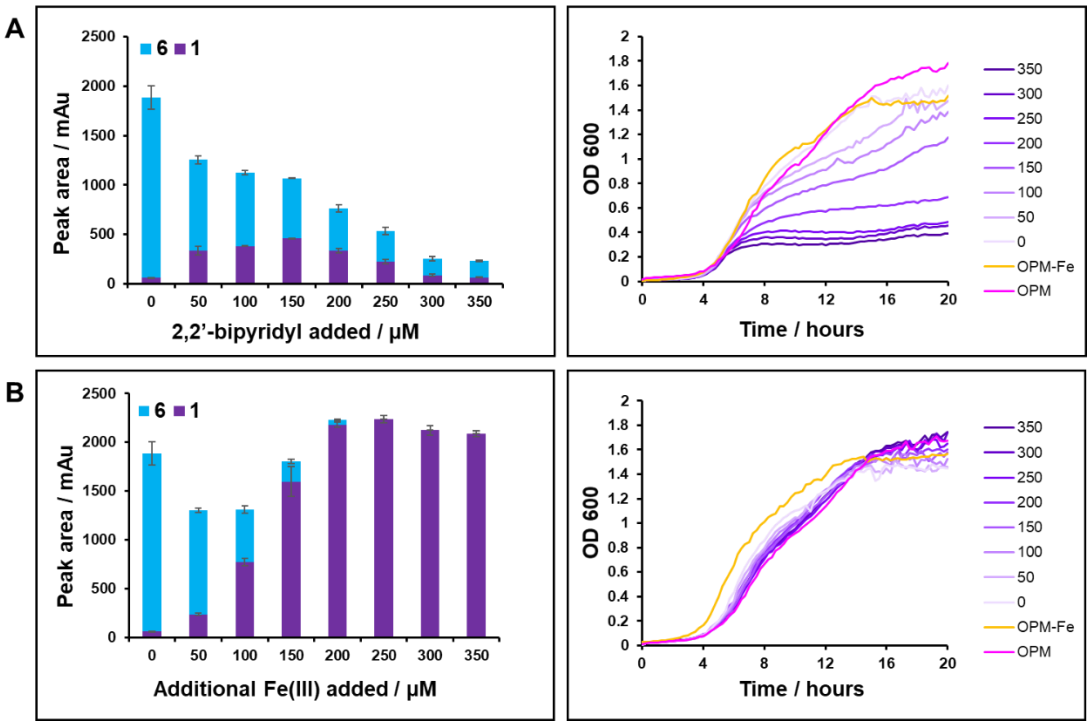

Figure 4.9: 1 does not function as a siderophore for *P. fluorescens*. The effect of A) iron depletion by addition of 2,2'-bipyridyl and B) iron replenishment by addition of $FeNO_3.9H_2O$ on metabolite production and growth of *P. fluorescens* was measured. The production of obafluorin, **1**, and its hydrolysis product, **6**, by *P. fluorescens* was monitored by measuring their respective peak areas at 270 nm from aliquots of cultures extracted after 14 hours of growth. The growth of the strain was monitored by UV-visible spectroscopy at OD_{600}. Experiments were performed in triplicate and the average values for peak area and OD_{600} are plotted.

During this experiment I noticed the colouration of the cultures changes with an increasing concentration of Fe(III); the purple colouration of the **1**-Fe(III) complex is increasingly prominent as Fe(III) concentration increases. However, this does not affect the OD_{600} measurements; comparable readings were seen for *P. fluorescens* Δ*obaL* cultures grown in the same concentrations of Fe(III), but these do not have any purple colouration due to their inability to produce **1**.

4.5 The hydrolytic breakdown of 1 and its limitation by Fe(III) binding

As we had shown the catechol moiety is essential for the Fe(III)-binding property of **1**, and following several indications that Fe(III)-binding could protect the β-lactone moiety of **1** from hydrolytic breakdown, I aimed to definitively test this by HPLC. I performed timed HPLC experiments where I prepared each sample (1 mg/mL samples of **1** buffered from pH 6.0 – 8.0) to give a 30-minute room temperature

incubation period before injection onto the HPLC column. This experimental set up ensured that analysis was performed at the same time-point for each sample, enabling a comparison to be made. The hydrolytic breakdown of **1** to **6** was monitored by comparing their relative peaks at 270 nm in HPLC chromatograms. As shown in Figure 4.11, the hydrolysis of **1** to **6** is pH dependent, with a higher proportion of **1** remaining stable to nucleophilic attack and β-lactone hydrolysis at lower pHs. To note here is that I chose a concentration of **1** of 1 mg/mL to ensure that, even upon breakdown to **6**, the concentrations would be sufficient to give detectable absorbance levels.

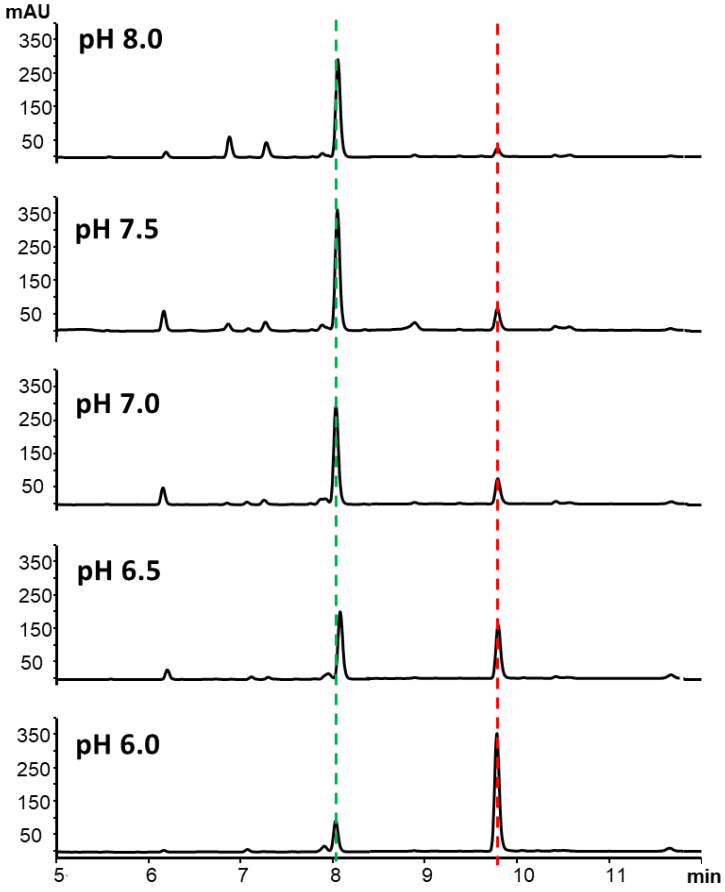

Figure 4.10: 1 hydrolysis with pH. UV chromatograms at 270 nm of solutions of **1** incubated in Tris buffer pH 6.0-8.0. The red and green dashed lines represent **1** and **6** respectively.

Next, I performed similar experiments in order to monitor the hydrolysis of **1** in comparison to the catecholate analogues, **3**-**5,** at pH 8.0 (the pH at which we see maximum hydrolysis) with and without the addition of Fe(III). A solution of compound or 1:1 compound:Fe(III) was incubated for 30 min at room temperature then analysed by HPLC. The proportion of ring-closed versus the hydrolysed product was

determined for each compound by analysis of the corresponding peak areas at 270 nm. This is shown in Figure 4.12.

Without the addition of Fe(III), the majority of **1** has hydrolysed to **6** or reacted with buffer components. But, when Fe(III) is present, approx. 92% remains as ring-closed **1**, indicating that binding to iron is protecting the β-lactone moiety from hydrolysis. Conversely, for the analogues **2** and **3** I do not see this effect, as would be expected due to the fact that the compounds are unable to bind to Fe(III). Unexpectedly, for compound **4**, which lacks both hydroxyl groups on the catechol moiety, no hydrolysis was observed, even in the absence of Fe(III). This might indicate that the hydroxyl groups themselves participate in the hydrolysis reaction which is consistent with observations made by others during synthetic studies of **1**. Pu *et al*. proposed that hydrolytic breakdown of **1** could be catalysed by basic impurities in samples, aided by a catecholate anion that enhances the attack by water to form a tetrahedral intermediate.[93] This could also explain why **1** has greater resistance to hydrolysis in weakly acidic conditions when the catecholate hydroxyls are protonated. Similarly, perhaps upon binding to iron, the catechol moiety participates in this interaction (as we know both hydroxyl groups are required for this) rendering it unable to catalyse the intramolecular hydrolysis reaction. The theoretical pKa values of the phenolic groups were calculated using MarvinSketch,[102] and are 8.30 and 11.92 for the 2' and 3' hydroxyl groups of the catechol moiety, respectively.

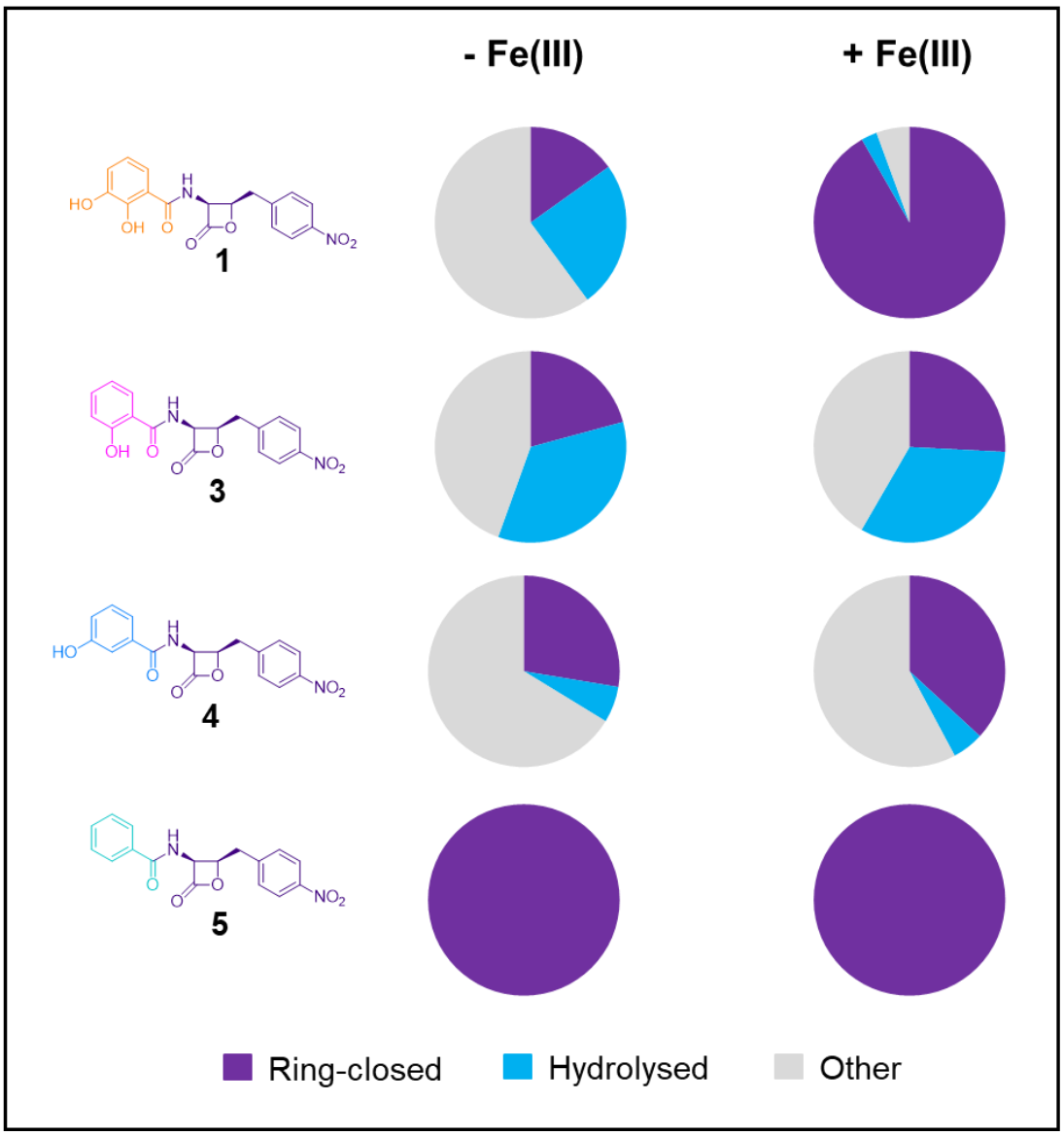

Figure 4.11: The catechol moiety is required to bind Fe(III) to protect 1 from hydrolysis. A representation of peak area data from HPLC UV chromatograms at 270 nm monitoring the hydrolysis of **1** and the catecholate analogues, **3**, **4** and **5** after incubation for 30 min with or without Fe(III). The proportion of ring-closed lactone (purple) is shown compared to the hydrolysed product (blue) and other compounds with absorbance at 270 nm (grey). LCMS analysis of the "other" compounds was consistent with them being products of reaction with buffer components – a peak with mass corresponding to **1**/analogue covalently attached to HEPES buffer was observed.

Further attempts were made to characterise hydrolysis of **1**. I performed HPLC experiments to characterise the rate of hydrolysis of **1** compared to one of the

catecholate analogues, **3**. Samples were taken regularly from the reaction which was conducted in an HPLC vial in the machines autosampler.

To achieve this, I also shortened the HPLC run time to obtain the maximum number of data points before complete breakdown of the compound. This was performed at a range of pH's from 6.0-8.0 to assess the effect of pH on the reaction.

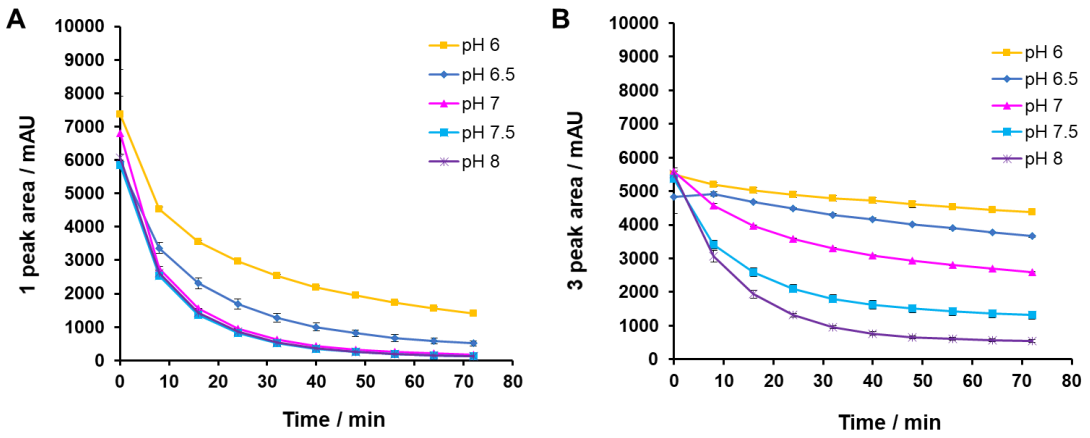

Figure 4.12: Effect of pH and catechol on β-lactone hydrolysis. Plots of peak area of A) **1** and B) the catecholate analogue **3**, against time after preparation of samples at a range of pH's (from 6.0-8.0). Data was collected in duplicate and analysed from UV chromatograms at 270 nm. Error bars are displayed (note an outlier data point for the pH 6.0, time=0 sample for **3** was removed). This was performed with 1 mM samples incubated at 25 ˚C.

These experiments were complicated by the reactivity of the compounds; they do not simply participate in a single hydrolysis reaction to the hydrolysed β-lactone products, they also react with buffer components (as determined by LCMS). Therefore, due to multiple reactions occurring, it was not possible to calculate rate constants for the hydrolysis reaction. However, a clear trend was observed. The peak area of parent compound decreases with time and with increasing pH meaning that ring opening of the lactone moiety occurs more easily at higher pH (Figure 4.13). For **1**, the pH effect only manifests itself below pH 7.0. In contrast, for **3**, an effect was observed at every change of pH and, overall, **3** was less prone to ring opening reactions than **1**. This could suggest that the ring-opening reactions are base catalysed, however for **1**, concentration of hydroxide ions is not the rate-limiting factor above pH 7.0. The main conclusion from these experiments, is that the rate of breakdown of the β-lactone ring increases with pH.

I also performed growth experiments to test whether the purple colouration of *P. fluorescens* cultures was due to the formation of the **1**-Fe(III) complex.

I set up cultures in normal production media (OPM) which contains 0.1 g/L $FeSO_4$ and production media with the $FeSO_4$ removed (OPM-Fe). After incubation for 14 hours under the standard conditions, I observed the absence of the characteristic purple colouration for cultures grown in OPM-Fe. I took extracts of these cultures for HPLC analysis which showed that, consistently with my earlier observations, in the cultures grown in OPM-Fe, the majority of **1** produced had been hydrolysed to **6** (Figure 4.14). To test whether addition of Fe(II) or Fe(III) would restore the culture colouration I added aliquots of stock solutions of each metal ion to give a final concentration equal to that of OPM (0.1g/L). Upon addition of Fe(II), a grey/purple colour change was observed over a period of ~30 minutes. However, upon addition of Fe(III), the colour change was observed immediately. These results show the colouration of the cultures is due to a complex with Fe(III). The slow colour change upon addition of Fe(II) must be due to *in situ* oxidation of the metal ions to Fe(III) in the cultures. The colouration of the cultures is shown in Figure 4.14.

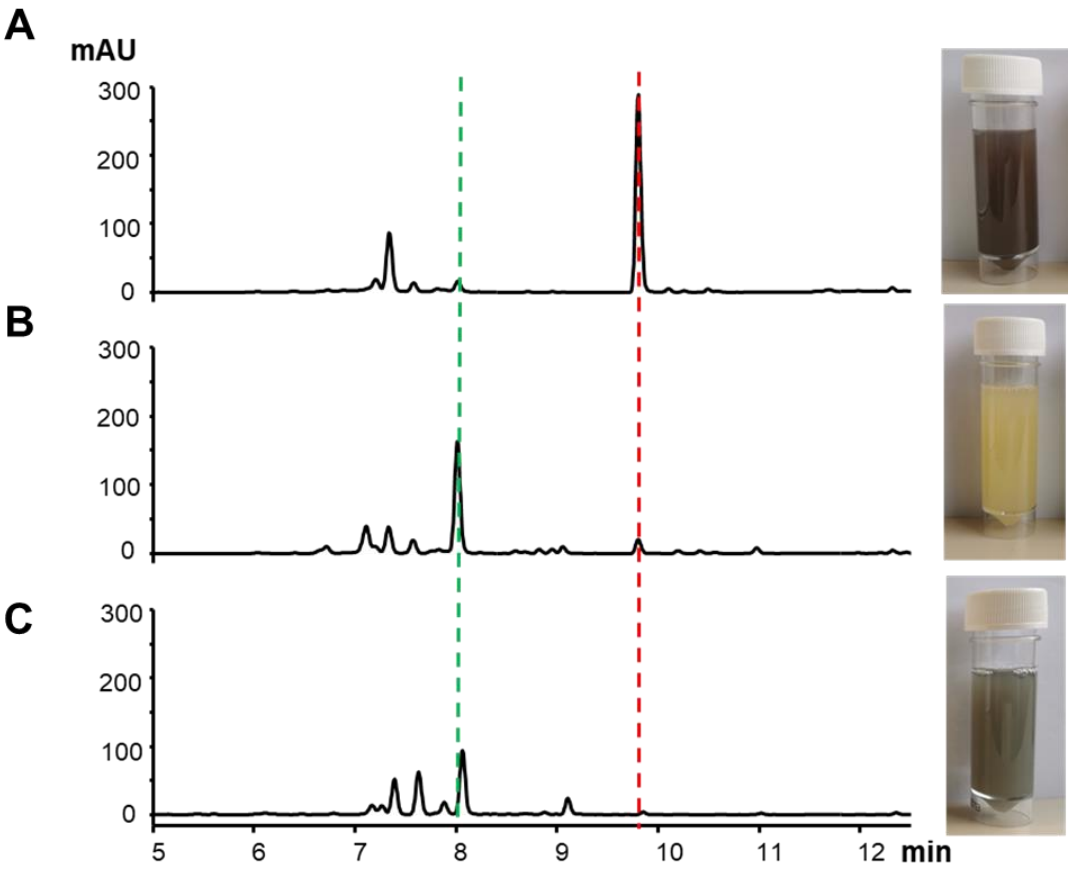

Figure 4.13: Fe(III) binding gives culture colouration. HPLC UV chromatograms at 270 nm from aliquots of *P. fluorescens* ATCC 35902 grown in A) obafluorin production media (OPM), B) OPM without iron (OPM-Fe), C) OPM-Fe which was supplemented with the equivalent concentration of $FeCl_3$ present in OPM after culture growth. The red and green dashed lines represent **1** and **6** respectively.

4.6 The β-lactone ring of 1 is essential for bioactivity

After results showing the susceptibility of the hydrolysis of the β-lactone moiety of **1** to hydrolysis to give **6**, and the protection effect upon binding to Fe(III), we wanted to investigate the properties of **6**. To do this, I hydrolysed an aliquot of **1** by simply stirring it in aqueous NaOH (0.05 mM) solution for 3 hours at room temperature then extracted **6** using liquid-liquid extraction with ethyl acetate. The first question to answer was, is it important to retain the β-lactone moiety for bioactivity as had been suggested previously? To probe this, I performed spot-on-lawn bioassays of **6** against a set of typical indicator strains; MRSA, *B. subtilis*, *E. coli* 25922 and *E. coli* NR698. MICs of **6** against these strains are shown in Table 4.5, with the MICs of **1** for comparison.

Table 4.5: The β-lactone of 1 is essential for full bioactivity. The minimum inhibitory concentrations (MICs) in μg/mL of compound **6** (hydrolysed β-lactone) and **1** against various indicator strains; methicillin-resistant *Staphylococcus aureus* (MRSA), *Bacillus subtilis*, *E. coli* 25922 and membrane permeabilised *E. coli* NR698.

Compound	**MIC / μg/mL**			
	MRSA	***B. Subtilis***	***E. coli* 25922**	***E. coli* NR698**
6	128	1000	>1000	1000
1	4	8	128	4

The MIC of **6** against MRSA is 128 μg/mL, so exhibits a distinctly weaker ability to inhibit the growth of this organism than **1** which shows an MIC of 4 μg/mL. These results show that the β-lactone of **1** is essential for a full spectrum of bioactivity.

Further to this, I also wanted to test the metal binding properties of **6** so I performed CAS and PAR assays with this compound. These showed that **6** can bind Fe(III) to a similar extent to **1** and is able to bind Zn(II) above a concentration of 1 mg/mL (Figure 4.14).

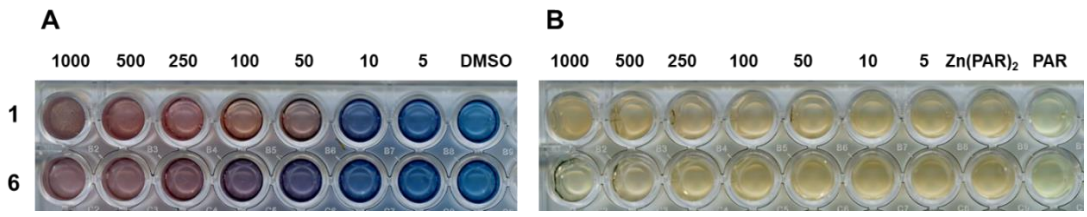

Figure 4.14: Metal binding assays of 6 with 1 shown for comparison. A) Chrome azurol S (CAS) assay monitoring the Fe(III) binding ability of **1**. 10% DMSO in CAS is used as a negative control. B) 4-(2-pyridylazo)-resorcinol (PAR) assay monitoring the Zn(II) binding ability. 10% DMSO in $Zn(PAR)_2$ solution is a negative control. 10% DMSO in PAR only solution is used as a positive control to show yellow colouration. Concentrations are in μg/mL.

4.6 Discussion

By application of chemical and biochemical techniques we have been able to gain insight into the biological role of the iron binding property of **1**. Chemical characterisation experiments gave additional information on the binding mode and properties of the **1**-Fe(III) complex. CAS assays described in Chapter 3 showed that the catechol moiety of **1** is essential for iron binding, with the 2'-hydroxyl group being

more important than the 3'-hydroxyl for the interaction (**3** can bind Fe(III) weakly at the highest concentrations tested). Further work showed that **1** selectively forms a complex with Fe(III) compared to a range of biologically relevant metal ions including Fe(II) and Ga(III); Ga(III) shares chemical properties with Fe(III) and is known to act as an Fe(III) mimic.[103] The **1**-Fe(III) complex can be detected by MS, which shows a shift in mass from 359.0872, **1** $[M+H]^+$, to 411.9980, **1**-Fe(III) $[M-2H+Fe(III)]^+$, Δ -3.40 ppm. MS experiments also showed that **1** seems to form a complex with Mn(II) through deprotonation of a single hydroxyl group on the catechol moiety. However, the proportion of **1**-only to **1**-complex peaks in **1**-Mn(II) and **1**-Fe(III) spectra, and the formation of the **1**-Fe(III) complex from a sample containing a mixture of the metal ions suggests that the **1**-Fe(III) complex presides. The masses observed by MS indicated the formation of a 1:1 **1**:Fe(III) complex which was confirmed by UV-visible spectroscopy using the Job's method of continuous variation.[92] A deep blue colouration is attributed to the formation of the **1**-Fe(III) complex, which is responsible for the characteristic colouration of **1**-producing *P. fluorescens* cultures. Several observations made during these experiments suggested the **1**-Fe(III) binding interaction could provide a stability enhancing effect by protecting **1** from hydrolysis.

Attempts were made to examine the structural binding mode of the complex via single-crystal XRD. Although the crystallographic solution was of **1**-Fe(III), unfortunately, no Fe(III) was present in the crystal structure. The structure solved was identical to that described by Tymiak *et al*.,[55] with **1** captured in a butterfly-like conformation due to pi-stacking interactions between the aromatic ring systems. An acetonitrile ligand is coordinating through hydrogen bonding with the catecholamide proton N7**H**. This and the fading of the blue colouration of solutions of **1**-Fe(III) observed in solvent systems containing acetonitrile leads us to hypothesise whether acetonitrile could be involved in competitive binding between Fe(III) to **1**. If this is the case, it could also give more information on the binding mode of Fe(III) to **1**. Therefore, considering the binding mode of acetonitrile to **1** via the catecholamide proton, I investigated the importance of this group in Fe(III)-binding interactions in the literature. Interestingly, the binding mode of Fe(III) to enterobactin has been characterised to show the catecholamide is important. At neutral pHs, the catechol is protonated and the 2'-hydroxyl proton participates in a hydrogen bonding interaction with the amide oxygen atom. Upon deprotonation, the confirmation changes to the trans form where the amide proton instead hydrogen bonds with the 2'-hydroxyl oxygen atom (Figure 4.15).[42]

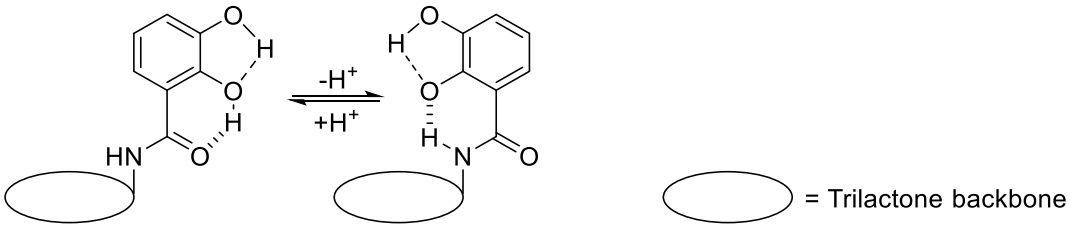

Figure 4.15: The conformational change of the catecholamide group in enterobactin's structure. This is driven by hydrogen bonding following deprotonation. Figure adapted from Raymond et al.[42]

It could be proposed that **1** acts in a similar way; upon deprotonation a conformational change occurs so the amide proton hydrogen bonds to the 2'-hydroxyl oxyanion of the catechol, preorganising the structure to adopt a conformation where it is able to bind Fe(III). This is an interaction mediated by the catechol hydroxyl groups but must be aided by another part of the structure (due to the fact **1** is better able to bind Fe(III) than DHBA), either the β-lactone or the aromatic nitro group. UV-visible spectroscopy experiments confirmed the stoichiometry of the **1**-Fe(III) complex is a 1:1 complex. This is a further indication that another group, in addition to the catechol and likely coordinated water molecules, must participate in Fe(III) binding, as to fulfil the octahedral field preference of Fe(III) ions.[32]

After characterisation of the **1**-Fe(III) complex, I aimed to understand the biological role of the iron binding properties of **1**. Firstly, I performed bioassays with additional Fe(III) to test whether the presence of additional Fe(III) would affect the MIC of **1** against several indicator strains. Indeed, a drastic decrease in the MIC of **1** was observed in the presence of additional Fe(III), and the effect is particularly clear for the Gram-negative bacteria, *E. coli* and *P. aeruginosa*. This was shown to be a **1**-specific effect as a decrease in antibacterial activity with additional Fe(III) was not seen for a series of other structurally varied antibiotics. This was an intriguing observation that suggested the **1**-Fe(III) complex may be relevant to the mechanism of action of **1** in some way. Specifically, could it: 1) directly partake in an interaction with ThrRS, 2) partake in an iron acquisition mechanism as a siderophore or THA, or 3) provide a stability effect for **1,** increasing its effective concentration?

To probe this, I first performed experiments to test whether the **1**-Fe(III) complex could be involved in active transport via a THA mechanism. I performed bioassays of **1** against *E. coli* in normal vs. iron depleted conditions (via the addition of bipy) in which you should see an increase in MIC if the antibiotic is a THA.[99] However, I saw no change in MIC with addition of bipy, indicating **1** does not act as a THA. To confirm

this, I also used *E. coli* BW25113, and mutants Δ3 and Δ6, in which the first 3 or all of the siderophore TBDTs, FhuA, FecA, CirA, FepA, FhuE and Fiu are deleted, as indicator strains. Again, I observed the same effect; no change in MIC upon addition of bipy. In fact, I saw the same effect as observed previously in that upon addition of extra Fe(III) to the media a drastic decrease in the MIC of **1** was observed. These experiments suggest that **1** does not act as a THA, perhaps as the molecular weight of the complex is small enough not to require active transport across the cell membrane. To note here is that the MIC of **1** against membrane permeabilised *E. coli* NR698 is 4 μg/mL, close to that of **1** against *E. coli* 25922 in bioassays with additional Fe(III), 2 μg/mL. This fact and the data described above suggest that the effect of Fe(III) is due to increasing the effective concentration of **1** *in situ* by protecting it against hydrolysis. Alternatively, the binding to Fe(III) could aid in uptake via passive transport. Therefore, I suggest this effect is more significant against Gram-negatives due to their membrane permeability barrier.

Next, I tested whether **1** acts as a siderophore for the producing organism, *P. fluorescens* by performing growth experiments with addition of increasing concentrations of Fe(III) or bipy. I showed by HPLC and OD_{600} measurements that depleting the concentration of available iron in the media (by addition of bipy) the production of **1** and related compounds decreases, as does the growth of *P. fluorescens*. This shows that **1** does not act as a siderophore, as you would expect the inverse to be true if this was the case. Conversely, with the addition of extra Fe(III) to the media, the production of **1** and related compounds increases with no significant effect on growth to the organism. Interestingly, the proportion of **1** vs. the hydrolysed product, **6**, also increases with additional Fe(III) indicating a stabilising effect is occurring.

After several observations that Fe(III) binding increases the stability of **1**'s β-lactone against hydrolytic breakdown, I investigated this using HPLC. Indeed, we saw a notable protection effect with Fe(III). This was only the case for **1**, the analogues **3** and **4**, we saw no significant difference in proportion of ring-closed compound to hydrolysed product with Fe(III). However, **5** was stable to hydrolysis at pH 8.0, supporting the hypothesis of Pu *et al*. that the catechol hydroxyl groups (particularly the 2'-hydroxyl) are involved in intramolecular catalysis of the hydrolysis reaction.[93] Finally, I tested the importance of the β-lactone of **1** remaining intact for bioactivity by performing bioassays with the hydrolysed compound, **6**, and found that it is essential for the full spectrum of bioactivity.

Overall, this chapter highlights the importance of investigating both the chemical and biological properties of metal complexes to gain a more complete understanding of their role in a biological system. The evidence suggests the Fe(III) binding property of **1** is not involved in an active transport mechanism and instead suggests that its main role could be provision of a stabilising effect to the molecule.

Chapter 5:

Analysis of the mode of action of obafluorin

Chapter 5 : *In vitro* analysis of the mechanism of action of obafluorin

5.1 Introduction

Following the delineation of the **1** BGC by mutational analysis[59] and identification of the target of **1** as ThrRS,[61] attention turned to mechansim of action studies. A variety of biochemical techniques can be applied to unpick the mechanism of drug inhibition. X-ray crystallography can provide a definitive snapshot of the interaction of an inhibitor and its target protein, as can mass spectrometry (MS) which is a highly valuable technique that can be applied to identification of protein-covalent adducts. This area of MS is often termed “adductomics” and studies can be further classified into two main areas. 1) Targeted, which focuses on the identification of covalent adducts upon exposure to a specific chemical agent and 2) untargeted, which aims to comprehensively characterise the total covalent conjugates bound to a specific nucleophilic residue of a protein.[104] As covalent adducts have great impact in health problems such as cancer and autoimmune diseases,[105] it is essential to identify the biochemical nature of covalent conjugates to understand the molecular events underlying diseases. Additionally, understanding covalency as a drug strategy will enable us to better our position to treat such diseases.

Targeted adductomics has been applied to identify the specific residue of covalent attachment of β-lactone inhibitors on their target proteins. Using a “bottom-up” methodology to analyse the tryptic peptides by high resolution liquid chromatography mass spectrometry (HR-LCMS) it is possible to identify which amino acid of a peptide is covalently modified by a molecule of specific mass.[104, 106] The residue of covalent modification of tetrahydrolipstatin (Orlistat) was found to be Ser^{152}, the active site serine residue of its target protein, pancreatic lipase.[107] Homoserine transacetylase, a key enzyme in the methionine biosynthetic pathway, is inhibited by β-lactones, including ebelactone A, through covalent attachment to Ser^{143} which forms part of the Ser-His-Asp catalytic triad. This demonstrates the power of MS for understanding the mechanism of β-lactone inhibitors.

Using mass spectrometric strategies applied to understand the mechanism of β-lactone inhibition we proposed a sequence of experiments to investigate the **1**-ThrRS interaction. Firstly, the EcThrRS target protein would be analysed by MS before and after incubation with **1**. By comparing the intact mass spectra, we should be able to identify a shift corresponding to the mass of **1** (358 Da) showing that it is covalently

attached to the protein. Subsequently, the sample would be proteolytically digested with trypsin to give a series of peptide fragments which can be analysed by liquid chromatography tandem mass spectrometry (LC-MS/MS). These would then be analysed against a database to enable the identification of a specific target residue of covalent modification by **1** based on differences between expected and observed peptide masses and fragmentation patterns. A schematic representation of this process is shown in Figure 5.1.

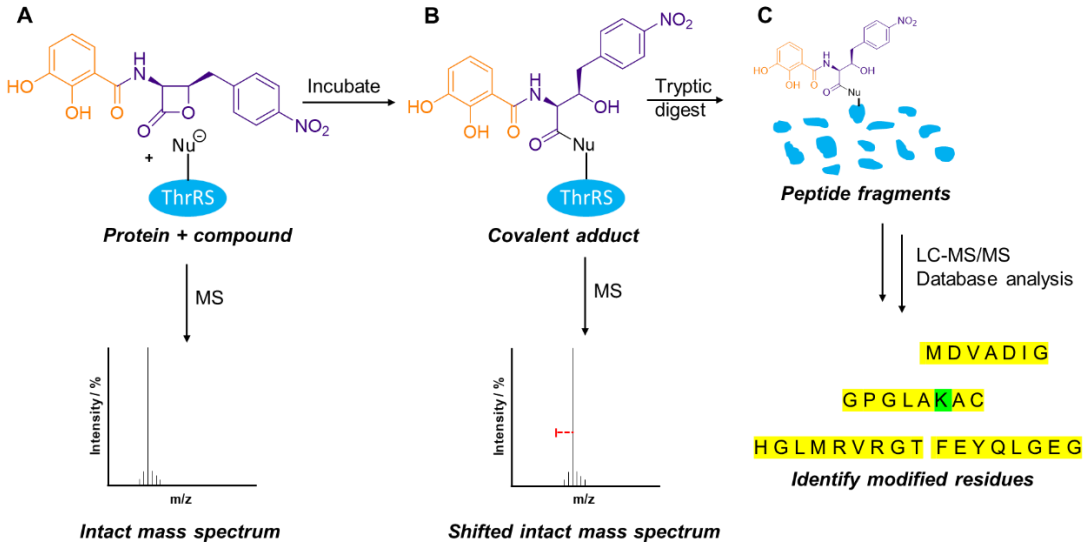

Figure 5.1: Schematic representation of experimental flow to identify target residue of covalent modification in protein-covalent adduct interaction. A) Enzyme (ThrRS) is analysed by mass spectrometry to give intact mass spectrum of unmodified enzyme. B) After incubation with compound (**1**) a covalent adduct forms which is analysed by MS to show a shift in mass corresponding to the mass of the compound. C) After digestion of the adduct complex, liquid chromatography - tandem mass spectrometry (LC-MS/MS) is used to detect a series of peptides which are analysed against a database (derived from the unmodified parent protein) to find a mass shift of a specific target residue of covalent modification (highlighted in green).

Additional methods to characterise the mode of action of antibiotics can use the innate ability of bacteria to respond and adapt to threats. Due to the selection pressure of the presence of antibiotic molecules produced by competing species in Nature, bacteria have evolved the genetic adaptability to generate antibiotic resistance.[108] There are a variety of resistance mechanisms including mutation of the target gene, rendering the antibiotic unable to execute its mechanism of action.[109] By growing an indicator strain in the presence of antibiotic over several generations it is possible to select for resistant mutants. These bacteria can be genetically analysed via genome

sequencing to identify changes in the DNA of the target gene, encoding for resistance. It is therefore possible to harness this natural mechanism to identify the mechanism of action of antibiotic activity. This approach was used to define the mechanism of quinolone antibiotics, including ciprofloxacin, which inhibit the DNA gyrase or topoisomerase IV enzymes and therefore inhibiting the activity of the bacterial replication fork. Mutations in the GyrA subunit of gyrase or the ParC subunit of topoisomerase IV result in amino acid changes that reduce the affinity of quinolones to their target enzymes.[108-111] Using this approach to identify antibiotic mechanism of action has been attempted previously by the Wilkinson group and it was hypothesised that this approach could be used to investigate the mode of action of **1**.

5.2 Using mass spectrometry to investigate the 1-ThrRS interaction

The first question to address was whether we would see a shift corresponding to the mass of covalently attached **1** in the intact mass spectrum of the target enzyme. I repeated this experiment multiple times with both full length EcThrRS and ΔN-EcThrRS, an N-terminally truncated version of the protein. The tryptic digest and mass spectrometric analysis were performed by Carlo de-Oliveira Martins from the proteomics facility at John Innes Centre.

EcThrRS/ΔN-EcThrRS was readily expressed as a soluble protein in a hexahistidine-tagged form in *E. coli* NiCo21(DE3):pLysS and purified using Ni-affinity and subsequent size exclusion chromatography. This was then incubated with **1** and analysed by MS. To note here is that these experiments were performed in pH 8.0 buffer to maintain protein stability. I observed variable results, most commonly multiple modifications of the full length or N-terminally truncated EcThrRS enzyme, ΔN-EcThrRS. (Figure 5.2). These results indicate that multiple molecules of **1** (up to four) are capable of binding to the enzyme under these conditions. The mass differences between sequential additions are not always exactly the mass of **1** (358 Da), this could be due to proton rearrangements during nucleophilic attack and covalent attachment to the protein. Alternatively, the chosen conditions in the sample preparation method could have influenced these results; the emission of a washing step after addition of **1** to protein and the excess concentration of **1** could result in adduct formation. However, I believe this to be unlikely due to the susceptibility of **1** to hydrolysis in the sample preparation conditions, as will be discussed later.

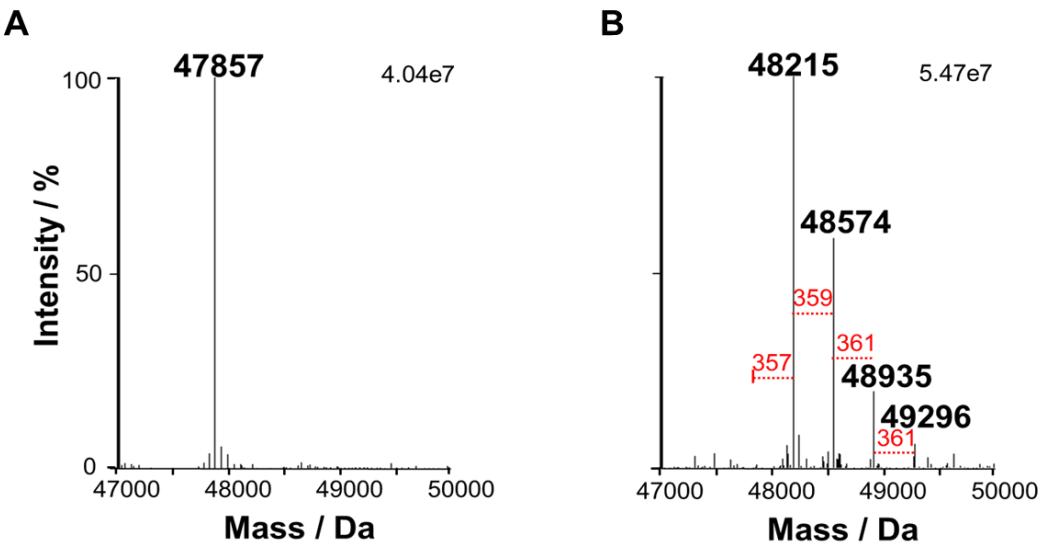

Figure 5.2: 1 covalently binds to ΔN-EcThrRS. The ESI HRMS spectrum of a) ΔN-EcThrRS only showing a mass of 47857 Da, and b) ΔN-EcThrRS incubated with **1,** showing complete consumption of the native mass and modification by the masses shown in red. This corresponds to modification of the enzyme with multiple molecules of **1**.

Following this, the samples of **1**-treated enzyme (or untreated for comparison) were digested with trypsin to give a series of peptides which were analysed by tandem MS. By adding a variable modification of the mass of **1** at the nucleophilic residues of cysteine, lysine, serine, threonine and tyrosine residues to a Mascot[112] database, the mass differences of peptide fragments were used to define amino acids modified by **1** in EcThrRS. These results were verified using Scaffold software and deemed significant if above a 95% confidence threshold.

Similar to the intact mass experiments, we observed highly variable results, with a **1**-modification (peptide mass shift of 358 Da) detected on residues in the protein which were inconsistent between repeats. These experiments indicated that **1** could be acting as a general acylating agent *in vitro*. To probe this, I performed the same experiment with ObaO protein, the partially resistant copy of ThrRS from *P. fluorescens* ATCC 39502, which might be expected to bind **1** but likely in a different way to a sensitive ThrRS; I also included ObaG, a L-threonine transaldolase enzyme[59] from the biosynthetic pathway which we would not expect to bind to **1**, as a negative control. These proteins were expressed and purified in essentially the same way as EcThrRS. SDS-PAGE gels are shown in Figure 5.3.

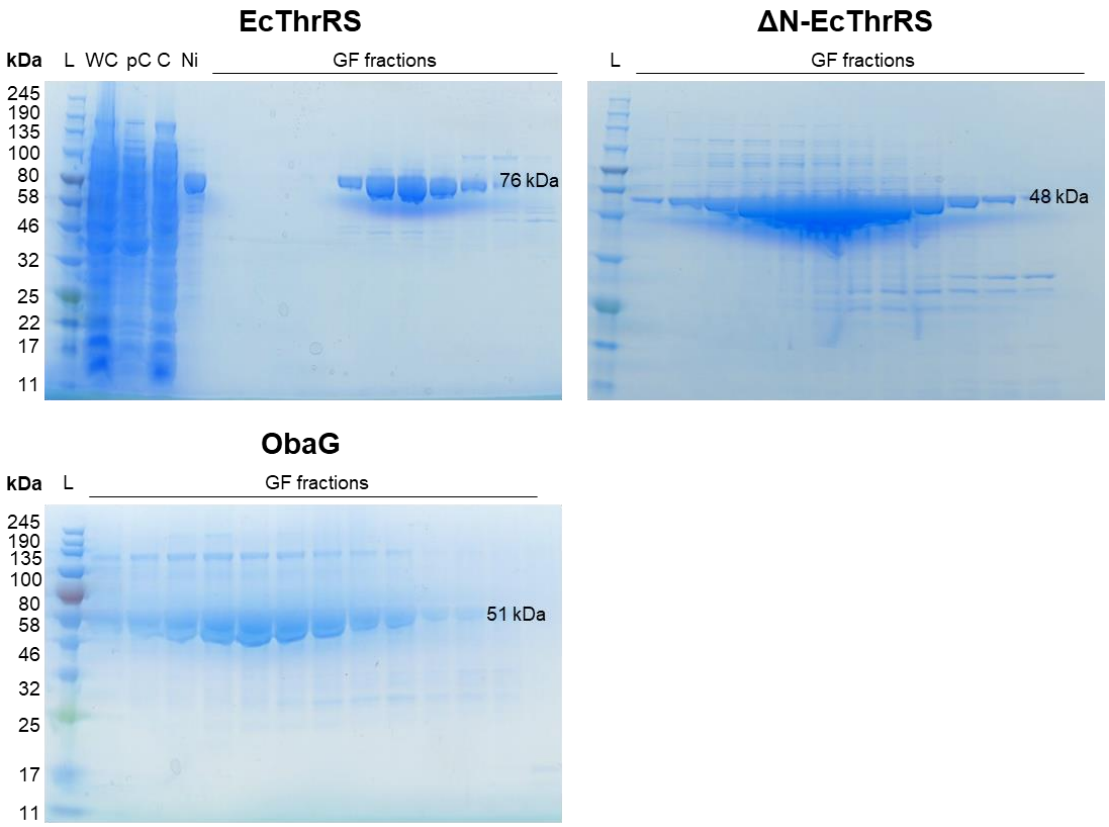

Figure 5.3: 12% SDS-PAGE gels of purified proteins. Fractions collected from size exclusion chromatography of His_6-EcThrRS, His_6-ΔN-EcThrRS and His_6-ObaG. Samples from previous purification steps are shown for EcThrRS. L = ladder (Colour Prestained Protein Standard, Broad Range (NEB), WC = whole cell lysate, pC = pre-chitin wash, C =chitin wash eluent, Ni = Ni-affinity purified sample. The expected molecular weights for His_6-EcThrRS, ΔN-EcThrRS and ObaG are 76, 48 and 51 kDa respectively.

EcThrRS, ObaO and ObaG were all found to be modified by **1** at variable residues, mainly lysines, indicating that **1** is binding non-specifically *in vitro*. Therefore, it was not possible to identify a single consensus residue which is modified by covalent attachment of **1** in EcThrRS by mass spectrometry. The Scaffold results of these experiments for EcThrRS and ObaO are shown in Figure 5.4.

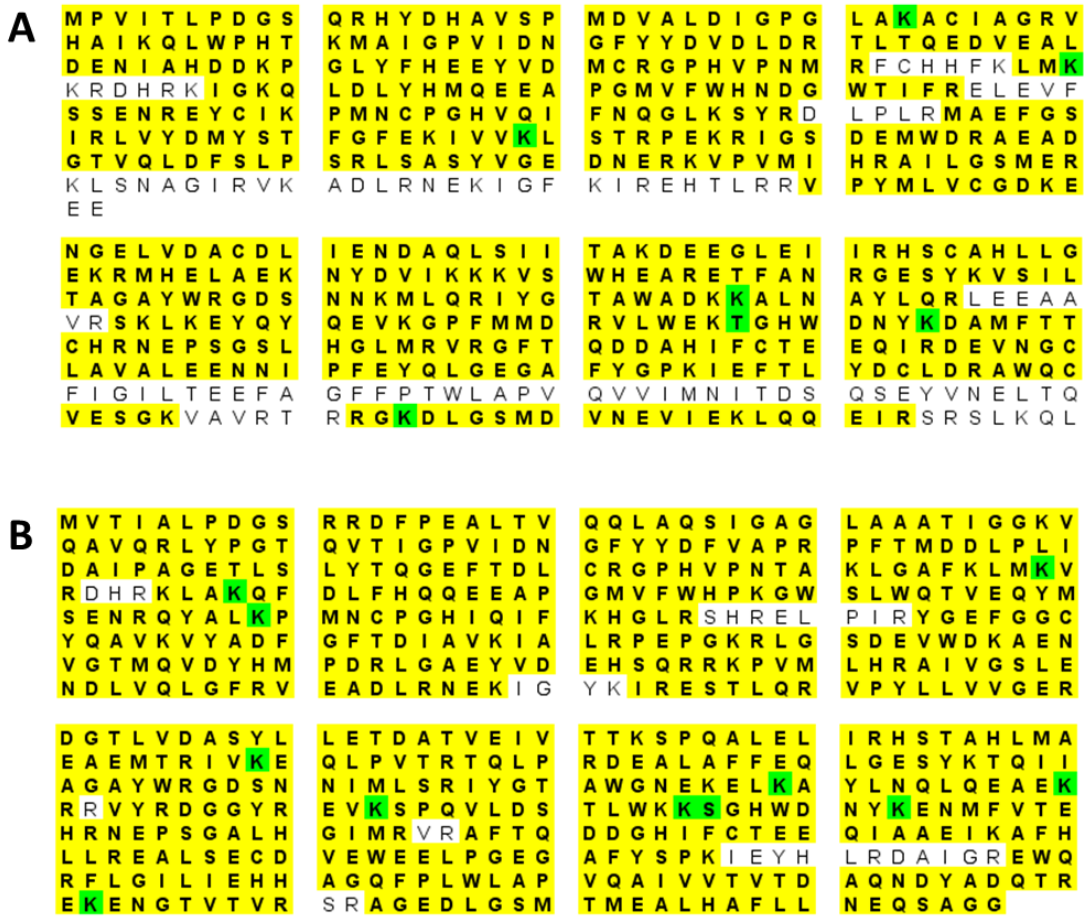

Figure 5.4: 1 binds to multiple variable lysine residues of ThrRSs. Examples of results from LC-MS/MS experiments of tryptic digest peptides of A) EcThrRS and B) ObaO proteins incubated with **1.** The sequences of the proteins are shown, highlighted in yellow are the amino acids in peptide sequences that were detected by MS. Residues which have been detected with a **1** covalent modification (mass shift of 358 Da) are highlighted in green.

Additionally, there are various reasons, apart from the reactivity of **1** *in-vitro*, that could provide explanation for these results. It is quite possible that the observation of multiple lysine modifications at random sites within the proteins could be due to the experimental conditions selected. For example, due to 1) exposure of the proteins to high concentrations of **1**; 2) prolonged reaction times; 3) protein destabilisation and unfolding leading to exposure of buried lysine residues. Therefore, these experiments will require optimisation if further investigations are attempted in the future.

5.3 QuikChange™ mutagenesis

To test whether the modification of these lysine residues in the ThrRS protein is involved in the mechanism of action of **1**, or simply an artefact of the reactivity of **1** in

in vitro experiments. I performed site-directed mutagenesis experiments of EcThrRS. After analysing all the Mascot results to find residues that were consistently modified in runs of the same protein, I chose three lysine residues of EcThrRS, K200, K314, K419, that were identified with a **1** modification in multiple experimental repeats. Using the QuikChange™ PCR protocol I mutated these three residues to alanine in pJH10TS-EcThrRS, a vector for the expression of EcThrRS in *Pseudomonas* and *E. coli* strains that was created by Dr. Thomas Scott[59]. To monitor whether these mutations are significant in the sensitivity of EcThrRS to **1**, I used the plasmids to transform *P. fluorescens* Δ*obaL*Δ*obaO*. This strain lacks ObaL and cannot biosynthesise DHBA; this means it cannot produce **1** unless DHBA is added exogenously. However, this strain also lacks the immunity determinant ObaO, and therefore upon addition of DHBA the strain cannot grow, but both growth and **1** production are restored when the *obaO* gene is complemented *in trans.*[61] Thus, if any of the K to A mutations introduced into EcThrRS confer resistance to **1**, then when expressed in *P. fluorescens* Δ*obaL*Δ*obaO* using the expression plasmid described above, the cultures should grow as normal and **1** production will be restored when DHBA is added exogenously. However, it was found that the mutations did not change the sensitivity of EcThrRS to **1**; none of the complemented Δ*obaL*Δ*obaO* cultures were able to grow in the presence of DHBA, as shown in Figure 5.5. Alternatively, it could be possible that the K to A mutations could have an adverse effect on protein function, therefore, to refute this, they should be expressed, purified and their activity compared to the WT protein monitored *in-vitro* by aminoacylation assays.

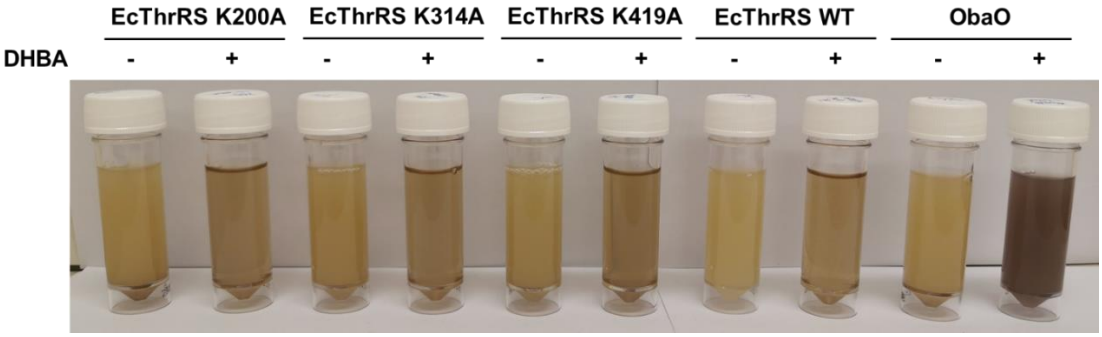

Figure 5.5: Singular lysine mutations of EcThrRS do not confer resistance to 1. *P. fluorescens* 39502 Δ*obaL*Δ*obaO* cultures complemented with EcThrRS K to A mutants or with ObaO as a control. The – and + symbols represent the absence or presence of DHBA which was added to a final concentration of 0.2 mM. The Δ*obaL*Δ*obaO*::EcThrRS mutants are unable to grow in the presence of DHBA, similar to the Δ*obaL*Δ*obaO*::EcThrRS control, whereas Δ*obaL*Δ*obaO*::ObaO is able to grow

and produce **1**, shown by the characteristic purple colouration of the culture; this was confirmed by HPLC analysis.

5.4 Protein-ligand crystallography

A crystal structure of EcThrRS liganded with **1** would allow a full understanding of the binding interactions of **1** with its target enzyme, helping us to define its mechanism of action. The structure of ΔN-EcThrRS was published by Sankaranarayanan *et al*.,[77, 80] and has been reproduced by the Wilkinson group. The crystal structure of EcThrRS was solved with another known ThrRS inhibitor, borrelidin, which simultaneously occupies each of the three binding pockets (for threonine, tRNA and ATP) as well as a non-catalytic fourth subsite.[59, 61, 64] It has also been solved with different ligands; tRNA and AMP,[77] and 5′-O-(N-(L-threonyl)-sulfamoyl)adenosine (Thr-AMS), which is a less-readily hydrolysable analogue of the intermediate L-threonyl-adenylate substrate.[80] Each of these structures showed a zinc ion in the active site which was shown to be essential and responsible for amino acid discrimination.[77, 80] These crystal structures will provide a basis for the mechanism of action studies of **1**.

Crystallisation trials were focused on ΔN-EcThrRS which crystallises far more easily than the full-length enzyme, and several attempts were made including co-crystallisations with **1** and with soaks into pre-formed crystals. I was successful in obtaining crystals using the vapour drop diffusion method in co-crystallisations of ΔN-EcThrRS with **1** in Morpheus screens, examples of which are shown in Figure 5.6. Due to the susceptibility of the β-lactone ring to hydrolytic breakdown[53] and indications that the hydroxyls on the catechol of **1** could participate in intramolecular catalysis of this process,[93] there were concerns about the stability of **1** under experimental conditions. Therefore, I also performed crystallisation trials with ΔN-EcThrRS and the catecholate analogues, **3** and **4** (**5** caused precipitation of the protein upon addition), which are likely less susceptible to hydrolysis, as well as **6** in anticipation that ring-opening of the **1** lactone moiety might be required for binding to its target residue.

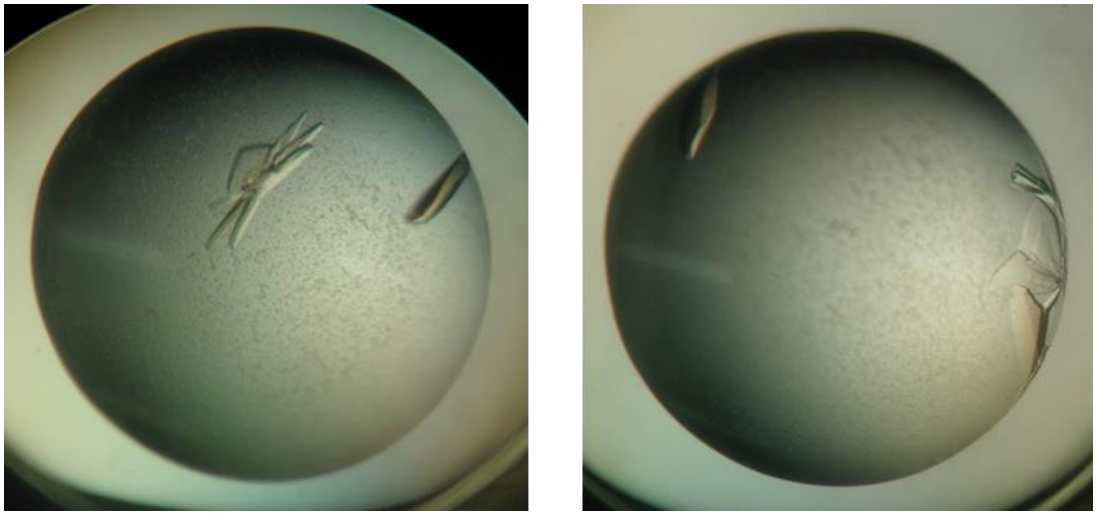

Figure 5.6: Crystals of ΔN EcThRS in a Morpehus (Molecular Dimensions) co-crystallisation screen with 1.

X-ray diffraction data were collected at Diamond Light Source to give structures of ΔN-EcThrRS which diffraction to 1.5-2.2 Å. These structures were checked for the presence of additional ligands using DIMPLE which generates electron density difference maps to search for putatively bound ligands.[113] Unfortunately, no non-native ligands bound to the protein structure were detected, but L-threonine was bound to the zinc ion in the active site.

As we know that the majority of **1** is hydrolysed at pH 8.0 (Figure 4.8), the pH at which ΔN-EcThrRS is purified and soluble. This could explain why we have been unable to obtain **1** liganded crystals. Due to the greater stability of **1** at lower pHs, I attempted to optimise the conditions to find a suitable pH to minimise **1**-hydrolysis but in which the protein remained stable. However, upon dialysis of EcThrRS protein into buffer at pH < 8.0, precipitation occurred, hindering the progress of these experiments further.

5.5 Isothermal Titration Calorimetry (ITC)

An attempt was made to characterise the **1**-ThrRS interaction via isothermal titration calorimetry (ITC). This technique is used to determine the thermodynamic parameters of interactions in solution by measuring the heat released or absorbed upon a bimolecular binding event.[114] A solution of **1** was injected into EcThrRS protein, in a matching buffer system, to monitor the heat released upon binding. An enthalpy change was observed upon the addition of **1** to protein (Figure 5.7) which was not seen for the control experiments. However, this would be expected if **1** is binding non-specifically to the protein, as previously described. To test this, I repeated the experiment using a readily available protein as a control, bovine serum albumin

(BSA), which also showed an enthalpy change on addition of sequential aliquots of **1**, suggesting that **1** acts as a general acylating agent for proteins *in vitro*. Additionally, HPLC analysis was performed on a solution of **1** in the buffer conditions used which showed that, during the time frame of the experiment, **1** is hydrolysed. This will cause complications during interpretation of results due to inaccuracies in concentrations of **1** and the possibility of multiple binding events. It was therefore decided that ITC is not a suitable method for studies on the **1**-ThrRS interaction.

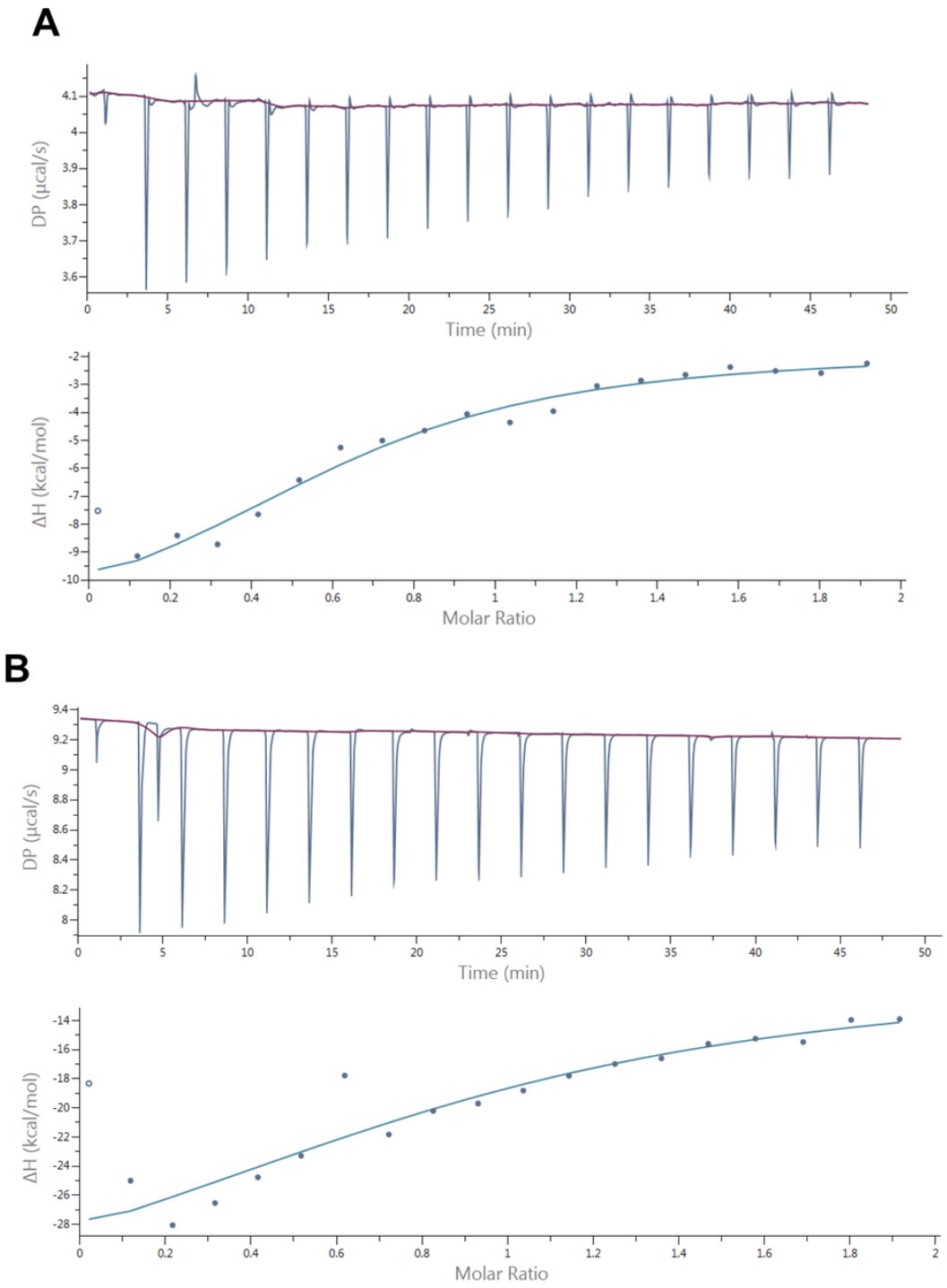

Figure 5.7: 1 binds non-specifically to proteins *in vitro*. Isothermal titration calorimetry (ITC) measuring the change in enthalpy (ΔH) on addition of sequential aliquots of 200 µM **1** to A) 20µM EcThrRS or B) control protein; bovine serum albumin (BSA). The change of differential power (DP) over time is also displayed and shows a constant baseline for both samples.

5.6 Attempts to use Fe(III) to stabilise 1 for mechanism of action studies

Results detailed in Chapter 4 which showed the protection effect against β-lactone hydrolysis of **1** upon binding to Fe(III), raised the question; could addition of Fe(III) resolve problems due to stability issues experienced during the mechanism of action studies of **1**?

Firstly, I repeated crystallisation trials of ΔN-EcThrRS with the addition of the **1**-Fe(III) complex as this should stabilise **1** to hydrolysis in the crystallisation conditions. Unfortunately, I found that the addition of Fe(III) at the concentrations required for crystallography resulted in the denaturation of the protein. This was characterised by precipitation and a complete loss of UV absorbance of protein in wells containing **1**-Fe(III), compared to crystals forming as normal in wells containing **1** only. I also repeated the MS experiments with the protein incubated with the **1**-Fe(III) complex compared to **1** only for comparison, to test the hypothesis that the Fe(III) binding protects **1** against nucleophilic attack from non-specific protein residues allowing identification of a consensus, target residue. However, these experiments gave inconclusive results; intact mass spectra showed sequential modification of ΔN-EcThrRS with **1** in both **1**-only and **1**-Fe(III) samples. However, tryptic digest experiments showed no modifications of **1** detected in either case although the protein was detected with 86 and 66% coverage, respectively. This shows that there was an issue with the experimental procedure that disrupted the ability of **1** to bind to the protein, as I would expect modifications of **1** to be detected in the control sample incubated with **1**-only.

5.6.1 Using Fe(III) to stabilise 1 in liquid culture in preparation for selection for resistance assays

As noted earlier, using the selection for bacterial resistance to study mode of action was always in mind. This might allow us to identify amino acid changes in the ThrRS target enzyme which are involved in the **1**-binding mechanism. However, a prerequisite of this experiment is the ability to grow indicator strains in media containing the antibiotic. The instability of **1** due to its susceptibility to hydrolysis was therefore an obstacle to performing this experiment. However, after results showing the protection effect of Fe(III) binding, it was reconsidered, i.e. could a selection for resistance experiment be performed with the **1**-Fe(III) complex to maximise the concentration of ring-closed **1** in solution?

Firstly, I probed the stability of **1**-only vs. the **1**-Fe(III) complex in growth conditions used for typical indicator strains, e.g. incubation in LB media at 37 ˚C (in a 96-well-

plate). I took aliquots for HPLC analysis at several time points, and this showed that incubation of **1** only results in complete hydrolysis to **6** after 21 hours. However, in the experiments containing the **1**-Fe(III) complex some ring-closed **1** remained after 21 hours (the proportion of **6**:**1** is 60:40). To note here is that the sum of total peak area of compounds detected at 270 nm in the HPLC chromatogram is much reduced compared to that of the initial sample (Figure 5.7 C). This could be to technical issues with the HPLC injection, sample evaporation or sequestration of **1** via reaction with peptides and/or other molecules in LB. However, the same was seen for all samples of the triplicate. Results are shown in Figure 5.8.

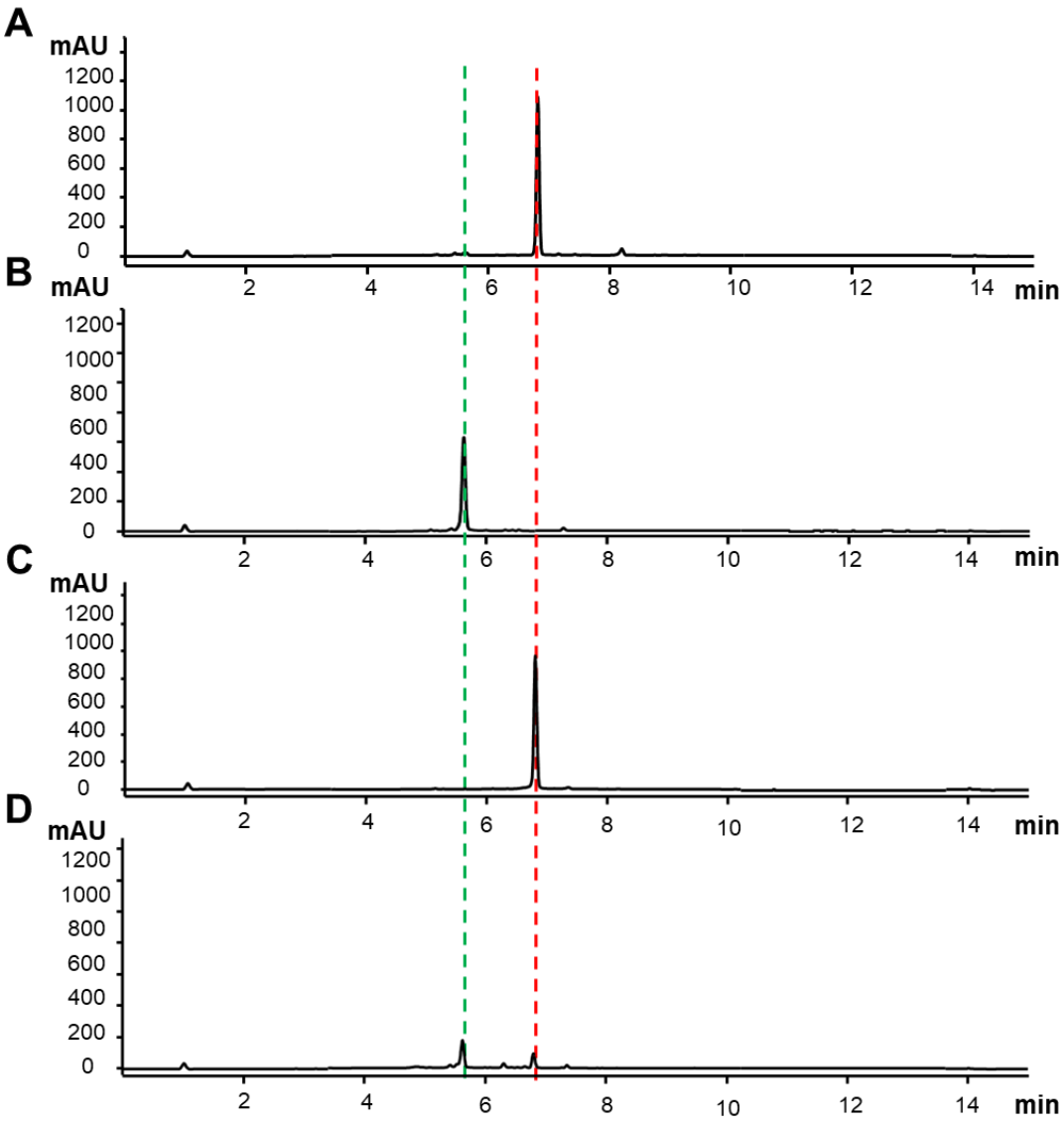

Figure 5.8: 1 hydrolysis in small volume of LB, effect of Fe(III) and time. HPLC UV chromatograms at 270 nm monitoring the hydrolysis of **1** with and without the addition of Fe(III) in LB cultures incubated at 37 ˚C in 96-well-plates (150 µL total

volume). A) Extract taken immediately after addition of **1** to LB and B) extract taken after 21 hours of incubation. C) Extract taken immediately after addition of **1**-Fe(III**)** to LB and D) extract taken after 21 hours of incubation. The red and green dashed lines represent **1** and **6** respectively.

The next question is, as Fe(III) can protect the β-lactone of **1** from hydrolysis in liquid culture to an extent in 96-well-plates, is the **1** left in solution at a concentration high enough to inhibit and/or arrest the growth of an indicator strain. To probe this, I aimed to perform cell viability assays. I prepared a set of serial dilutions of **1** only, Fe(III) only and **1**-Fe(III) into LB media which was inoculated with *E. coli* or MSSA and incubated the cultures overnight at 37 ˚C. I and noted the inhibition of growth by visible reduction in cell viability (Figure 5.9). For *E. coli* growth inhibition occured above 128 μg/mL **1** and **1**-Fe(III) and for MSSA, above 32 μg/mL **1** and 8 μg/mL **1**-Fe(III), as shown in Figure 5.9. To quantitatively analyse the inhibitory effect of **1** compared to **1**-Fe(III), these assays should be performed in a spectrophotometer to measure changes in OD_{600} over time.

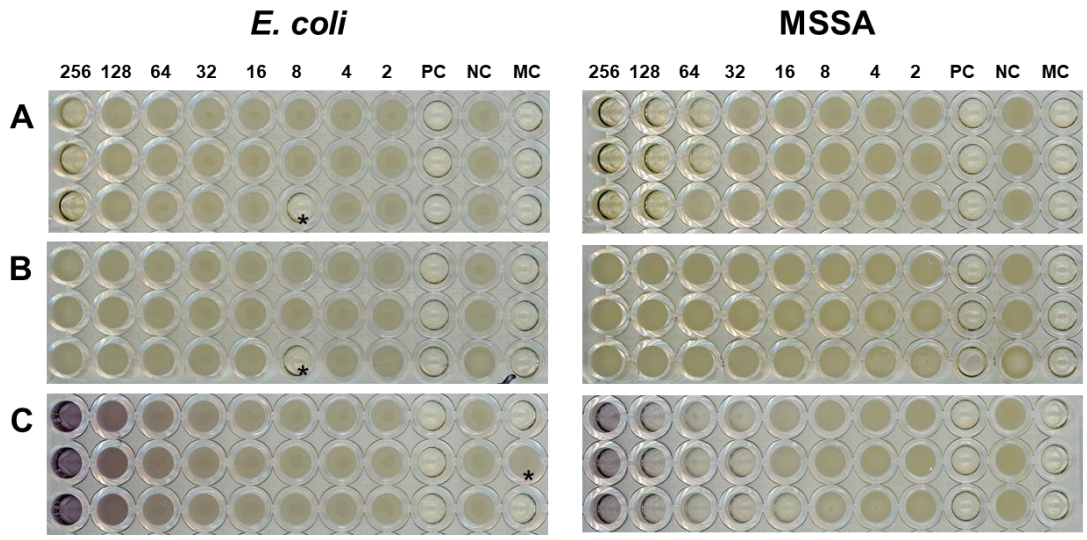

Figure 5.9: 1/1-Fe(III) has some ability to inhibit growth of indicator strains in liquid culture. Cell viability assays of *Escherichia coli* (*E. coli*) and methicillin-resistant *Staphylococcus aureus* (MSSA) against A) **1** only, B) Fe(III) only and C) the **1**-Fe(III) complex. PC (positive control) = Apramycin, NC (negative control) = DMSO only, MC (media control) = no bacterial inoculum. Concentrations of **1** are shown above each column and are in μg/mL. Note the results in wells highlighted with an asterisk are due to human error in experimental set-up.

These results show that **1** and **1**-Fe(III) have some ability to inhibit the growth of these indicator strains in liquid culture. There is no difference in MIC of **1** compared to **1**-

Fe(III) for *E. coli*, but **1**-Fe(III) has a lower MIC against MSSA than **1** only. I did attempt to perform resazurin assays with these plates which would give a colorimetric read out of cell viability. Resazurin, however, is an indicator dye that exhibits a colour change in the presence of *any* metabolically active cells,[115, 116] and therefore cannot distinguish inhibition of growth. Thus, I decided to present this data without the addition of dye.

5.7 Discussion

A variety of techniques has been used to probe the **1**-ThrRS interaction. The typical MS strategy used to identify the specific target residue of β-lactone covalent attachment was unsuccessful in this case. Instead of identifying one specific residue, analysis showed the modification of multiple residues throughout the target protein, EcThrRS, and for control proteins. This suggests that **1** can act as a general acylating agent *in vitro*, non-specifically binding to lysine residues. Additionally, the inability to identify a consensus residue of **1** binding to EcThrRS suggests that **1** acts in a different way to other β-lactone antibiotics and could present a novel mechanism of action. However, I believe that the mechanism of **1** does indeed involve covalent attachment to a specific target residue, as with other β-lactone containing antibiotics, and that it is simply the behaviour of the compound under laboratory conditions that is impeding our studies.

To combat these problems, I attempted to apply the discovery of the protection effect against hydrolysis of **1** upon Fe(III) binding to mechanism of action studies. Unfortunately, the high concentrations of **1**-Fe(III) required for co-crystallisations or soaks resulted in denaturation of the ΔN-EcThrRS protein, therefore crystallography was an unsuitable technique to characterise the interaction. MS experiments with **1**-only compared to **1**-Fe(III) gave inconclusive results. Intact mass showed the same results as previously for both conditions (sequential covalent modifications of **1**, which suggests that **1** acts as a general acylating agent irrespective of the presence of Fe(III). On the other hand, tryptic digest experiments showed no modifications of **1**-only control. This indicates issues with experimental procedures so further repeats are required.

Experiments to monitor the stability of **1** in liquid culture and conditions that would be suitable for performing a selection for resistance assay also showed varied results. Figure 5.7 shows that if no Fe(III) is present, **1** is completely hydrolysed after 21 hours of incubation in LB media at 37 ˚C. However, if inoculated as the **1**-Fe(III) complex, a proportion of ring-closed **1** remains after this time. Therefore, further experiments to

probe the ability of **1** vs.**1**-Fe(III) to inhibit the growth of an indicator strain in liquid media were performed in 96-well-plates. These showed the ability of **1** and **1**-Fe(III) to inhibit growth of *E. coli* above 128 μg/mL and for MSSA above 32 and 8 μg/mL, respectively. I expected there to be a greater difference between the MICs of **1** vs. **1**-Fe(III) due to the significant drop in MIC observed upon addition of Fe(III) to solid spot-on-lawn bioassays. However, it could be the case that, in these conditions, the hydrolysis protection effect of Fe(III) is not as significant. Further experiments towards a selection for resistance assay could be completed in future although conditions must be optimised to ensure a sufficient concentration of ring-closed **1** is present in solution for the duration of the experiment.

In summary, I experienced significant problems working with **1** under the experimental conditions described that are due to its inherent instability. Thus, producing more stable analogues of **1** should be a future priority. Would it be possible to create an analogue that can participate in the same mechanism of action of **1** but have lower susceptibility to hydrolysis? The catecholate analogues are much less susceptible to hydrolysis, however their bioactivity is also greatly reduced relative to **1**. Therefore, analogues must be less susceptible to hydrolysis but retain the full catecholate moiety. Previously, unsuccessful attempts were made in our group (by Dr. Thomas Scott) to generate analogues with variation at the nitrophenolate group, using a mutasynthesis approach (substrates were fed to the *ΔobaC* mutant lacking the ability to produce the β-hydroxyamino acid **2**).

The remaining structural feature that can be altered is the β-lactone, a key functional group required for the bioactivity of **1**. We were aware of the chemical similarity but less electrophilic nature of β-lactam groups compared to β-lactones; moreover, **1** was discovered during screening for β-lactam containing antibacterial compounds.[57] Therefore, we hypothesised converting the β-lactone moiety to a β-lactam might lead to a compound that would behave in a similar way to **1** but retain higher stability against nucleophilic attack and ring-opening. Extensive attempts were made by Dr. Edward Hems in our group to pursue a semi-synthetic approach to create the β-lactam analogue from a purified sample of **1** which were unfortunately unsuccessful. Further attempts could focus on a fully synthetic approach. However, due to the incompatibilities of the different functional groups in the structure of **1**, this would likely require a highly complicated, multi-step synthesis.

Overall, it seems there is a large disparity between how **1** behaves in laboratory conditions vs. how it must act in its environmental niche to be effective. *P. fluorescens*

and the other **1**-producing organisms have evolved, acquired, and maintained the ability to biosynthesise **1**. This means the production of the antibiotic must give the organisms a significant selective advantage which overrules the energetic cost. Additionally, the β-lactone of **1** is susceptible to break down *in vitro*/laboratory conditions. In the environment, there is likely to be a highly complex mechanism, involving a plethora of different interactions that stabilise it until the point it must react with the target enzyme. I believe that it is unlikely that those conditions can be recreated in the laboratory and so it will be difficult to definitively characterise the mode of action of **1**. Therefore, we have been unsuccessful with using the techniques described.

Further investigations into the mechanism of action of **1** should focus on an *in vivo* approach to minimise difficulties attributed to compound stability. Dr. Sibyl Batey is doing so by designing a targeted mutagenesis approach which aims to identify target residue/s of EcThrRS responsible for changes in **1** sensitivity. This could provide a method to identify regions of the protein which are significant in the mechanism of action of **1**.

Chapter 6:

Discussion

Chapter 6 : Discussion

6.1 Summary of Results

In this work, the antibiotic and metal binding properties of obafluorin, **1**, were explored in detail with an aim to understand their role in its mechanism of action. The mutasynthetic approach for the creation of analogues of **1** with a modified catechol, developed previously in the Wilkinson group, was applied as a platform to assess the role of the catechol moiety. Firstly, the analogues **3**, **4** and **5**, with a modified catechol, were isolated in good yield after fermentation of the mutant strain of *P. fluorescens* ATCC 39502/Δ*obaL* to which exogenous catechol analogues had been fed. To achieve this, I worked in a collaborative manner with Drs Sibyl Batey and Edward Hems to scale-up the procedure. Bioassays of these analogues against typical indicator strains and metal binding assays showed that the catechol moiety is essential for both the antibacterial activity and the Fe(III)-binding properties of **1**. This correlation indicated a role of Fe(III) binding in the mechanism of action of **1** and led me to these questions: could Fe(III)-binding be involved in 1) an interaction with the target enzyme, ThrRS; 2) an uptake mechanism such as a siderophore or THA; or 3) provide a stability enhancing effect for the molecule? Or might it involve some combination of these effects?

To investigate these questions, experiments were first performed to assess the ability of the *in situ* biosynthesised analogues **3**-**5** to inhibit the housekeeping ThrRS enzyme of *P. fluorescens*, and thus its growth, in the absence of the immunity determinant ObaO. These experiments indicated that there was no detrimental effect on growth and thus that the analogues **3**-**5** could be biosynthesised inside the *P. fluorescens* cell in the absence of ObaO. This contrasts to equivalent experiments for the biosynthesis of **1** *in situ*, indicating that the catechol moiety is required for interaction with, and inhibition of, sensitive ThrRS. Next, we wondered whether the Fe(III)-binding properties of the catechol moiety may play an additional role in the biology of **1**, so experiments were performed to investigate the **1**-Fe(III) interaction further. The aims here were to understand: 1) the chemical characteristics of complex formation; 2) the effect of Fe(III) on **1** bioactivity; 3) the potential of **1** to act as a THA or a siderophore. MS experiments showed that **1** selectively binds to Fe(III), from a selection of other biologically-relevant metals, and UV-visible spectroscopy showed that it forms a 1:1 complex with Fe(III) which has a characteristic deep-blue colouration. Unexpectedly, spot-on-lawn antibacterial assays performed in the presence of an increased concentration of Fe(III) in the soft nutrient agar medium showed a drastic decrease in MIC of **1** against indicator strains, particularly for the

Gram-negative organisms *E. coli* and *P. aeruginosa*. However, when these assays were performed in iron depleted conditions, achieved through the addition of the iron chelator bipy, they showed no change in MIC of **1** against *E. coli* 25922. These results were the opposite of what would be expected for a Trojan-horse antibiotic (THA) which show a decrease in MIC in iron-depleted conditions due to enhanced cellular uptake via active transport.[99-101]

Spot-on-lawn antibacterial assays were performed against TonB-dependent transporter (TBDT) deficient strains, which showed the same result as those against *E. coli* 25922; there was no change in MIC upon addition of bipy, strongly suggesting that **1** does not act as a THA. Likely, the **1**-Fe(III) complex is low enough in MW not to require active transport across the cell membrane.[32] To investigate the ability of **1** to act as a siderophore, the effect of increasing and decreasing the availability of Fe(III) on the growth and the **1**-production by *P. fluorescens* was monitored. By measuring both the OD_{600} and peak area of **1**-related metabolites in HPLC UV chromatograms it was found that increasing the concentration of bipy, and therefore depleting the concentration of free Fe(III), led to decreased growth and **1**-related metabolite production. Again, this is the opposite of what would be expected if the biological role of **1** was to act as a classic siderophore.[32, 117, 118] In fact, increasing the concentration of Fe(III) resulted in increased **1** production, with no effect on cell growth. Interestingly, it also resulted in a reduction in the amount of **1** produced in fermentations that had been hydrolysed to **6**.

These results ruled out **1** acting as a siderophore and strongly suggested against it acting as a THA, but did indicate that binding of **1** to Fe(III) could provide protection from hydrolysis. Therefore, this latter observation was investigated further. The concept of protection from hydrolysis was particularly interesting due to observations by us[59] and others[93] that the β-lactone of **1** is highly susceptible to breakdown by hydrolysis, especially at alkaline pH. To examine this phenomena, **1** and **3**-**5** were incubated between pH 6.0-8.0 (at 0.5 pH unit increments) and the level of hydrolysis with or without added Fe(III), was monitored by HPLC. Results showed that **1** is more susceptible to hydrolysis in basic conditions. Also, that the catechol hydroxyls, particularly the 2'-hydroxyl, are required for hydrolysis suggesting that they intramolecularly catalyse this reaction. An exciting finding was that binding to Fe(III) protected the β-lactone of **1** from hydrolysis; in the presence of Fe(III), the proportion of **1** that was hydrolysed to **6** was greatly reduced. Additionally, it was verified that the β-lactone moiety is important for the antibacterial activity of **1**; **6** has greatly

reduced bioactivity compared to **1** exemplified by an increase in MIC against MRSA to 128 μg/mL from 4 μg/mL.

In summary, these results show that the catechol moiety is essential for the antibiotic and Fe(III) binding properties of **1**. We hypothesise that it participates in a direct interaction with the target enzyme, ThrRS, and that Fe(III) binding protects the β-lactone from hydrolysis.

6.2 Hypotheses for mechanism of action of 1

Considering these findings, my hypothesis for the mechanism of action of **1** is that the ring-closed β-lactone is required for covalent attachment to a specific residue in the ThrRS target, as is the case for other β-lactone NPs.[52, 67] However, due to the susceptibility of **1** to hydrolysis or ring opening with biological nucleophiles, it must be protected until it reaches its target enzyme; we suggest this is one benefit of the Fe(III) binding propensity of **1**. Although, considering the low availability of Fe(III) inside the cell due to the detrimental effects it causes via oxidative stress,[29] it is likely that the binding of **1** to Fe(III) could be protein-mediated. The data from our experiments with analogues **3**-**5** on their susceptibility to hydrolysis, and from the published results of others,[93] suggest that binding to Fe(III) via the phenolic groups on the catechol moiety renders them unable to engage in an intramolecular hydrolysis mechanism. This leads to an increased concentration of **1** relative to **6** that can access the target enzyme *in situ.* Once in position, a specific nucleophilic target residue of ThrRS will attack the carbonyl of the β-lactone and open the ring to leave **1** covalently attached to the protein. However, the electrophilic nature of **1** means that non-specific acylation of amino acid residues could also occur, in theory leading to off target effects (although no overt toxicity was reported for published *in vivo* antibacterial studies for **1** in mice).[55] Other functional groups in the structure of **1**, such as the aromatic nitro group and catechol moiety likely also participate in interactions with nearby active site residues in the protein.

On the other hand, it is also important to consider literature which shows that lysine residues of aaRSs are aminoacylated by their respective amino acid in signal transduction pathways.[119-121] This was first described by Gillet *et al.* who demonstrated that *E. coli* methionyl-tRNA synthetase could auto-aminoacylate,[119] a finding that was later confirmed by Hountondji *et al*.[122] The lysyl residue ε-NH_2 group of the aaRS reacts with the carboxylate of the amino acid, which is bound in its reactive aminoacyl-adenylate intermediate, to form an isopeptide bond. This leaves the amino acid covalently attached to the aaRS lysine residue which transduces

signals in various important cellular pathways.[121] It is also known that aaRSs can sense sufficient levels of their cognate amino acid using this process; they act as amino acid sensors. Additionally, it was found that leucine and leucyl-tRNA synthetase activate mTORC1, essential in protein translation, using this process. Therefore, aaRSs are able to aminoacylate lysine residues of both their own protein and other proteins with their cognate amino acid via a process that is directly sensitive to amino acid levels.[121, 123] This modification also decreases the capacity of aaRSs to aminoacylate their cognate tRNA, which, in turn, is directly proportional to their lysine aminoacyl transferase activity.[121] Therefore, this is a circular process and so its disruption could lead to a cascade of negative effects.

This leads me to an alternative hypothesis for the mechanism of action of **1** considering this information and the results described in Section 5.2. Perhaps, instead of this being an artefact of the reactivity of **1** *in vitro*, the covalent attachment of **1** to lysine residues that was observed by MS, could inhibit this process. Instead of the reaction of these lysine residues with their cognate reactive threonyl-adenylate intermediates, it is the β-lactone of **1** that reacts with them. This would give justification for the molecule's reactivity; it does not require activation by the formation of an adenylate intermediate as the strained 4-membered ring means the carbonyl is already primed for nucleophilic attack. Furthermore, once the β-lactone has been ring-opened by reaction with a nucleophile, its structure resembles that of threonine (with the addition of the periphery aromatic groups). This proposed reaction is shown in Figure 6.1.

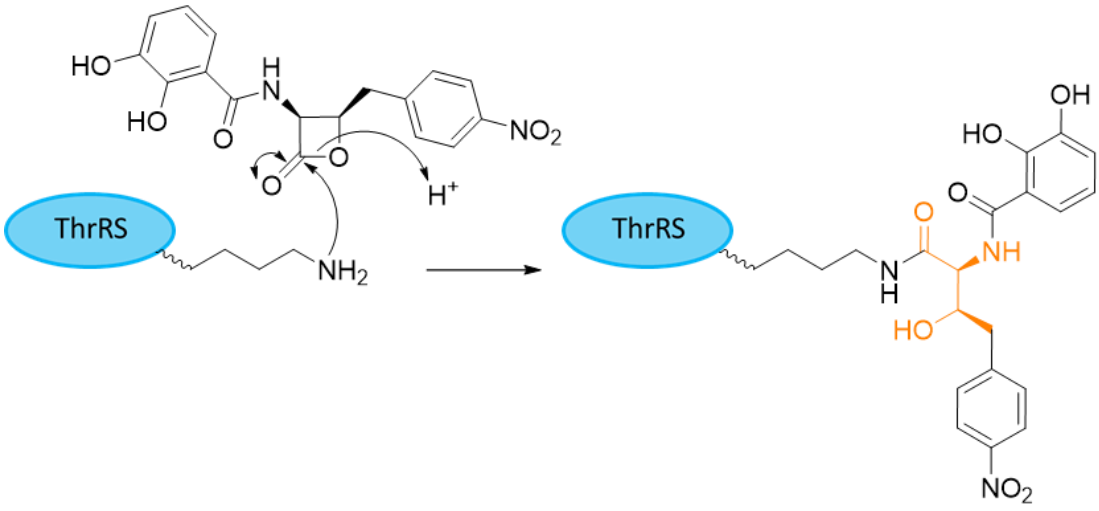

Figure 6.1: The proposed mechanism for 1-modification of lysine residues of ThrRS. The part of the resultant structure that resembles threonine is highlighted in orange.

One could therefore propose that, **1** covalently attaches to ThrRS lysine residues instead of its cognate threonine substrate and acts as a competitive inhibitor. This could inhibit the ability of ThrRS to sense levels of threonine sufficiency and cause subsequent imbalances in threonine homeostasis. Alternatively, the modification of lysine residues of ThrRS by **1** could inactivate the enzyme via an allosteric effect, preventing conformational changes required for enzyme activity. The observed lysine modifications of ObaG by **1**, a non-aaRS enzyme that was used as a control, could suggest that **1** is able to inhibit the aminoacylation (with threonine) of other proteins as well as ThrRS itself. Perhaps it inhibits the ability of ThrRS to threonylate interacting proteins and therefore inhibits signal transduction pathways. A similar phenomenon has been described for halofuginone, a prolyl-tRNA synthetase inhibitor, which suppresses tissue damage by mimicking amino acid stress and therefore disrupting the immune response.[124] However, considering this hypothesis for the **1** mechanism of action, we must address the selectivity of binding i.e. how would **1** not just act as a general acylating agent *in vivo*. This is important to consider, especially after MS results showing **1** can modify ObaG, a non-aaRS control protein. But, after the results of the MS experiments described here and the literature precedent for lysine aminoacylation of aaRSs, I believe this hypothesis would be interesting to investigate further.

6.3 Future Directions

The results described here, although have increased our insight into the mechanism of action and biochemical properties of **1**, also raise a lot more questions. Below, I will describe the key areas I believe should be investigated further.

6.3.1 Investigating the catechol moiety and Fe(III) binding

An important piece of information that is still unknown is whether the catecholate analogues **3**, **4** and **5** can inhibit ThrRS *in vitro*. Therefore, this must be tested via the aminoacylation assays described in Section 1.4.2. This would give conclusive evidence that the catechol is essential for the bioactivity of **1** by direct interaction with the target enzyme. Following this, further studies should focus on the **1**-Fe(III) complex; it could have potential as antimicrobial agent due to the considerable decrease in the MIC of **1** observed in bioassays with additional Fe(III). This could be particularly useful considering the activity against Gram-negative pathogens, *E. coli* and *P. aeruginosa*. The fact that MIC of **1** against *E. coli* NR698 (a membrane-permeabilised strain) is almost equal to that against *E. coli* 25922 when additional Fe(III) is present should be considered. This could suggest that the **1**-Fe(III) complex

penetrates the cell membrane better than **1**-only, but the results described strongly suggest **1** does not act as a THA to increase uptake via active transport. These results could be due to the following: 1) the **1**-Fe(III) complex can be passively transported inside the cell to a greater extent than **1**-only; 2) the hydrolysis protection effect upon binding to Fe(III) decreases the level of hydrolysis of **1** before entry to the cell; or 3) a combination of these effects.

For further investigations into the antibacterial activity of the **1**-Fe(III) complex it is vital that we further understand the effect of Fe(III) on the activity of **1**. We must be able to interpret differences due to the hydrolysis protection effect (and so **1** activity) or simply due to addition of Fe(III). This is important as we know that Fe(III) is essential for cellular processes but, in too high concentration, can also lead to cell damage via the formation of ROSs.[29] Therefore, a prerequisite of the use of **1**-Fe(III) as an antibiotic would be a complete understanding of the efficacy, toxicity and binding characteristics of the complex.

The inherent reactivity of **1** *in vitro*, sometimes even in the presence of Fe(III), will likely lead to difficulties with the design and execution of further experiments. But here I will provide suggestions as to what should be attempted. Future experimental investigations into the activity of the **1**-Fe(III) complex should be completed with **1** only, Fe(III) only and the **1**-Fe(III) complex so that the differences due to the addition of Fe(III) can be distinguished. Additionally, after/during steps in each experiment, the proportion of **1** compared to **6** should be monitored by HPLC, to ensure results can be attributed to the concentration of β-lactone present. Unfortunately, the crystallography and MS experiments attempted here, described in Section 5.6, to understand the efficacy of the **1**-Fe(III) complex *in vitro* were unsuccessful. After observing hydrolysis of **1** in the ThrRS crystallography conditions, I attempted to use Fe(III) to provide a hydrolysis protection effect, but this instead resulted in denaturation of the protein. MS experiments of ThrRS with **1**-Fe(III) gave inconclusive results and so should be repeated. The sample preparation method should be optimised; the effect of reaction time, compound concentration and a protein wash step on the number of **1**-modifications to both the intact protein mass and the lysine residues in the digested protein should be monitored. Therefore, to test the ability of the **1**-Fe(III) complex to inhibit ThrRS, I suggest that it should be subjected to aminoacylation assays. The efficacy of the antibiotic should also be tested using an infection model able to monitor activity and toxicity *in vivo*. Methods have been established which use the larvae of the Greater wax moth, *Galleria mellonella*, as a surrogate for a mammalian infection model.[125, 126] The use of *G. mellonella* is a more

rapid, ethically acceptable and reliable system for investigation of the *in vivo* toxicity and efficacy of antimicrobials.[127] Therefore, it is an ideal platform to investigate the *in vivo* potential of **1** compared to **1**-Fe(III), in the first instance.

The chemical characterisation of the **1**-Fe(III) complex should be supplemented by a key piece of data; the stability constant of the complex, K_{stab}. This would provide information on the stability of the complex in cellular conditions, its susceptibility to ligand exchange and release of free Fe(III). Additionally, it would provide insight as to whether the concentrations of Fe(III) required for formation of the complex are feasible to suggest this mechanism of **1**-Fe(III) binding for hydrolysis protection occurs intracellularly upon **1** production. Attempts were made, to characterise the stability constant via UV-visible spectrophotometric titration experiments (Figure 4.7) which are commonly used for this purpose in literature.[32, 94, 95] Unfortunately, interpretation of the results was limited by the requirement for additional software (HypSpec[98]) and expertise that was not available to us. Additionally, the pK_a values of the binding moieties (specifically of the catechol hydroxyl groups) should be included in calculations which could not be obtained experimentally due to complications with the hydrolysis of **1**. To combat these problems, I also attempted ITC experiments to determine the stability constant as has been described previously,[114, 128, 129] but again, the experiments were hindered by the hydrolysis of **1** in the experimental conditions. Therefore, further investigations should be conducted to identify a method for determination of the complex stability that it applicable to **1**.

6.3.2 Mechanism of action studies

In mechanism of action studies, the selectivity of **1** should be considered carefully. The lack of toxicity in *in vivo* antibacterial studies for **1** in mice[55] suggests it acts by a specific mechanism. Additionally, aminoacylation assays showed that **1** inhibits the activity of EcThrRS *in vitro.*[61] The presence of ObaO in the biosynthetic gene cluster (BGC) for **1** production and its partial inhibition by **1** indicate that is present as an immunity copy of the target, ThrRS. On the other hand, the results of MS and ITC experiments described in Chapter 5 showed that **1** acts as a general acylating agent *in vitro* and covalently attaches to lysine residues of proteins. Therefore, this leads me to question the specificity of **1** and whether it can inhibit other proteins in addition to ThrRSs. The inhibition of ThrRS/ObaO by **1** should be investigated further but I believe we should also consider whether **1** can covalently attach to lysine residues *in vivo* and so whether general acylation is part of its mechanism of action.

Due to difficulties experienced with experiments to investigate the mechanism of action of **1** on ThrRS *in vitro*, I propose that further studies should focus on an *in vivo* approach. The goal would be to identify a target residue/s for **1** covalent attachment via a mutagenesis strategy. As mentioned in Section 5.7, Dr. Sibyl Batey aims to do so by generating a set of EcThrRS/ObaO chimeric proteins to identify which part of ObaO contains the **1** resistance determinant. The chimeric proteins will be expressed in the *P. fluorescens* Δ*obaL*Δ*obaO* strain and the growth will be monitored in the presence of increasing concentrations of DHBA to initiate the biosynthesis of **1**. Initially, the three main domains of the proteins will be swapped, after which iterations will be performed for subregions of a domain shown to be important for conferring resistance to **1**. Then, the *in vitro* experiments can be repeated with these proteins to identify changes in how they interact with **1** compared to the EcThrRS. These will include the aminoacylation assays and the MS experiments described in Section 5.2.

To probe the alternative hypothesis of the mechanism of action of **1**, we should aim to validate the significance and investigate the biological role of covalent modification of lysine residues of ThrRS by **1**. Firstly, the MS tryptic digest experiments described here should be performed with ThrRS to monitor for auto-acylation with threonine itself. Then, I suggest investigating the ability of **1** to competitively inhibit this process by performing the experiment with ThrRS, threonine, ATP and **1** incubated together; do we observe modifications of **1** rather than threonine on lysine residues? Following this, experiments could be attempted to monitor the ability of **1** to inhibit lysine threonylation *in vivo*. It is possible to globally analyse the *in vivo* incorporation of specific amino acids in/onto proteins using a SILAC (stable isotope labelling by amino acids in cell culture) and quantitative MS approach.[130, 131] This would allow us to monitor changes to lysine threonylation in cell cultures challenged by **1** production; allowing us to determine whether **1** can disrupt lysine threonylation by ThrRS. I would suggest performing this experiment in the Δ*obaL*Δ*obaO* strain due to difficulties experienced upon addition of purified **1** to liquid culture.

Furthermore, it could be possible that Fe(III) is directly involved in the mechanism of action of **1** in some way. There are several examples of antibiotics that interact with iron in their mechanism of action. Bleomycin is a glycopeptide antibiotic with anti-tumour properties which exerts its activity by creating DNA breaks in a mechanism that is dependent on the generation of a free radical in the presence of iron.[30, 132, 133] Streptonigrin exerts its toxicity via binding irreversibly to DNA in the presence of certain metal ions, including Fe(III), so forming a streptonigrin– metal–DNA

complex.[132] It could be that the mechanism of action of **1** involves Fe(III)-mediated binding to ThrRS.

6.3.3 Regulation of the biosynthesis of 1

Another aspect of **1** biosynthesis that has not been discussed in this work but would be an interesting addition to our understanding of the biology of **1**, is its regulation. The **1** BGC contains two genes, *obaA* and *obaB*, which are predicted to be involved in quorum sensing (QS). This is a bacterial communication mechanism which allows synchronisation of gene expression as a function of population density by the release of signalling molecules detected above a minimum threshold concentration.[134] For Gram-negative bacteria these tend to be *N*-acylhomoserine lactone (HSL) compounds which are produced and recognised by LuxI synthases and LuxR receptors, respectively. ObaB and ObaA are predicted homologues of these proteins and so imply that the "switching-on" of the **1** biosynthetic pathway is through QS. It has also been reported that many organisms, including *P. aeruginosa*,[135] regulate siderophore biosynthesis using a QS system.[136, 137] In these systems, it is expected that there is a potential coregulation of siderophore production by QS and iron, although this is underexplored in the literature.[137]

Studies into the regulation of **1** should include disruption and/or overexpression of *obaA* and *obaB*, then monitoring the production levels of **1** and related metabolites by HPLC. If a change in production is observed, it would be interesting to see whether the phenotype could be restored by addition of exogenous HSLs. Upon deletion of *obaA* and *obaB*, the mutant strains, along with WT and the relevant controls, could be subjected to RNA-sequencing (RNA-seq) analysis to quantify levels of gene expression of the **1** BGC. It would also be interesting to investigate the effect of Fe(III) on gene expression of the **1** BGC. Results of experiments to monitor the effect of Fe(III) concentrations on the production of **1** and related metabolites by HPLC described in Section 4.4, show an increased proportion of **1** compared to **6** with increased Fe(III) levels (Figure 4.9). They also suggest that increasing Fe(III) has some effect on increasing the total level of **1** and related metabolites produced and so could implicate that Fe(III) is involved in the regulation of **1** biosynthesis. Perhaps the stability enhancing effect of Fe(IIII) is involved in this; *P. fluorescens* will only produce **1** with sufficient concentrations of Fe(III) to bind and protect the molecule from hydrolysis. It could be possible that iron is directly involved in regulation of the cluster and so the presence of binding sites, eg. a Fur box, near the **1** BGC should be investigated bioinformatically. Additionally, an RNA-seq experiment can be

designed to monitor the effect of Fe(III) on the levels of expression of **1** biosynthetic genes; I suggest WT, Δ*obaA* and Δ*obaB* strains are grown in OPM and OPM-Fe.

6.3.4 Key points for future investigations

To summarise the future directions, here are the key questions and areas that I believe should be the focus of future work.

1) Can the analogues **3**-**5** inhibit ThrRS *in vitro*?
2) The **1**-Fe(III) interaction:
    a. Is the antibacterial activity of **1**-Fe(III) enhanced compared to **1**-only due to increased cellular uptake via passive transport or protection against hydrolysis leading to increased concentration of **1** *in situ*?
    b. What is the stability constant of the complex formation?
    c. Is Fe(III) involved in the regulation of the biosynthesis of **1**?
3) Mechanism of action studies and the selectivity of **1**:
    a. Is **1** selectively able to inhibit threonyl tRNA synthetases?
    b. Does **1** act as a general acylating agent *in vivo*? The lack of toxicity in *in vivo* antibacterial studies for **1** in mice[55] suggests not so how and why?
    c. Is the covalent attachment of **1** to lysine residues of proteins biologically relevant *in vivo*, and if so, how is this selective?

6.4 Concluding Remarks

This study described a biochemical approach to understanding the bioactivity of the antibiotic obafluorin, **1**, by unpicking the role of its different structural motifs and chemical properties. Application of mutasynthesis and biochemical analysis led to identification of the role of the catechol moiety of **1**; it is essential for antibiotic activity and Fe(III)-binding. Chemical characterisation and investigation into biological effects of the **1**-Fe(III) complex led to identification of its hydrolysis protection effect of the β-lactone. This was found to be important in maintaining the bioactivity of **1**. These findings have aided investigations into the mechanism of action of **1**, which seems to be more complicated than other characterised β-lactone NPs. This study highlights the potential of revisiting antibiotics that were previously disregarded before the genome mining era using modern biochemical techniques. It also exemplifies the importance of interactions between iron and antibiotics and highlights the important role metal-binding can play in antibiotic activity. Antibiotics that interact with iron could

be an underexplored avenue to antimicrobials with a potentially higher barrier to resistance, critical in this age of rising AMR.

Chapter 7:

References

Chapter 7 : References

1. Katz, L.; Baltz, R. H., Natural product discovery: past, present, and future. *J. Ind. Microbiol. Biotechnol.* **2016,** *43*, 155-176.

2. Hutchings, M. I.; Truman, A. W.; Wilkinson, B., Antibiotics: past, present and future. *Curr. Opin. Microbiol.* **2019,** *51*, 72-80.

3. Shen, B., A New Golden Age of Natural Products Drug Discovery. *Cell* **2015,** *163*, 1297-1300.

4. Dias, D. A.; Urban, S.; Roessner, U., A Historical overview of natural products in drug discovery. *Metabolites* **2012,** *16*, 303-336.

5. Cragg, G. M.; Newman, D. J., Natural products: a continuing source of novel drug leads. *Biochim Biophys Acta* **2013,** *1830* (6), 3670-95.

6. Abraham, E. P.; Chain, E.; Fletcher, C. M.; Gardner, A. D.; Heatley, N. G.; Jennings, M. A.; Florey, H. W., FURTHER OBSERVATIONS ON PENICILLIN. *The Lancet* **1941,** *238* (6155), 177-189.

7. Genilloud, O., Actinomycetes: still a source of novel antibiotics. *Natural Product Reports* **2017,** *34* (10), 1203-1232.

8. Waksman, S. A.; Reilly, H. C.; Johnstone, D. B., Isolation of streptomycin-producing strains of Streptomyces griseus. *J. Bacteriol.* **1946,** *52*, 393-7.

9. Duggar, B. M., Aureomycin; a product of the continuing search for new antibiotics. *Ann. N. Y. Acad. Sci.* **1948,** *51* (Art. 2), 177-81.

10. Ehrlich, J.; Bartz, Q. R.; Smith, R. M.; Joslyn, D. A.; Burkholder, P. R., Chloromycetin, a New Antibiotic From a Soil Actinomycete. *Science* **1947,** *106* (2757), 417.

11. Geraci, J. E.; Heilman, F. R.; Nichols, D. R.; Wellman, E. W.; Ross, G. T., Some laboratory and clinical experiences with a new antibiotic, vancomycin. *Antibiot Annu* **1956**, 90-106.

12. Pham, J. V.; Yilma, M. A.; Feliz, A.; Majid, M. T.; Maffetone, N.; Walker, J. R.; Kim, E.; Cho, H. J.; Reynolds, J. M.; Song, M. C.; Park, S. R.; Yoon, Y. J., A Review of the Microbial Production of Bioactive Natural Products and Biologics. *Front Microbiol* **2019,** *10*, 1404.

13. Peláez, F., The historical delivery of antibiotics from microbial natural products--can history repeat? *Biochem. Pharmacol.* **2006,** *71* (7), 981-90.

14. Brown, E. D.; Wright, G. D., Antibacterial drug discovery in the resistance era. *Nature* **2016,** *529* (7586), 336-343.

15. Li, J. W.; Vederas, J. C., Drug discovery and natural products: end of an era or an endless frontier? *Science* **2009,** *325* (5937), 161-5.

16. Ortholand, J. Y.; Ganesan, A., Natural products and combinatorial chemistry: back to the future. *Curr. Opin. Chem. Biol.* **2004,** *8* (3), 271-80.

17. O'Shea, R.; Moser, H. E., Physicochemical Properties of Antibacterial Compounds: Implications for Drug Discovery. *J. Med. Chem.* **2008,** *51* (10), 2871-2878.

18. Bentley, S. D.; Chater, K. F.; Cerdeño-Tárraga, A. M.; Challis, G. L.; Thomson, N. R.; James, K. D.; Harris, D. E.; Quail, M. A.; Kieser, H.; Harper, D.; Bateman, A.; Brown, S.; Chandra, G.; Chen, C. W.; Collins, M.; Cronin, A.; Fraser, A.; Goble, A.; Hidalgo, J.; Hornsby, T.; Howarth, S.; Huang, C. H.; Kieser, T.; Larke, L.; Murphy, L.; Oliver, K.; O'Neil, S.; Rabbinowitsch, E.; Rajandream, M. A.; Rutherford, K.; Rutter, S.; Seeger, K.; Saunders, D.; Sharp, S.; Squares, R.; Squares, S.; Taylor, K.; Warren, T.; Wietzorrek, A.; Woodward, J.; Barrell, B. G.; Parkhill, J.; Hopwood, D. A., Complete genome sequence of the model actinomycete Streptomyces coelicolor A3(2). *Nature* **2002,** *417*, 141-147.

19. Blin, K.; Shaw, S.; Kloosterman, A. M.; Charlop-Powers, Z.; van Wezel, G. P.; Medema, M. H.; Weber, T., antiSMASH 6.0: improving cluster detection and comparison capabilities. *Nucleic Acids Res.* **2021,** *49* (W1), W29-W35.

20. Blin, K.; Medema, M. H.; Kazempour, D.; Fischbach, M. A.; Breitling, R.; Takano, E.; Weber, T., antiSMASH 2.0--a versatile platform for genome mining of secondary metabolite producers. *Nucleic Acids Res.* **2013,** *41* (Web Server issue), W204-12.

21. Bibb, M. J., Regulation of secondary metabolism in streptomycetes. *Curr. Opin. Microbiol.* **2005,** *8* (2), 208-15.

22. Fisch, K. M., Biosynthesis of natural products by microbial iterative hybrid PKS-NRPS. *Rsc Advances* **2013,** *3* (40), 18228-18247.

23. Winn, M.; Fyans, J. K.; Zhuo, Y.; Micklefield, J., Recent advances in engineering nonribosomal peptide assembly lines. *Nat. Prod. Rep.* **2016,** *33* (2), 317-47.

24. Miller, B. R.; Gulick, A. M., Structural Biology of Nonribosomal Peptide Synthetases. *Methods in molecular biology (Clifton, N.J.)* **2016,** *1401*, 3-29.

25. Staunton, J.; Weissman, K. J., Polyketide biosynthesis: a millennium review. *Natural Product Reports* **2001,** *18* (4), 380-416.

26. Wilkinson, B.; Micklefield, J., Mining and engineering natural-product biosynthetic pathways. *Nat. Chem. Biol.* **2007,** *3*, 379-386.

27. Scott, T. A.; Piel, J., The hidden enzymology of bacterial natural product biosynthesis. *Nat Rev Chem* **2019,** *3* (7), 404-425.

28. Martínez-Núñez, M. A.; López, V. E. L. y., Nonribosomal peptides synthetases and their applications in industry. *Sustainable Chemical Processes* **2016,** *4* (1), 13.

29. Andrews, S. C.; Robinson, A. K.; Rodriguez-Quinones, F., Bacterial iron homeostasis. *FEMS Microbiol Rev* **2003,** *27* (2-3), 215-37.

30. Ezraty, B.; Barras, F., The 'liaisons dangereuses' between iron and antibiotics. *FEMS Microbiol Rev* **2016,** *40* (3), 418-35.

31. Cassat, J. E.; Skaar, E. P., Iron in infection and immunity. *Cell Host Microbe* **2013,** *13* (5), 509-519.

32. Hider, R. C.; Kong, X., Chemistry and biology of siderophores. *Nat. Prod. Rep.* **2010,** *27* (5), 637-57.

33. Möllmann, U.; Heinisch, L.; Bauernfeind, A.; Köhler, T.; Ankel-Fuchs, D., Siderophores as drug delivery agents: application of the “Trojan Horse” strategy. *BioMetals* **2009,** *22* (4), 615-624.

34. Barry, S. M.; Challis, G. L., Recent advances in siderophore biosynthesis. *Curr. Opin. Chem. Biol.* **2009,** *13* (2), 205-15.

35. Crosa, J. H.; Walsh, C. T., Genetics and assembly line enzymology of siderophore biosynthesis in bacteria. *Microbiol. Mol. Biol. Rev.* **2002,** *66* (2), 223-49.

36. Challis, G. L.; Ravel, J.; Townsend, C. A., Predictive, structure-based model of amino acid recognition by nonribosomal peptide synthetase adenylation domains. *Chem. Biol.* **2000,** *7* (3), 211-24.

37. Kramer, J.; Ozkaya, O.; Kummerli, R., Bacterial siderophores in community and host interactions. *Nat. Rev. Microbiol.* **2020,** *18* (3), 152-163.

38. Chandrangsu, P.; Rensing, C.; Helmann, J. D., Metal homeostasis and resistance in bacteria (vol 15, pg 338, 2017). *Nature Reviews Microbiology* **2017,** *15* (6).

39. Carrano, C. J.; Raymond, K. N., Coordination chemistry of microbial iron transport compounds: rhodotorulic acid and iron uptake in Rhodotorula pilimanae. *J. Bacteriol.* **1978,** *136* (1), 69-74.

40. Moynie, L.; Milenkovic, S.; Mislin, G. L. A.; Gasser, V.; Malloci, G.; Baco, E.; McCaughan, R. P.; Page, M. G. P.; Schalk, I. J.; Ceccarelli, M.; Naismith, J. H., The complex of ferric-enterobactin with its transporter from Pseudomonas aeruginosa suggests a two-site model. *Nat Commun* **2019,** *10* (1), 3673.

41. Grinter, R.; Lithgow, T., The structure of the bacterial iron-catecholate transporter Fiu suggests that it imports substrates via a two-step mechanism. *J. Biol. Chem.* **2019,** *294* (51), 19523-19534.

42. Raymond, K. N.; Dertz, E. A.; Kim, S. S., Enterobactin: an archetype for microbial iron transport. *Proc Natl Acad Sci U S A* **2003,** *100* (7), 3584-8.

43. Foley, T. L.; Simeonov, A., Targeting iron assimilation to develop new antibacterials. *Expert Opin Drug Discov* **2012,** *7* (9), 831-47.

44. Stefanska, A. L.; Fulston, M.; Houge-Frydrych, C. S.; Jones, J. J.; Warr, S. R., A potent seryl tRNA synthetase inhibitor SB-217452 isolated from a Streptomyces species. *J Antibiot (Tokyo)* **2000,** *53* (12), 1346-53.

45. Ito-Horiyama, T.; Ishii, Y.; Ito, A.; Sato, T.; Nakamura, R.; Fukuhara, N.; Tsuji, M.; Yamano, Y.; Yamaguchi, K.; Tateda, K., Stability of Novel Siderophore Cephalosporin S-649266 against Clinically Relevant Carbapenemases. *Antimicrob Agents Chemother* **2016,** *60* (7), 4384-6.

46. Mushtaq, S.; Sadouki, Z.; Vickers, A.; Livermore, D. M.; Woodford, N., In Vitro Activity of Cefiderocol, a Siderophore Cephalosporin, against Multidrug-Resistant Gram-Negative Bacteria. *Antimicrob Agents Chemother* **2020,** *64* (12).

47. Zhanel, G. G.; Golden, A. R.; Zelenitsky, S.; Wiebe, K.; Lawrence, C. K.; Adam, H. J.; Idowu, T.; Domalaon, R.; Schweizer, F.; Zhanel, M. A.; Lagace-Wiens, P. R. S.; Walkty, A. J.; Noreddin, A.; Lynch Iii, J. P.; Karlowsky, J. A., Cefiderocol: A Siderophore Cephalosporin with Activity Against Carbapenem-Resistant and Multidrug-Resistant Gram-Negative Bacilli. *Drugs* **2019,** *79* (3), 271-289.

48. Robinson, S. L.; Christenson, J. K.; Wackett, L. P., Biosynthesis and chemical diversity of beta-lactone natural products. *Nat. Prod. Rep.* **2019,** *36* (3), 458-475.

49. Lane, J. F.; Koch, W. T.; Leeds, N. S.; Gorin, G., On the Toxin of Illicium Anisatum. I. The Isolation and Characterization of a Convulsant Principle: Anisatin1. *Journal of the American Chemical Society* **1952,** *74* (13), 3211-3215.

50. Pemble, C. W. t.; Johnson, L. C.; Kridel, S. J.; Lowther, W. T., Crystal structure of the thioesterase domain of human fatty acid synthase inhibited by Orlistat. *Nat. Struct. Mol. Biol.* **2007,** *14* (8), 704-9.

51. Badros, A.; Singh, Z.; Dhakal, B.; Kwok, Y.; MacLaren, A.; Richardson, P.; Trikha, M.; Hari, P., Marizomib for central nervous system-multiple myeloma. *Br. J. Haematol.* **2017,** *177* (2), 221-225.

52. Kluge, A. F.; Petter, R. C., Acylating drugs: redesigning natural covalent inhibitors. *Curr. Opin. Chem. Biol.* **2010,** *14* (3), 421-7.

53. Robinson, S. L.; Christenson, J. K.; Wackett, L. P., Biosynthesis and chemical diversity of β-lactone natural products. In *Nat Prod Rep* 2019.

54. Sykes, R. B.; Bonner, D. P.; Bush, K.; Georgopapadakou, N. H.; Wells, J. S., Monobactams--monocyclic beta-lactam antibiotics produced by bacteria. *J. Antimicrob. Chemother.* **1981,** *8 Suppl E*, 1-16.

55. Tymiak, A. A.; Culver, C. A.; Malley, M. F.; Gougoutas, J. Z., Structure of Obafluorin: An Antibacterial β-Lactone from Pseudomonas fluorescens. *J. Org. Chem.* **1985,** *50*, 5491−5495.

56. Herbert, R. B.; Knaggs, A. R., The biosynthesis of the antibiotic obafluorin from p-aminophenylalanine in Pseudomonas fluorescens. *Tetrahedron Lett.* **1988,** *29*, 6353–6356.

57. Wells, J. S.; Trejo, W. H.; Principe, P. A.; Sykes, R. B., Obafluorin, a novel β-lactone produced by pseudomonas fluorescens. taxonomy, fermentation and biological properties. *J. Antibiot.* **1984,** *37*, 802–803

58. Herbert, R. B.; Knaggs, A. R., The biosynthesis of the pseudomonas antibiotic obafluorin from p-aminophenylalanine and glycine (glyoxylate). *Tetrahedron Lett.* **1990,** *31*, 7517–7520.

59. Scott, T. A.; Heine, D.; Qin, Z.; Wilkinson, B., An L-threonine transaldolase is required for L-threo-β-hydroxy-α-amino acid assembly during obafluorin biosynthesis. *Nat. Commun* **2017,** *8*, 15935.

60. Schaffer, J. E.; Reck, M. R.; Prasad, N. K.; Wencewicz, T. A., beta-Lactone formation during product release from a nonribosomal peptide synthetase. *Nat. Chem. Biol.* **2017,** *13* (7), 737-744.

61. Scott, T. A.; Batey, S. F. D.; Wiencek, P.; Chandra, G.; Alt, S.; Francklyn, C. S.; Wilkinson, B., Immunity-Guided Identification of Threonyl-tRNA Synthetase as the Molecular Target of Obafluorin, a beta-Lactone Antibiotic. *ACS Chem Biol* **2019,** *14* (12), 2663-2671.

62. Kreitler, D. F.; Gemmell, E. M.; Schaffer, J. E.; Wencewicz, T. A.; Gulick, A. M., The structural basis of N-acyl-alpha-amino-beta-lactone formation catalyzed by a nonribosomal peptide synthetase. *Nat Commun* **2019,** *10* (1), 3432.

63. Hurdle, J. G.; O'Neill, A. J.; Chopra, I., Prospects for aminoacyl-tRNA synthetase inhibitors as new antimicrobial agents. *Antimicrob. Agents Chemother.* **2005,** *49* (12), 4821-33.

64. Fang, P.; Yu, X.; Jeong, S. J.; Mirando, A.; Chen, K.; Chen, X.; Kim, S.; Francklyn, C. S.; Guo, M., Structural basis for full-spectrum inhibition of translational functions on a tRNA synthetase. *Nat Commun* **2015,** *6*, 6402.

65. Hughes, J.; Mellows, G., Inhibition of isoleucyl-transfer ribonucleic acid synthetase in Escherichia coli by pseudomonic acid. *Biochem J* **1978,** *176* (1), 305-18.

66. Agarwal, V.; Nair, S. K., Aminoacyl tRNA synthetases as targets for antibiotic development. *MedChemComm* **2012,** *3* (8), 887-898.

67. De Pascale, G.; Nazi, I.; Harrison, P. H.; Wright, G. D., beta-Lactone natural products and derivatives inactivate homoserine transacetylase, a target for antimicrobial agents. *J Antibiot (Tokyo)* **2011,** *64* (7), 483-7.

68. O'Rourke, S.; Widdick, D.; Bibb, M., A novel mechanism of immunity controls the onset of cinnamycin biosynthesis in Streptomyces cinnamoneus DSM 40646. *J. Ind. Microbiol. Biotechnol.* **2017,** *44* (4-5), 563-572.

69. Hanahan, D., Studies on transformation of Escherichia coli with plasmids. *J. Mol. Biol.* **1983,** *166* (4), 557-80.

70. Ruiz, N.; Falcone, B.; Kahne, D.; Silhavy, T. J., Chemical Conditionality: A GeneticStrategy to Probe Organelle Assembly. *Cell* **2005,** *121* (2), 307-317.

71. Simon, R.; Priefer, U.; Pühler, A., A Broad Host Range Mobilization System for In Vivo Genetic Engineering: Transposon Mutagenesis in Gram Negative Bacteria. *Bio/Technology* **1983,** *1* (9), 784-791.

72. Alexander, D.; Zuberer, D., Use of chrome azurol S reagents to evaluate siderophore production by rhizosphere bacteria. *Biol. Fertility Soils* **1991,** *12*, 39-45.

73. Petre, B.; Win, J.; Menke, F. L. H.; Kamoun, S., Protein-Protein Interaction Assays with Effector-GFP Fusions in Nicotiana benthamiana. *Methods Mol Biol* **2017,** *1659*, 85-98.

74. Bender, K. W.; Blackburn, R. K.; Monaghan, J.; Derbyshire, P.; Menke, F. L.; Zipfel, C.; Goshe, M. B.; Zielinski, R. E.; Huber, S. C., Autophosphorylation-based Calcium (Ca(2+)) Sensitivity Priming and Ca(2+)/Calmodulin Inhibition of Arabidopsis thaliana Ca(2+)-dependent Protein Kinase 28 (CPK28). *J. Biol. Chem.* **2017,** *292* (10), 3988-4002.

75. Tyanova, S.; Temu, T.; Cox, J., The MaxQuant computational platform for mass spectrometry-based shotgun proteomics. *Nat Protoc* **2016,** *11* (12), 2301-2319.

76. Reid, K. R.; Meyerhoff, M. E.; Mitchell-Koch, J. T., Salicylate Detection by Complexation with Iron(III) and Optical Absorbance Spectroscopy. An Undergraduate Quantitative Analysis Experiment. *J. Chem. Educ.* **2008,** *85* (12), 1658.

77. Sankaranarayanan, R.; Dock-Bregeon, A. C.; Romby, P.; Caillet, J.; Springer, M.; Rees, B.; Ehresmann, C.; Ehresmann, B.; Moras, D., The structure of threonyl-tRNA synthetase-tRNAThr complex enlightens its repressor activity and reveals an essential zinc ion in the active site. *Cell* **1999,** *97*, 371−381.

78. Schwyn, B.; Neilands, J. B., Universal chemical assay for the detection and determination of siderophores. *Anal. Biochem.* **1987,** *160* (1), 47-56.

79. Behnsen, J.; Raffatellu, M., Siderophores: More than Stealing Iron. *mBio* **2016,** *7*, 1906-16.

80. Sankaranarayanan, R.; Dock-Bregeon, A. C.; Rees, B.; Bovee, M.; Caillet, J.; Romby, P.; Francklyn, C. S.; Moras, D., Zinc ion mediated amino acid discrimination by threonyl-tRNA synthetase. *Nat. Struct. Biol.* **2000,** *7*, 461–465.

81. Hunt, J. B.; Neece, S. H.; Ginsburg, A., The use of 4-(2-pyridylazo)resorcinol in studies of zinc release from Escherichia coli aspartate transcarbamoylase. *Anal. Biochem.* **1985,** *146* (1), 150-7.

82. Page, M. G.; Dantier, C.; Desarbre, E., In vitro properties of BAL30072, a novel siderophore sulfactam with activity against multiresistant gram-negative bacilli. *Antimicrob Agents Chemother* **2010,** *54* (6), 2291-302.

83. Page, M. G. P., The Role of Iron and Siderophores in Infection, and the Development of Siderophore Antibiotics. *Clin. Infect. Dis.* **2019,** *69* (Suppl 7), S529-S537.

84. Nikaido, H.; Rosenberg, E. Y., Cir and Fiu proteins in the outer membrane of Escherichia coli catalyze transport of monomeric catechols: study with beta-lactam antibiotics containing catechol and analogous groups. *J. Bacteriol.* **1990,** *172* (3), 1361-7.

85. Ju, K. S.; Parales, R. E., Nitroaromatic compounds, from synthesis to biodegradation. *Microbiol. Mol. Biol. Rev.* **2010,** *74* (2), 250-72.

86. Tsednee, M.; Huang, Y.-C.; Chen, Y.-R.; Yeh, K.-C., Identification of metal species by ESI-MS/MS through release of free metals from the corresponding metal-ligand complexes. *Sci Rep* **2016,** *6*, 26785-26785.

87. Keith-Roach, M. J., A review of recent trends in electrospray ionisation–mass spectrometry for the analysis of metal–organic ligand complexes. *Anal. Chim. Acta* **2010,** *678* (2), 140-148.

88. Amin, S. A.; Green, D. H.; Kupper, F. C.; Carrano, C. J., Vibrioferrin, an unusual marine siderophore: iron binding, photochemistry, and biological implications. *Inorg. Chem.* **2009,** *48* (23), 11451-8.

89. Butler, A.; Theisen, R. M., Iron(III)-siderophore coordination chemistry: Reactivity of marine siderophores. *Coord. Chem. Rev.* **2010,** *254* (3-4), 288-296.

90. Vosburgh, W. C.; Cooper, G. R., Complex Ions. I. The Identification of Complex Ions in Solution by Spectrophotometric Measurements. *Journal of the American Chemical Society* **1941,** *63* (2), 437-442.

91. Gaspar, M.; Grazina, R.; Bodor, A.; Farkas, E.; Amélia Santos, M., Siderophore analogues: a new macrocyclic tetraamine tris(hydroxamate) ligand;

synthesis and solution chemistry of the iron(III), aluminium(III) and copper(II) complexes†. *J. Chem. Soc., Dalton Trans.* **1999,** (5), 799-806.

92. Renny, J. S.; Tomasevich, L. L.; Tallmadge, E. H.; Collum, D. B., Method of continuous variations: applications of job plots to the study of molecular associations in organometallic chemistry. *Angew. Chem. Int. Ed. Engl.* **2013,** *52* (46), 11998-2013.

93. Pu, Y.; Lowe, C.; Sailer, M.; Vederas, J. C., Synthesis, Stability, and Antimicrobial Activity of (+)-Obafluorin and Related β-Lactone Antibiotics. *J. Org. Chem.* **1994,** *59*, 3642–3655.

94. Harris, W. R.; Carrano, C. J.; Cooper, S. R.; Sofen, S. R.; Avdeef, A. E.; McArdle, J. V.; Raymond, K. N., Coordination chemistry of microbial iron transport compounds. 19. Stability constants and electrochemical behavior of ferric enterobactin and model complexes. *Journal of the American Chemical Society* **1979,** *101* (20), 6097-6104.

95. Carrano, C. J.; Drechsel, H.; Kaiser, D.; Jung, G.; Matzanke, B.; Winkelmann, G.; Rochel, N.; Albrecht-Gary, A. M., Coordination Chemistry of the Carboxylate Type Siderophore Rhizoferrin: The Iron(III) Complex and Its Metal Analogs. *Inorg. Chem.* **1996,** *35* (22), 6429-6436.

96. Crumbliss, A. L.; Harrington, J. M., Iron sequestration by small molecules: Thermodynamic and kinetic studies of natural siderophores and synthetic model compounds. In *Adv. Inorg. Chem.*, van Eldik, R.; Hubbard, C. D., Eds. Academic Press: 2009; Vol. 61, pp 179-250.

97. Zhang, G.; Amin, S. A.; Kupper, F. C.; Holt, P. D.; Carrano, C. J.; Butler, A., Ferric stability constants of representative marine siderophores: marinobactins, aquachelins, and petrobactin. *Inorg. Chem.* **2009,** *48* (23), 11466-73.

98. Gans, P.; Sabatini, A.; Vacca, A., Investigation of equilibria in solution. Determination of equilibrium constants with the HYPERQUAD suite of programs. *Talanta* **1996,** *43* (10), 1739-1753.

99. Southwell, J. W.; Black, C. M.; Duhme-Klair, A. K., Experimental Methods for Evaluating the Bacterial Uptake of Trojan Horse Antibacterials. *ChemMedChem* **2021,** *16* (7), 1063-1076.

100. Kohira, N.; West, J.; Ito, A.; Ito-Horiyama, T.; Nakamura, R.; Sato, T.; Rittenhouse, S.; Tsuji, M.; Yamano, Y., In Vitro Antimicrobial Activity of a Siderophore Cephalosporin, S-649266, against Enterobacteriaceae Clinical Isolates, Including Carbapenem-Resistant Strains. *Antimicrob Agents Chemother* **2016,** *60* (2), 729-34.

101. Ito, A.; Nishikawa, T.; Matsumoto, S.; Yoshizawa, H.; Sato, T.; Nakamura, R.; Tsuji, M.; Yamano, Y., Siderophore Cephalosporin Cefiderocol Utilizes Ferric Iron

Transporter Systems for Antibacterial Activity against Pseudomonas aeruginosa. *Antimicrob Agents Chemother* **2016,** *60* (12), 7396-7401.

102. .

103. Chitambar, C. R., Gallium and its competing roles with iron in biological systems. *Biochim Biophys Acta* **2016,** *1863* (8), 2044-53.

104. Nunes, J.; Charneira, C.; Morello, J.; Rodrigues, J.; Pereira, S. A.; Antunes, A. M. M., Mass Spectrometry-Based Methodologies for Targeted and Untargeted Identification of Protein Covalent Adducts (Adductomics): Current Status and Challenges. *High Throughput* **2019,** *8* (2).

105. Antoniak, D. T.; Duryee, M. J.; Mikuls, T. R.; Thiele, G. M.; Anderson, D. R., Aldehyde-modified proteins as mediators of early inflammation in atherosclerotic disease. *Free Radic Biol Med* **2015,** *89*, 409-18.

106. Phillips, M. B.; Sullivan, M. M.; Villalta, P. W.; Peterson, L. A., Covalent modification of cytochrome c by reactive metabolites of furan. *Chem. Res. Toxicol.* **2014,** *27* (1), 129-35.

107. Hadvary, P.; Sidler, W.; Meister, W.; Vetter, W.; Wolfer, H., The lipase inhibitor tetrahydrolipstatin binds covalently to the putative active site serine of pancreatic lipase. *J. Biol. Chem.* **1991,** *266* (4), 2021-7.

108. Reygaert, W. C., An overview of the antimicrobial resistance mechanisms of bacteria. *AIMS Microbiol* **2018,** *4* (3), 482-501.

109. Munita, J. M.; Arias, C. A., Mechanisms of Antibiotic Resistance. *Microbiol Spectr* **2016,** *4* (2).

110. Reygaert, W., Methicillin-resistant Staphylococcus aureus (MRSA): molecular aspects of antimicrobial resistance and virulence. *Clin Lab Sci* **2009,** *22* (2), 115-9.

111. Lowy, F. D., Antimicrobial resistance: the example of Staphylococcus aureus. *J. Clin. Invest.* **2003,** *111* (9), 1265-73.

112. Perkins, D. N.; Pappin, D. J. C.; Creasy, D. M.; Cottrell, J. S., Probability-based protein identification by searching sequence databases using mass spectrometry data. *Electrophoresis* **1999,** *20* (18), 3551-3567.

113. Wojdyr, M.; Keegan, R.; Winter, G.; Ashton, A., DIMPLE - a pipeline for the rapid generation of difference maps from protein crystals with putatively bound ligands. *Acta Crystallographica Section A Foundations of Crystallography* **2013,** *69*, s299-s299.

114. Damian, L., Isothermal titration calorimetry for studying protein-ligand interactions. *Methods Mol Biol* **2013,** *1008*, 103-18.

115. Sarker, S. D.; Nahar, L.; Kumarasamy, Y., Microtitre plate-based antibacterial assay incorporating resazurin as an indicator of cell growth, and its application in the in vitro antibacterial screening of phytochemicals. *Methods* **2007,** *42* (4), 321-4.

116. Travnickova, E.; Mikula, P.; Oprsal, J.; Bohacova, M.; Kubac, L.; Kimmer, D.; Soukupova, J.; Bittner, M., Resazurin assay for assessment of antimicrobial properties of electrospun nanofiber filtration membranes. *AMB Express* **2019,** *9* (1), 183.

117. Rachid, D.; Ahmed, B., Effect of iron and growth inhibitors on siderophores production by Pseudomonas fluorescens. *Afr J Biotechnol* **2005,** *4* (7), 697-702.

118. Budzikiewicz, H., Secondary metabolites from fluorescent pseudomonads. *FEMS Microbiol. Rev.* **1993,** *10* (3-4), 209-228.

119. Gillet, S.; Hountondji, C.; Schmitter, J. M.; Blanquet, S., Covalent methionylation of Escherichia coli methionyl-tRNA synthetase: Identification of the labeled amino acid residues by matrix-assisted laser desorption-ionization mass spectrometry. *Protein Sci.* **1997,** *6* (11), 2426-2435.

120. Yanagisawa, T.; Sumida, T.; Ishii, R.; Takemoto, C.; Yokoyama, S., A paralog of lysyl-tRNA synthetase aminoacylates a conserved lysine residue in translation elongation factor P. *Nat. Struct. Mol. Biol.* **2010,** *17* (9), 1136-U14.

121. He, X. D.; Gong, W.; Zhang, J. N.; Nie, J.; Yao, C. F.; Guo, F. S.; Lin, Y.; Wu, X. H.; Li, F.; Li, J.; Sun, W. C.; Wang, E. D.; An, Y. P.; Tang, H. R.; Yan, G. Q.; Yang, P. Y.; Wei, Y.; Mao, Y. Z.; Lin, P. C.; Zhao, J. Y.; Xu, Y. H.; Xu, W.; Zhao, S. M., Sensing and Transmitting Intracellular Amino Acid Signals through Reversible Lysine Aminoacylations. *Cell Metab* **2018,** *27* (1), 151.

122. Hountondji, C.; Beauvallet, C.; Pernollet, J. C.; Blanquet, S., Enzyme-induced covalent modification of methionyl-tRNA synthetase from Bacillus stearothermophilus by methionyl-adenylate: Identification of the labeled amino acid residues by matrix-assisted laser desorption-ionization mass spectrometry. *J. Protein Chem.* **2000,** *19* (7), 563-568.

123. Chantranupong, L.; Scaria, S. M.; Saxton, R. A.; Gygi, M. P.; Shen, K.; Wyant, G. A.; Wang, T.; Harper, J. W.; Gygi, S. P.; Sabatini, D. M., The CASTOR Proteins Are Arginine Sensors for the mTORC1 Pathway. *Cell* **2016,** *165* (1), 153-164.

124. Kim, Y.; Sundrud, M. S.; Zhou, C.; Edenius, M.; Zocco, D.; Powers, K.; Zhang, M.; Mazitschek, R.; Rao, A.; Yeo, C. Y.; Noss, E. H.; Brenner, M. B.; Whitman, M.; Keller, T. L., Aminoacyl-tRNA synthetase inhibition activates a pathway that branches from the canonical amino acid response in mammalian cells. *P Natl Acad Sci USA* **2020,** *117* (16), 8900-8911.

125. Thomas, R. J.; Hamblin, K. A.; Armstrong, S. J.; Müller, C. M.; Bokori-Brown, M.; Goldman, S.; Atkins, H. S.; Titball, R. W., Galleria mellonella as a model system to test the pharmacokinetics and efficacy of antibiotics against Burkholderia pseudomallei. *Int. J. Antimicrob. Agents* **2013,** *41* (4), 330-336.

126. Tsai, C. J.; Loh, J. M.; Proft, T., Galleria mellonella infection models for the study of bacterial diseases and for antimicrobial drug testing. *Virulence* **2016,** *7* (3), 214-29.

127. Desbois, A. P.; Coote, P. J., Chapter 2 - Utility of Greater Wax Moth Larva (Galleria mellonella) for Evaluating the Toxicity and Efficacy of New Antimicrobial Agents. In *Adv. Appl. Microbiol.*, Laskin, A. I.; Sariaslani, S.; Gadd, G. M., Eds. Academic Press: 2012; Vol. 78, pp 25-53.

128. Wyrzykowski, D.; Pilarski, B.; Jacewicz, D.; Chmurzynski, L., Investigation of metal-buffer interactions using isothermal titration calorimetry. *J. Therm. Anal. Calorim.* **2013,** *111* (3), 1829-1836.

129. Wszelaka-Rylik, M.; Gierycz, P., Isothermal titration calorimetry (ITC) study of natural cyclodextrins inclusion complexes with tropane alkaloids. *J. Therm. Anal. Calorim.* **2015,** *121* (3), 1359-1364.

130. Weinert, B. T.; Iesmantavicius, V.; Wagner, S. A.; Scholz, C.; Gummesson, B.; Beli, P.; Nystrom, T.; Choudhary, C., Acetyl-Phosphate Is a Critical Determinant of Lysine Acetylation in E. coli. *Mol. Cell* **2013,** *51* (2), 265-272.

131. Ong, S. E.; Blagoev, B.; Kratchmarova, I.; Kristensen, D. B.; Steen, H.; Pandey, A.; Mann, M., Stable isotope labeling by amino acids in cell culture, SILAC, as a simple and accurate approach to expression proteomics. *Molecular & Cellular Proteomics* **2002,** *1* (5), 376-386.

132. Sekhon, B. S. In *Metalloantibiotics and antibiotic mimics - an overview*, 2010.

133. Burger, R. M.; Peisach, J.; Horwitz, S. B., Activated Bleomycin - a Transient Complex of Drug, Iron, and Oxygen That Degrades DNA. *J. Biol. Chem.* **1981,** *256* (22), 1636-1644.

134. Camilli, A.; Bassler, B. L., Bacterial small-molecule signaling pathways. *Science* **2006,** *311* (5764), 1113-1116.

135. Stintzi, A.; Evans, K.; Meyer, J. M.; Poole, K., Quorum-sensing and siderophore biosynthesis in Pseudomonas aeruginosa: lasR/lasI mutants exhibit reduced pyoverdine biosynthesis. *FEMS Microbiol. Lett.* **1998,** *166* (2), 341-345.

136. Guan, L. L.; Onuki, H.; Kamino, K., Bacterial growth stimulation with exogenous siderophore and synthetic N-acyl homoserine lactone autoinducers under iron-limited and low-nutrient conditions. *Appl Environ Microbiol* **2000,** *66* (7), 2797-803.

137. McRose, D. L.; Baars, O.; Seyedsayamdost, M. R.; Morel, F. M. M., Quorum sensing and iron regulate a two-for-one siderophore gene cluster in Vibrio harveyi. *P Natl Acad Sci USA* **2018,** *115* (29), 7581-7586.

Appendix:

^{1}H NMR Spectra

Appendix: ^{1}H NMR Spectra

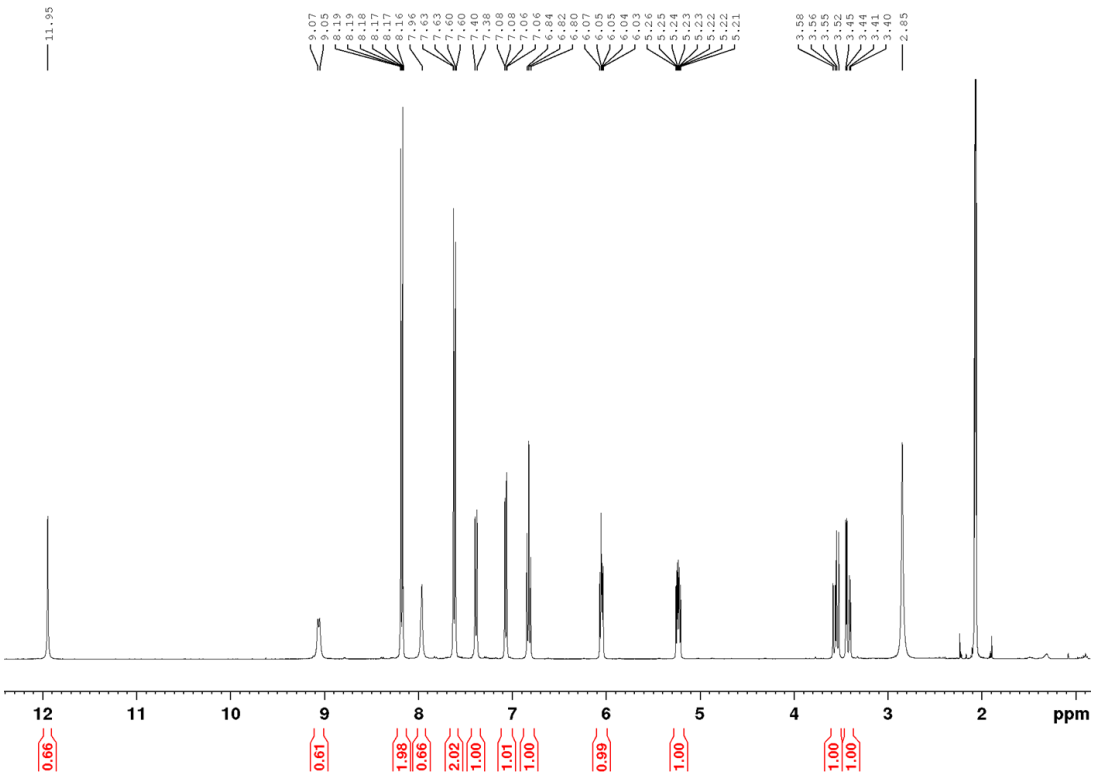

Supplementary Figure 1: ^{1}H NMR spectrum of obafluorin, **1** (400 MHz in C_3D_6O).

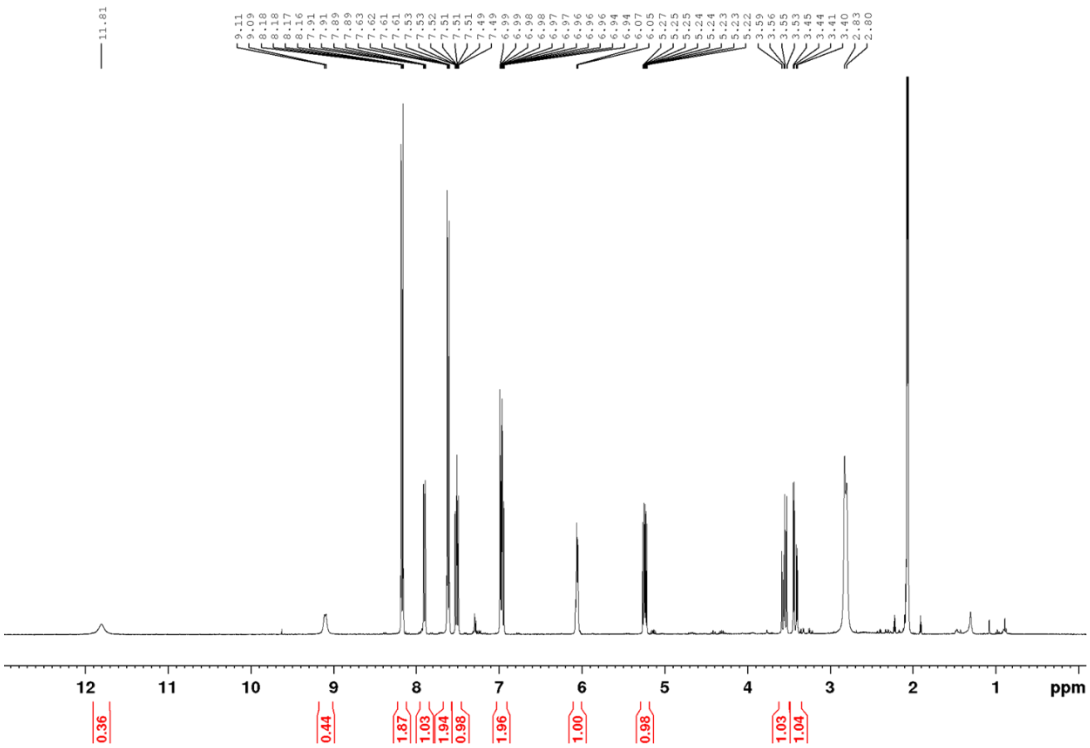

Supplementary Figure 2: ^{1}H NMR spectrum of analogue **3** (400 MHz in C_3D_6O).

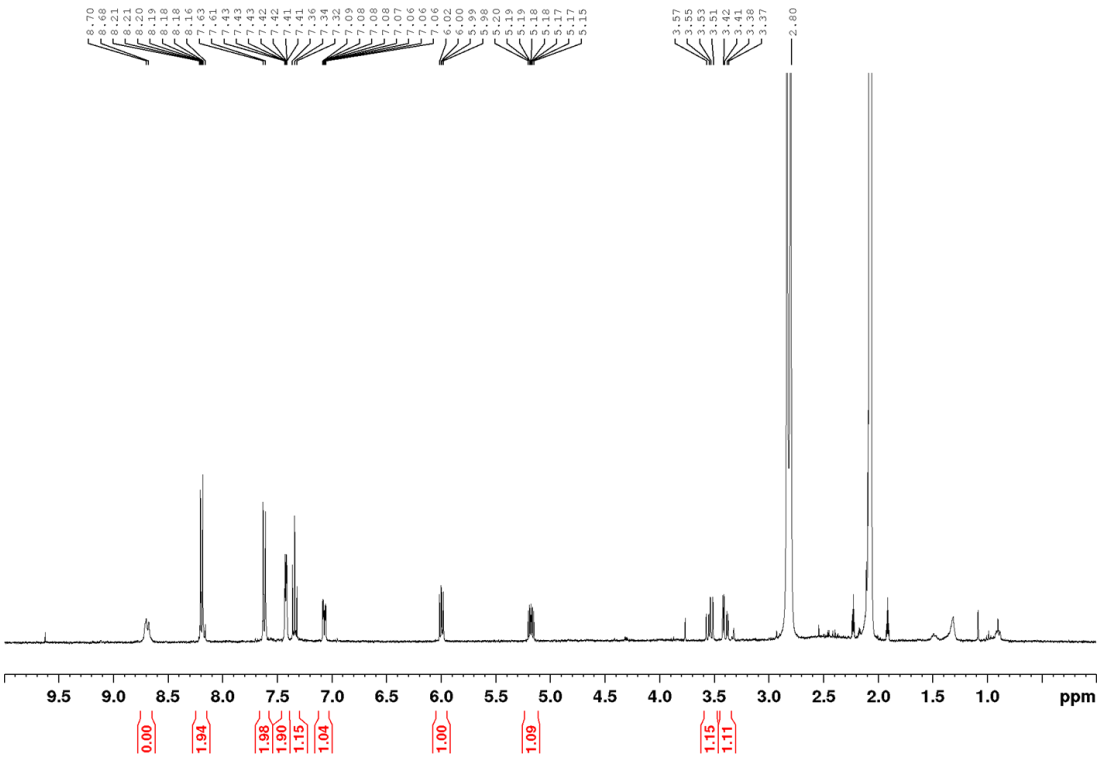

Supplementary Figure 3: ^{1}H NMR spectrum of analogue **4** (400 MHz in C_3D_6O).

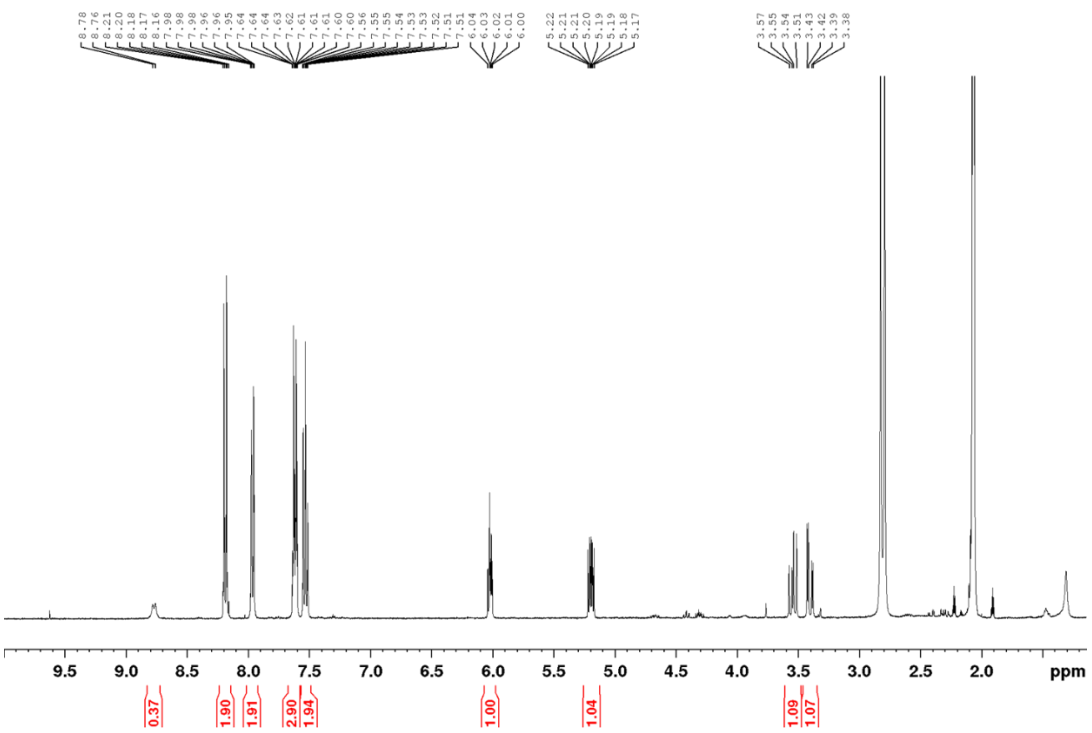

Supplementary Figure 4: ^{1}H NMR spectrum of analogue **5** (400 MHz in C_3D_6O).

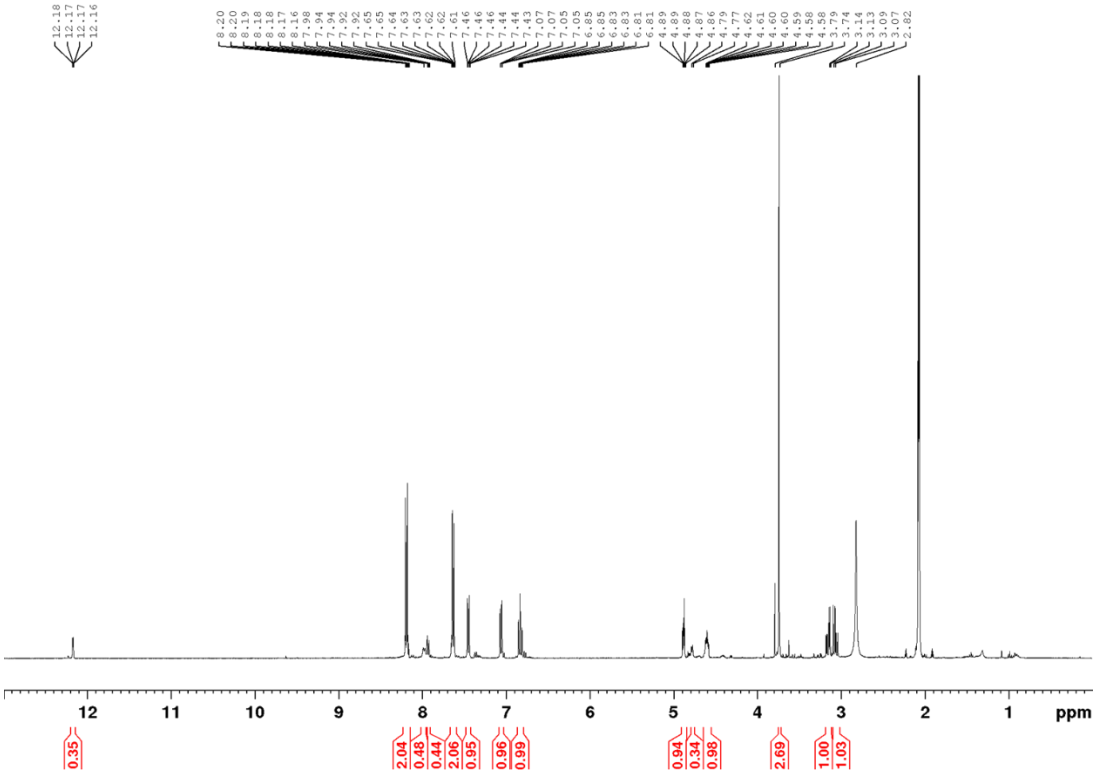

Supplementary Figure 5: ^{1}H NMR spectrum of hydrolysed obafluorin, **6** (400 MHz in C_3D_6O).